NONINVASIVE DETECTION OF CENTRAL VENOUS WAVEFORM USING PHOTOPLETHYSMOGRAPHY

Gideon Aniagyei-Mensah

A thesis submitted to the Faculty of Graduate and Postdoctoral Studies in partial fulfillment of the requirements for the degree of

MASTER OF APPLIED SCIENCE

in Biomedical Engineering

Ottawa-Carleton Institute for Biomedical Engineering
University of Ottawa
And
Medical Devices Innovation Institute of
The University of Ottawa Heart Institute
Ottawa, Canada

January 2014

Abstract

Information about the central venous pressure is important in evaluating several clinical conditions including cardiac failure and volume overload. The jugular veins serve as a primary route for the indirect estimation of the central venous pressure or waveform. The conventional methods for acquiring the central venous pressure in these veins have been through neck visualization and the insertion of catheters. Even though these procedures are effective if done properly, they have various downsides such as being invasive, inaccurate and time consuming.

In this research, a sensor is proposed for the noninvasive detection of central venous waveforms within the jugular veins. The sensor is a reflectance configured probe which utilizes laser based on the photoplethysmography principle. The effectiveness of the sensor was tested in-vitro using a mock circulatory loop and was also tested on a single human subject. The results from the tests indicated a very good sensor response in estimating pressure waveforms.

Acknowledgements

This work will not have been possible without the strength and life given to me by the almighty God, whose grace and mercies has brought me this far. I would also like to thank my supervisor, Professor Liang Ming, for assisting me throughout my graduate studies and research work. Profound gratitude also goes to my co-supervisor, Dr. Mussivand Tofy, for suggesting this research with immense support. My deepest gratitude goes out to my family (Aniagyei-Mensah family) for their support, love and encouragement. I will also like to give thumbs up to the Antwi family who helped me realize the dream of graduate education by supporting me financially.

I will like to appreciate the Mechanical Engineering department of the University of Ottawa for the administrative help they offered during my graduate study. I am also grateful to Dr. Marianne Fenech for providing a pressure meter to support the research. I want to say a big thank you to the following people for their help and contributions towards this work; Isaac Mencer, Jamie Vanderadt, Matthew Decan, Arda Bedirian, Kevin Derrah and Jocelyn Bergeron. Last but not least, I want to acknowledge the websites of Wikipedia and MedlinePlus for providing the explanations to the terms listed in the glossary.

Table of contents Page

List of Figures

Figure **Page**

List of Tables

Table **Page**

Glossary

Cardiac tamponade – The inability of the heart ventricles to expand fully due to the collection of blood or fluid in the pericardium sac surrounding the heart.

Cardiogenic shock – The inadequate circulation of blood due to primary failure of the ventricles of the heart to function effectively.

Congestive heart failure – Inappropriate blood flow to provide the body's organs with oxygen and nutrients due to damaged or weakened heart.

Couplant – A substance such as water, oil, grease, or paste used to avoid the retarding of sound in ultrasound technology.

Damping – Process of producing a slower response from instrumentation by applying a filter to the instrumentation output.

Dark current – The current a photodiode produces when there is no light present.

Diastole – The phase of the heartbeat when the heart muscle relaxes and allows the chambers to fill with blood.

Emboli – The formation of air bubbles in the blood stream which obstructs blood flow.

Hematoma – The collection of blood into tissues outside a vessel.

Hypervolemia – The medical condition where there is too much fluid in the blood. Opposite scenario is Hypovolemia.

Pericardial constriction – An inflammation of the sac-like covering of the heart (the pericardium) with thickening, scarring, and muscle tightening.

Phlebostatic axis – A point located by drawing an imaginary line from the fourth intercostal space at the sternum and finding its intersection with an imaginary line drawn down the center of the chest below the armpits.

Pulmonary hypertension – An increased pressure level in the pulmonary artery.

Sepsis – An overwhelming immune response of the body to bacterial infection where the chemicals released into the blood to fight the infection trigger widespread inflammation, leading to blood clots and leaky blood vessels.

Spectral response – The wavelength of a radiation that can be detected by a photodiode. It usually given in a range.

Supine – Lying flat on the back with a slight elevation of the head.

Systole – The phase of the heartbeat when the heart muscle contracts and pumps blood from the chambers into the arteries.

Tarchycardia – When the heart beats faster than normal. Opposite scenario is Bradycardia.

Thrombosis – The clotting of blood in the blood stream which obstructs blood flow.

Trendelenburg – A position where the body laid flat on the back with a slight elevation of the legs.

Tricuspid regurgitation – A disorder, in which the heart's tricuspid valve does not close properly causing blood to flow backward (leak) into the right upper heart chamber (atrium) when the right lower heart chamber (ventricle) contracts.

Tricuspid stenosis – A heart disease which results in the narrowing of the orifice of the tricuspid valve of the heart.

Valsalva – Performed by forceful exhalation against a closed airway, usually done by closing one's mouth and pinching one's nose shut.

Valvular disorder – Any disease process involving one or more of the four valves of the heart (the aortic and mitral valves on the left and the pulmonary and tricuspid valves on the right).

Abbreviations

CPR – Cardiopulmonary Resuscitation

CVC – Central Venous Catheterization

CVP – Central Venous Pressure

DAQ – Data Acquisition

EJV – External Jugular Vein

IJV – Internal Jugular Vein

JVP – Jugular Venous Pressure

LED – Light Emitting Diode

MCL – Mock Circulatory Loop

PIN – Positive Intrinsic Negative

PPG – Photoplethysmography

PWM – Pulse Width Modulator

SpO_2 – Oxygen Saturation

Chapter 1

1.0. Introduction

Physicians and health professionals have always reiterated the importance of the early detection of diseases using signs and symptoms. They have often testified on how early detection has been an important asset in saving many lives during the treatment of various diseases. This has made medical monitoring very crucial in our day to day activities. Doctors in their role are faced with a task to keep a constant watch on patients so that serious and life-threatening situations can be detected early enough for counter measures to be taken.

One very common practice in a typical clinical setting is the monitoring of central venous pressure (CVP). In acute and critically ill patients, it serves as a predominant tool in assessing volume status and cardiac preload. This variable can be monitored continuously or intermittently depending on the method of measurement being administered, as well as the patient's need. CVP also helps in diagnosing failure in the right side of the heart, as well as finding the relationship between venous blood return and ventricular ejection. The linkage of CVP to volume status is primarily exploited by physicians to guide them during the process of fluid resuscitation. This is usually done to manage patients who have abnormal perfusion generated from increased or decreased levels of body fluids. When there is inadequate body fluid, it translates to the volume of blood in the body which affects optimum heart preload. Although CVP monitoring is not the sole source of the aforementioned conditions, it has become an adjunct that is highly recommended for surgical and medical patients with problems of hypotension,

hypovolemia, circulatory failure, and massive fluid replacement needs (Graves and Klein 1968).

The internal jugular vein (IJV) and external jugular vein (EJV) have often served as channels for estimating CVP. A majority of methods employed in estimating CVP rely on the jugular veins. This correlation is possible due to the fact that these veins have a link to the central superior vena cava which connects to the right atrium. Since the cardiovascular system is a closed loop, a change in any part will have repercussions throughout the system (Russell 1974). This makes the pressures in the right atrium indirectly accessible through the central veins. Therefore, the CVP can interchangeably be referred as jugular venous pressure (JVP) or right arterial pressure.

1.1. Methods of estimating CVP

Sir Thomas Louis in 1930 described a technique for estimating the CVP by measuring the height of the column of blood in the jugular veins (Lipton, 2000). Louis showed that the jugular veins could be regarded as natural manometers connected to the right atrium, and stated the CVP could be determined by observing the height of the venous column in the jugular veins (Short, 1957).

Based on Louis' findings, visualization of neck veins for distention still serves as a useful tool in the physical examination of critical ill patients. His method of using jugular veins has been the principal technique used by many health professionals and physicians in estimating CVP. Some concerns have however been raised by researchers on the validity of the Louis method. Whiles some claim it is not accurate, others claim the results are subjective and inconsistent. In contrast, other researchers have supported the theories of Louis. Colquhoun and Jenkins (2010) stated that over the past few decades

several studies had confirmed the validity of the original findings of Louis, indicating there was no significant difference in JVP whether measured from the internal or external jugular vein. Nevertheless, Donahue *et al* (2009) believes the Louis' approach, which relies on visualizing jugular veins on the neck, requires much clinical experience from the observer which can cause CVP estimations to differ.

Alternatives for determining CVP by the use of jugular veins have also been documented. One classical approach is the use of catheters which have pressure transducers that are inserted into the IJV/EJV (Ward *et al* 2006). Siva *et al* (2012) believe the invasive measurement of the CVP via a central venous catheter (CVC) is still the standard criterion. This approach of accessing CVP gives accurate results with a very good level of precision. On the contrary, the method is invasive to the human and comes with a certain level of risk. Muralidhar (2002) in his paper spoke about various complications associated with the use of CVC. Just to name a few, it included puncturing the carotid artery which lies close to the IJV, hematoma, emboli, nerve injury, thrombosis and infections.

Some scientists and physicians have alternatively used ultrasound techniques in estimating CVP. By neck ultrasound, the physical appearance of the jugular veins can be viewed for distention. Lipton (2000) in his article described the use of ultrasound in measuring CVP as well as the sonographic patterns in the IJV with low, normal, and elevated CVP. The noninvasiveness of this approach makes it a convenient method and has shown glimpses of good and accurate results. However, it has not been widely accepted probably because of the cost and training involved for ultrasound technology. Brennan *et al* (2007) supported this by stating that conventional ultrasound measurement

of the inferior vena cava accurately predicted the CVP. However the cost, lack of portability, and specialized training required to acquire and interpret the data rendered the modality impractical for routine clinical use.

Clearly, the ability to accurately estimate CVP is of top priority to physicians, patients and researchers. Although methods are available to complete this task, they fall short in one way or the other. Other methods have been used by other researchers to evaluate the CVP. However, these methods emerged from the approaches already discussed. The new techniques either sought to improve upon the methods or correct the flaws inherent in the existing approach. Consequently, there is a need to evaluate the CVP in a simple, noninvasive, portable, accurate, less time consuming and inexpensive manner.

1.2. Research approach

In this research, an effort was made to find a new noninvasive approach to acquire pressure information from the jugular veins in order to estimate the CVP. This was accomplished by relying on the principle of photoplethysmography to construct a novel reflectance configured sensor using laser and a pair of photodiodes.

Photoplethysmography (PPG) is literally coined from two words. ‘Photo’ relates to light and ‘plethysmography’ means the measurement of a specific quantity using the changes occurring within a body or medium. Thus, PPG utilizes light properties to measure specific quantities in a medium by relying on the changes occurring in the medium. A typical scenario is using the changes caused by the periodic pulsations of a superficial artery to estimate quantities like pressure or volume within it. One conventional device which thrives on this technique is the pulse oximeter which measures

oxygen concentration and pulse rate within the body. It is manufactured using relatively cheap electronic components including light emitting diodes (LED) and photodiodes. The LED shines light through the body at one end and the photodiode receives the light emerging from the body at another end. Based on the varying light intensity at the photodiode, a modulated signal is produced which represents the measured quantity.

As stated in the abstract, a mock circulatory loop (MCL) was used to test the sensor. The MCL served as an in-vitro setup which replicated the conditions of the jugular veins. The MCL was made up of a series of components such as pumps, dampeners, pressure monitors, and a blood mimicking fluid. With the correct adjustments of these components, a pressure similar to what exists in the jugular veins was replicated and was used to test the sensor.

1.3. Structure of the thesis

This thesis is organized as follows; Chapter 2 serves as a literature review where more knowledge is given about the jugular veins. This chapter also explains in detail how the existing approaches work in evaluating the CVP. The fundamental of photoplethysmography, upon which the research idea is based, is also presented in this chapter. Chapter 3 presents the proposed methods and how the idea was implemented. This includes the process of fabricating the sensor as well as the assembling of the MCL parts for the in vitro setup. Chapter 4 entails the in vitro test, its results and the analysis of the results. The single subject in vivo test and analysis will also be outlined in this chapter. Chapter 5 then rounds up the thesis with discussions, conclusions and recommendations for future research.

Chapter 2

2.0. Literature Review

2.1. The cardiac and blood circulatory system

Undoubtedly, every organ in the human body is regarded as important and each plays a major role in contributing to the sustenance of life. However, the heart plays one of the most prominent roles in the human body. It has been regarded as the 'power house' of the body, as its role involves keeping the other organs alive by supplying them with oxygen-rich blood. The human body is made up of network of veins and arteries which are linked directly or indirectly to the heart. In Figure 2.1, Enderle (2005) illustrates the comparison between the two different blood networks within the human body. It shows the major arteries and veins which make up the circulatory system and how they are respectively linked to the left and right parts of the heart. Due to the linkage of blood vessels to the heart, the pressures within the heart generated through its pumping action are transmitted through the network of vessels. Grubb *et al* (2013) clarified the level of pressures in the heart and major blood vessels in Figure 2.2. They further stated that the right part of the heart (right atrium and ventricle) pumps deoxygenated blood returning from the systemic veins into the pulmonary circulation at relatively low pressures. In similar fashion, the left side of the heart (left atrium and ventricle) receives blood from the lungs and pumps it round the body through the arteries to the tissues at higher pressures.

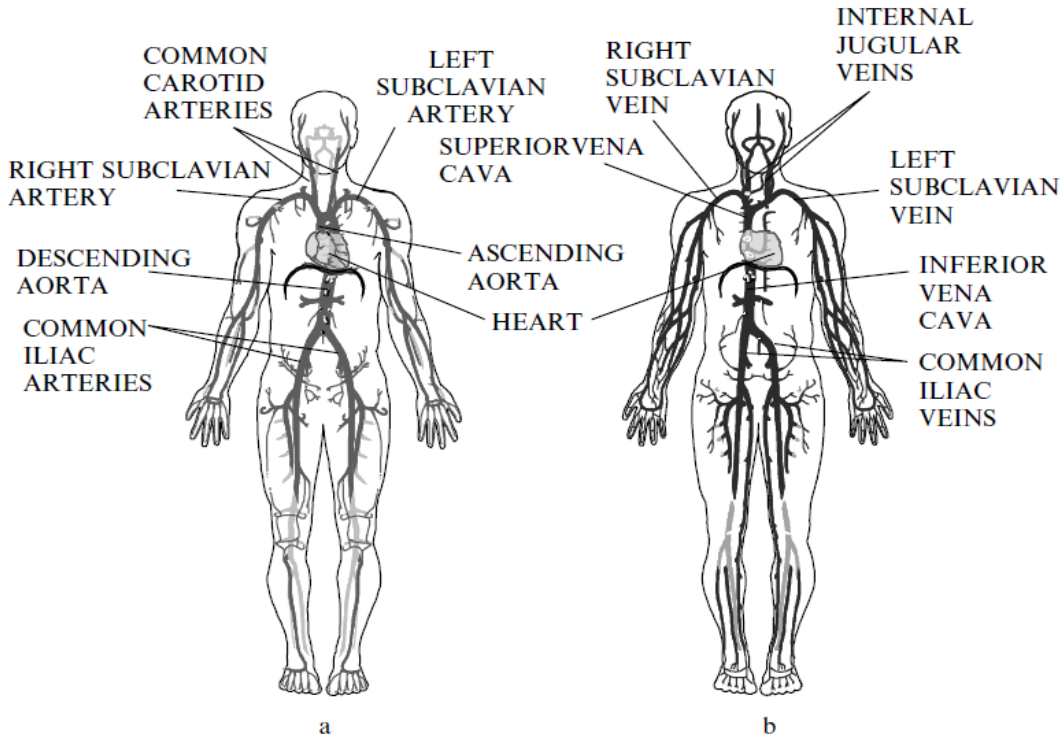

Figure 2.1. The blood circulatory network: (a) the distribution of the main arteries in the body which carry blood away from the heart, and (b) the distribution of the main veins in the body which return the blood to the heart. Reproduced from (Enderle 2005).

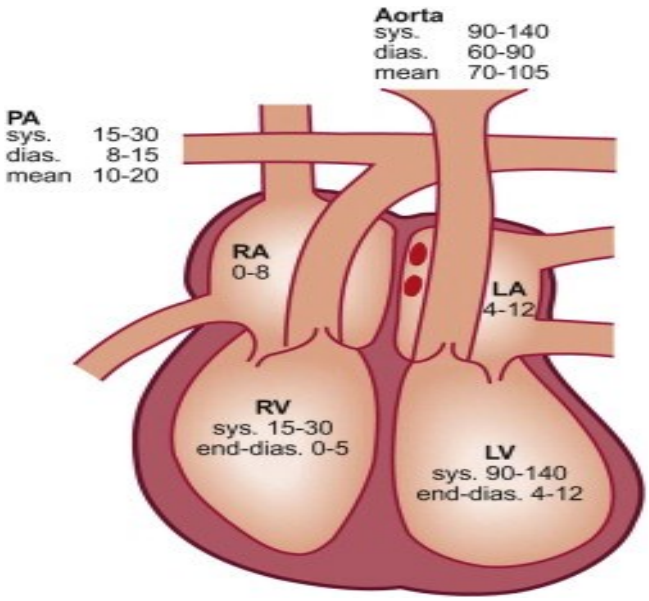

Figure 2.2. Normal resting pressures (mmHg) in the heart and great vessels. PA, pulmonary artery; RA, right atrium; LA, left atrium; RV, right ventricle; LV, left ventricle; sys., systolic; dias., diastolic. Reproduced from (Grubb *et al* 2013).

The link between the heart and the networked veins and arteries forms the peripheral venous and arterial system respectively. This networked system has given scientist and physicians the opportunity to derive cardiac information from the vessels which can easily by accessible. Typical examples include the brachial artery which is found in the arm. This artery can be felt around the region close to the crease of the elbow and this is the site normally used for the measurement of systolic and diastolic pressures. Another good example is the use of the carotid artery located in the frontal section of the neck. This artery is usually the first place to palpate on a critically injured person to ascertain if the heart is beating or not. In other words, it serves as a check on the person's status as being dead or alive. Not only does the peripheral system help in diagnosing the cardiac status. Because the vessels are networked throughout the body, present conditions existing within the body can be evaluated from a single peripheral site. This can be elaborated in the use of the pulse oximeter. Although the pulse oximeter may be applied to the tip of the finger or the ear lobe, it gives the average oxygen saturation level within the body. Likewise, this research draws motivation from the usefulness of the peripheral venous network. Where, information is translated from the right side of the heart through the jugular veins.

2.2. Central venous pressure (CVP)

Mangione (2008) and Pittman *et al* (2004) similarly defined the CVP as the pressure within the right atrium/superior vena cava system (i.e., the right ventricular filling pressure). This means CVP reflects right ventricular end-diastolic pressure (in the absence of tricuspid valve stenosis). In general, deoxygenated blood flows from the veins

into the right atrium through the superior and inferior vena cava. At diastole, the blood moves from the right atrium into the right ventricle. The tricuspid valve is the valve which separates the right atrium from the right ventricle and it function is to prevent the backflow of blood into the right atrium during ventricular contraction (systole). Tricuspid valve stenosis on the other hand is a medical condition which results to the narrowing of these valves. Hence in the absence of such a medical condition, the CVP is equal to the pressure in the right atrium or the pressure in the right ventricle after the diastolic phase ends. Rhodes *et al* (2011) alternatively defined the CVP as the intravascular pressure in the great thoracic veins, measured relative to atmospheric pressure. They additionally stated that it is conventionally measured at the junction of the superior vena cava and the right atrium. This site for CVP measurement is known to deliver accurate results especially through the use of catheters.

2.2.1. Importance of measuring CVP

Knowledge of a patient's CVP can be helpful in the diagnosis and management of a variety of critical illnesses and injuries including trauma, burns, sepsis, congestive heart failure, cardiogenic shock, traumatic brain injury and others (Ward *et al*, 2006). According to Magder (2005), two reasons that are commonly given for measuring the CVP are for the assessment of volume status and assessment of the preload of the heart. This agrees with Cole (2007) who claims the benefits of measuring CVP include the ability to:

- Monitor central intravascular blood volume and assess whether the patient is dehydrated, overhydrated or hypovolemic.

- Measure the effectiveness of intravenous (IV) fluid therapy, and
- Assess right-sided heart failure.

To clarify the relationship between CVP and intravenous blood volume, Easby and Dalrymple (2009) made it clear that a low CVP suggests a patient is under filled (i.e. intravascular depletion). A normal CVP means the patient is replete and a high CVP indicates overfilling. Also in agreement with Cole (2007), they reiterated a good cardiac output relies on an adequate CVP.

It should however be noted that intravascular blood volume and venous blood return are not always the cause or indicators of a higher or lower CVP. There can be other physiological causes of raised CVP, including cardiac tamponade, massive pulmonary embolus, superior vena cava obstruction, valvular disorders, venous tone and intra-thoracic pressure due to spontaneous respiration. Increased intra-thoracic pressure with intermittent positive pressure ventilation and positive end-expiratory pressure is translated to the central veins, artificially raising the CVP reading. Therefore, clinicians are encouraged to take isolated CVP measurements at the end of expiration. As an additional remedy to the other factors affecting CVP, it is has been advised that CVP should always be interpreted in conjunction with other measures of cardiac function and hemodynamic status such as pulse and blood pressure (Easby and Dalrymple 2009, and Watson and Wilkinson 2012).

Over the years, the jugular veins (both internal and external) have been the sites mostly used for CVP estimation. However, the use of the internal jugular vein (IJV) has usually been the favorite over the use of the external jugular vein (EJV). Since most methods as well as this research make reference to the jugular veins during CVP

estimation, it will be beneficial to give a brief insight into the anatomy and characteristics of these veins.

2.3. The jugular veins

The IJV and EJV both carry deoxygenated blood towards the superior vena cava which leads to the right atrium of the heart. According to Uflacker (2006), the IJV drains most of the blood from the skull, brain, superficial and deep parts of the face and neck whiles the EJV drains mainly the scalp, face and some deeper tissues. He further illustrated the anatomy and location of these veins using Figure 2.3. As shown in the figure, these veins run in a vertical fashion at the right side of the neck. However, similar anatomical features exist on the left side as well.

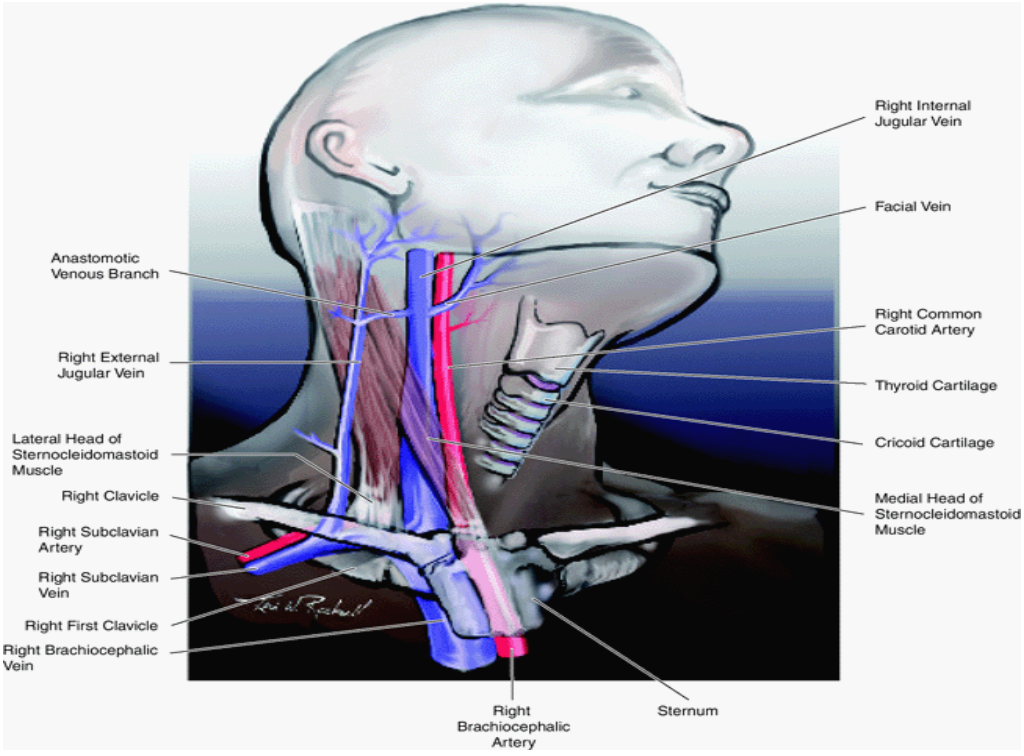

Figure 2.3. Internal jugular vein, external jugular vein and subclavian vein anatomy at the level of the neck. Reproduced from (Uflacker 2006).

The IJV emerges from the base of the skull, directly anterior and lateral to the internal carotid artery. It terminates after reaching the subclavian vein at the inner boarder of the anterior end of the first rib and posteriorly to the sternal end of the clavicle. The subclavian vein continues to the superior vena cava which leads to the right atrium. The landmark used to locate the distal portion of the internal jugular vein is the apex of the bifurcation of the two heads of the sternocleidomastoid muscle. During its course through the neck the IJV runs medial to the anterior portion of the sternocleidomastoid muscle in its upper part. Towards the middle, the IJV emerges from the apex of the triangle formed between the two inferior heads of the sternocleidomastoid muscle and the clavicle (Uflacker 2006, English *et al* 1969, and Defalque 1974). The EJV is much superficial to the skin as compared to the IJV. It begins just below the mandibular angle and runs down the neck towards the middle of the clavicle. It crosses the sternocleidomastoid muscles obliquely and in the subclavian triangle, perforates the deep fascia to end in the subclavian vein (Nishihara *et al* 1996).

2.3.1. IJV versus EJV

The IJV has traditionally been used in preference to the EJV. As Muralidhar (2002) puts it, the reason for the IJV popularity is directed towards its landmarks. This relates to its short, straight, valve less course to the superior vena cava and right atrium. Also, its position at the patient's neck provides easy access for anesthetists in more intra operative settings. Furthermore, the success rate for its use in catheterization exceeds 90% in most series of adults and children. This agrees with Troianos *et al* (1991) who also asserts the right IJV is the standard approach and a commonly used route for access to the central circulation. It was also disclosed that the IJV catheterization success rate of

95% is due to its accessibility during surgery, direct route into the right atrium, and predictable location.

There is an uncertainty about the use of the EJV in estimating CVP because some researchers claim it does not correctly estimate the CVP. Others also believe it is a good alternative for the IJV and the ease at which it can be visualized makes it a preferred choice. Vinayak *et al* (2006) hypothesized the EJV as an appealing alternative to the IJV, because it is easy to visualize. However, they were not clear about the usefulness of EJV in the assessment of CVP. Their argument was directed towards the purported obstacles in the EJV. This included the non-direct route of the EJV to the right atrium, the effect of neck fascial planes on the EJV, the smaller caliber of the EJV relative to the IJV, and the presence of venous valves. Based on the results of experiments conducted, they concluded by confirming the assertion that the EJV is easier to visualize than the IJV and also depicts abnormally low and high CVP with remarkable precision.

2.3.2. Characteristics of jugular veins

Unlike arteries, the jugular veins are primarily characterized by a very flexible vascular wall. The pressure within these vessels are very low and even though blood flowing within them is pulsatile, the low pressure makes it very difficult to palpate (feel and examine). Its flexibility makes it very susceptible to both physiological and anatomical changes. In a research conducted by Lin *et al* (2009), it is revealed that a jugular venous Doppler signal on ultrasound is represented by a continuous spectral waveform of low pulsatility, modulated by respiratory activity and the cardiac cycle. Results also indicate postural changes have an influence on the IJV flow and correlates to its variable lumen diameter. Sirovic *et al* (2003) also justifies posture has a strong effect

on the flow in the IJV saying, although the blood velocity in the jugular vein increases with transition from the supine to the sitting position, the estimated flow rate drops due to the narrowing of the jugular lumen. Lipton (2000) supported the latter with ultrasound images (Figure 2.4) showing a patient's IJV in the sitting position. It demonstrated a normal CVP will have an IJV that is almost completely collapsed. In the transverse plane it will either be non-visualized or appear as a small crescent or slit. Furthermore, Lobato *et al* (1998) conducted an experimental study using a two-dimensional surface ultrasound to view the cross sectional area of the jugular veins. It was documented on how clinical maneuvers such as the valsalva maneuver, an abdominal binder, or the trendelenburg position alone or in combination, increased the cross-sectional area of the right IJV.

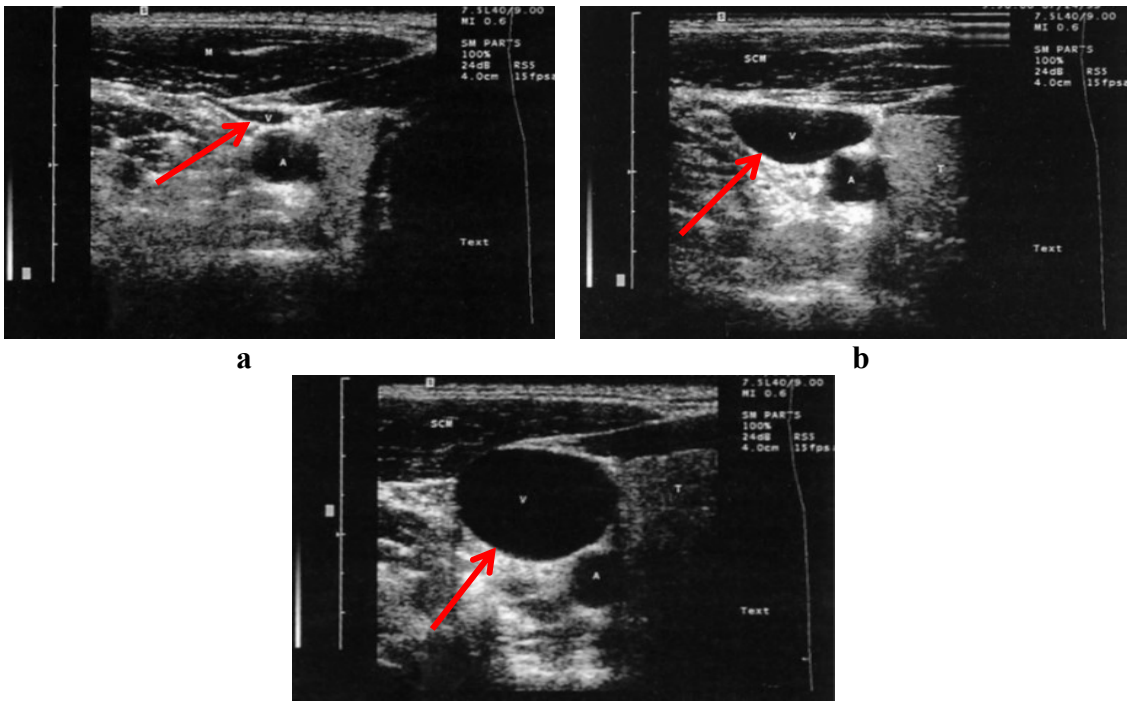

Figure 2.4. Transverse view of the right side of a neck showing differences in IJV lumen indicated by the red arrow: (a) collapsed IJV, (b) IJV at supine position, and (c) IJV with valsalva maneuver. A-The common carotid artery, SCM-the overlying sternocleidomastoid muscle. Reproduced from (Lipton 2000).

Pressure within the jugular veins is supposed to have a good correlation with the right arterial pressure. As was showed earlier, pressures in the right atrium during normal resting has values from 0 - 8mmHg. However this is not always the case recorded for estimated pressure in jugular veins. For example, a normal JVP in one posture could be abnormal in another. This therefore gives varying ranges and degrees when it comes to measuring JVP. Evidence of this can be seen in Table 2.1 which gives results of pressures in the right IJV at different postures (Lobato *et al* 1998). Nevertheless, Applefield (1990) believes a mean JVP greater than 10cmH_2O [7.36 mmHg] usually indicates volume overload, while a low JVP (i.e., less than 5cmH_2O [3.68 mmHg]) usually indicates hypovolemia.

Table 2.1 Effect of positive intrathoracic pressure induced by an inspiratory hold, hepatic compression, or both. Combined on the cross-sectional area and pressure of the right IJV with supine, and 10^o and 20^o trendelenburg positions. Reproduced from (Lobato *et al* 1998).

Position	**Control**	**Inspiratory hold**	**Hepatic Compression**	**Both Maneuvers**
	Cross sectional area of right IJV [cm^2 (% increase)]			
Supine	1.6 ±0.86	1.86 ±0.94 (14%)*	2.16 ±1.20 (26%)*	2.44 ±1.12 (35%)*
Trendelenburg				
10^0	2.13 ±1.12 (25%)*	2.22 ±1.12 (28%)*	2.37 ±1.12 (33%)*	2.54 ±1.12 (16%)*†
20^0	2.34 ±1.12 (32%)*	2.51 ±1.16 (36%)*	2.39 ±1.12 (34%)*	2.41 ±1.12 (34%)*
	Right IJV pressure [mmHg (% increase)]			
Supine	9.4 ±2.99	12.9 ±2.62 (23%)*	13.4 ±4.86 (30%)*	13.6 ±3.37 (42%)*
Trendelenburg				
10^0	13.5 ±3.74*	17.3 ±4.49 (22%)†	17.8 ±4.86 (24%)†	20.8 ±4.49 (35%)†
20^0	16.9 ±5.24*	19.5 ±4.86 (14%)‡	20.0 ±5.61 (16%)‡	23.4 ±4.86 (28%)‡

Note: Values are means ±Standard deviation
p<0.05 compared with *control supine, †control 10^0 trendelenburg, or ‡control 20^0 trendelenburg. The percent increase is based on supine control for right IJV cross-sectional area or right IJV pressure

On the other hand, EJV pressures may differ slightly but not significantly from IJV pressure and CVP. Parker *et al* (2002) saw that, a cannula placed in the EJV has a mean pressure 0.3 mmHg greater than the corresponding CVP. It was also realized that

over a wide range of venous pressure (1-22 mmHg), 95% of EJV pressure values were between 3.5 mmHg above and 3.0 mmHg below the CVP. However these results were for mechanically ventilated patients. For spontaneous respiration, the mean EJV pressure was 9.6 ±5.2 mmHg and the mean right atrial pressure (CVP) was 8.9 ±4.8 mmHg, which was not significantly different. Vinayak *et al* (2006) similarly used a benchmark categorized as low pressure ($\leq 5cmH_20$) and high pressure ($\geq 10cmH_20$) in determining the usefulness of the EJV's correlation to CVP. From their experiment, 118 observations were recorded among 35 patients and the resulting range for EJV pressure values was 2 - $20cmH_20$ (1.47 – 14.71mmHg). Based on their findings, it was concluded that the reliability for determining low and high CVP was excellent in the EJV.

2.4. Methods of measuring CVP

The measuring of CVP is a routine clinical practice carried out frequently on most critically ill patients. As Magder (2005) pointed out, it can be obtained with transducers and electronic monitors, or with a simple water manometer, and also by simply measuring jugular venous distension during physical examination. Currently, methods documented in literature for estimating CVP include the use of a central venous catheter which is inserted into a primary vein in the neck. This invasive method delivers accurate results because the catheter has a pressure transducer at its tip which measures pressures directly in the vicinity of the right atrium. One other classical method for CVP measurements is the visualization of neck veins. It has been demonstrated that the changes in the right atrium correlate with the properties of the major veins in the neck. So by critically observing the patient's neck, doctors are able to see the variations within the

vein which are reflected onto the skin surface. Alternatively, the use of ultrasound technology is being used to estimate CVP. Although this approach is not widely used, some researchers have carried out ultrasound on various veins in the neck and have used different criteria in estimating the CVP.

Certainly, there are several other methods which have been proposed by many researchers to estimate the CVP. Most of these methods sought to improve the methods already mentioned. Such as, correct flaws or make the existing method more robust. In the next few sections of this chapter, the methods will be discussed by explaining into detail how they are carried out. Also, some concerns and flaws about these methods will be addressed.

2.4.1. Central venous catheterization

Placement of a central venous catheter or central venous catheterization (CVC) is a frequent procedure during cardiac anesthesia and intensive care. This method is very useful in critically ill patients where the continuous monitoring of the patient's CVP is often required. It involves threading a catheter along a major vein until it is within vicinity of the right atrial compartment. Pressure readings are then collected directly inside the vein. These catheters have sensors at the tip in the form of pressure transducers which converts the mechanical pressure waves into electrical signals for display or storage. It is recommended that the CVC is placed in the distal superior vena cava i.e., outside of the cardiac chamber (Aggarwal *et al* 2006 and Shah *et al* 2013). With the use of CVC, one advantage is the possibility to rapidly infuse large volumes of intravenous fluids or deliver blood products and medications directly into patient's central circulation.

In view of CVC, Zamani *et al* 2012 mentioned various sites of catheter insertion which includes the femoral, subclavian, external jugular, internal jugular, antecubital and, rarely, saphenous veins. Several distinct approaches are discussed for placement of a CVC. Pfenninger and Fowler (2011) shared a similar opinion as they also said, CVC approaches included the cannulation of the subclavian vein (using both the supra- and infraclavicular routes), the jugular veins, and the femoral vein. They also added that the generally preferred veins are on the right side of the patient. Their premise for this preference is because the right-sided veins have a more direct course to the right atrium and thus, can be utilized for placement of a catheter with greater ease than the left-sided veins. The left-sided veins tend to have a more tortuous course and are in closer proximity to the thoracic duct and dome of the lung pleura.

2.4.1.1. Procedure for CVC

A lot of techniques have been developed towards the CVC approach. As mentioned earlier, there are various sites on the body through which CVC can be performed. Using a series of tables, Feldman (2003) summarized the following;

- The advantages and disadvantages of four different routes for central venous access (Table 2.2),
- The comparison of three catheterization techniques (Table 2.3),
- The comparison between three types of central venous catheters (Table 2.4), and
- The different approaches to IJV catheterization (Table 2.5).

In this thesis, explanation to the procedure for CVC will be limited to the seldinger technique using the right IJV. More information about the other techniques can be found in Feldman (2003).

Table 2.2. Advantages and disadvantages of four different routes for central venous access (Feldman 2003).

	IJV	**EJV**	**Subclavian vein**	**Femoral vein**
Risk of infection	Low	Low	Low	High
Patient mobility	Fair	Poor	Good	Bedridden
Trendelenburg required?	Yes	Yes	Yes	No, best for CHF or dyspnea
Need to stop Cardio Pulmonary Resuscitation (CPR)?	Probably	Probably	Yes	No, may continue CPR
Suitable for long-term use?	Yes, but not if ambulatory	No	Yes—best choice	No, remove within 2–3 days
Risk of venous thrombosis	Low	Low	Low	High

Table 2.3. Comparison of three catheterization techniques (Feldman 2003).

	Seldinger	**Catheter-over-the-needle**	**Catheter-through-the-needle**
Insertion needle	Small	Large	Largest
Speed	Slowest	Fastest	Fast
Number of steps	4+	1	2
Risk of catheter shear	None	Low	Highest
Catheters and lumens available	Single- or multiple-lumen,sheath/introducer	Single-lumen only	Single-lumen only
Rate of infusion	Highest (with sheath)	Moderate	Low to moderate

Table 2.4. Comparison between three types of catheter (Feldman 2003).

	Single-lumen	**Multiple-lumen**	**Sheath (Cordis)**
Minimum outer diameter	Smallest	Intermediate	Largest
Infusion rate	Moderate	Lowest (resuscitation catheters with larger lumen available)	Fastest (for central lumen; side port is slower)
Simultaneous infusions, or infusion while monitoring	No	Yes	Yes, if central lumen and side port both used
Length	Varies, fairly long	Long	Short
Allows device insertion (pulmonary artery lines and transvenous pacemakers)	No	No	Yes

Table 2.5. Different approaches to IJV catheterization (Feldman 2003).

	Central	**Anterior**	**Posterior**
Insertion landmark	Superior apex of the triangle formed by the two heads of the sternocleidomastoid muscle and the clavicle	Medial edge of the sternocleidomastoid muscle at level of thyroid cartilage	Lateral edge of sternocleidomastoid muscle, 1/3 of the way from the clavicle to the mastoid process
Angle with skin	30° (child), 45–60° (adult)	30° (child), 45° (adult)	30–45°, dive under the border of the sternocleidomastoid muscle
Aim toward	Ipsilateral nipple	Ipsilateral nipple	Sternal notch
Internal jugular vein depth in an adult	Within 3 cm	Within 3 cm	Within 5 cm

The procedure starts with the appropriate identification of the IJV. Some clinicians commence the process by first mapping out the triangle formed between the sternocleidomastoid muscles and the clavicle. This makes the prediction of the IJV location simpler. One assured way of locating the IJV is to let the patient lie in the supine or trendelenburg position with the head elevated at an angle of about 15 to 25 degrees. This keeps the vein engorged with blood and makes it visible enough to puncture. The process of engorging the vein can also be achieved by a valsalva maneuver. Once the vein is located, it is carefully pierced with a needle. A guide wire is threaded through the needle's bore into the jugular vein. However, this is only done with the assurance of the needle tip rightly situated in the lumen of the vein. When the guide wire has successfully reached the lumen of the vein, the needle is withdrawn leaving only the wire in place. An appropriate catheter having a lumen is slide gently over the guide wire into the vein's lumen until it reaches the desired location for pressure to be measured. Finally, the guide wire is withdrawn through the inserted catheter. The procedure is illustrated in Figure 2.5 (Muralidhar 2002).

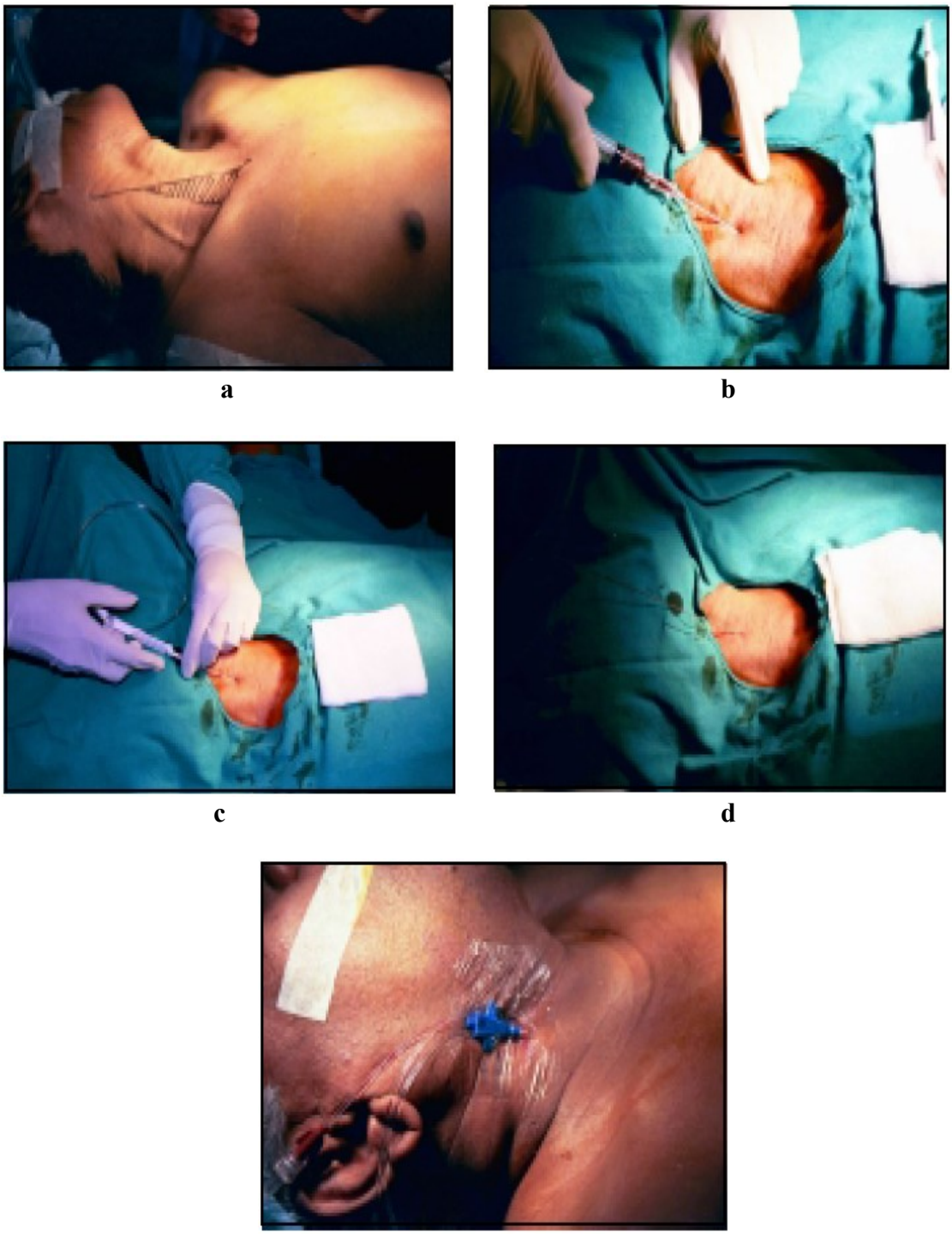

Figure 2.5. Procedure for CVC of the IJV: (a) head turned to left, trendelenberg position, two heads of sternocleidomastoid identified, (b) IJV located at the apex of the triangle, (c) guide wire passed through the needle, (d) guide wire left in place, and (e) A triple lumen CVP catheter inserted over the guide wire, guide wire reserved and CVP catheter in place. Reproduced from (Muralidhar 2002).

2.4.1.2. Complications associated with CVC

Despite the high level of accuracy associated with CVC methods in estimating CVP, its procedure is marred by several drawbacks. From the time of catheter insertion through to its removal, lots of care and caution is required in order to successfully carry out the procedure. Additionally, a high level of knowledge and experience is required for such an operation to be done. Sometimes, several trials have to be done when finding the jugular veins in order to complete the catheterization process. In other words, a series of needle puncture is done on a single patient which leads to discomfort and nerve injuries.

The complications of CVC are normally classified in two ways. Thus, complications which occur during the insertion of the catheter and the ones that comes about when the catheter is resident in the IJV. According to Lee *et al* (2007), Easby and Dalrymple (2008), and Muralidhar (2002), complications like hematoma, nerve injury, air embolism, pneumothorax and hemothorax can arise during the process of inserting a catheter, whiles issues like thrombosis, infection and arrhythmias come up when the catheter is resident in the IJV.

Out of the lot, one of the commonest complications associated with IJV catheterization is the puncturing of the common carotid artery. As shown earlier in this chapter, the carotid artery lies very close to the IJV and can be punctured during the step of needle insertion. This causes the collection of blood outside the vessels into tissues (Hematoma). In rare cases, the CVC line can be disconnected which can lead to excessive bleeding. Thrombosis emanates from the presence of foreign structures within the body. With such an occurrence, there is a probability of blood cells clotting within the vessels and blocking pathways preventing the flow of blood. Likewise, there are chances of

forming air bubbles within the veins (air embolism) which occur during catheter insertion and this phenomenon can also obstruct blood flow. Almost every invasive approach has to address the issue of infection and CVC methods are no exception. The insertion site has to be prepared adequately and full barrier precautions needs to be considered in order to eliminate the occurrence of infections. One other serious complication of the CVC method is arrhythmias. When care is not taken during the guide wire insertion, the wire can advance further than prescribed and enter the right atrium leading to this abnormality.

One may argue that the advent of technology such as ultrasound has lessened the burdens and complications of the CVC method. The ultrasound can now be used to assist clinicians as they locate the IJV and guide them during the catheter insertion process. As Trianos *et al* (1991) rightly puts it, ultrasound guided cannulation of the IJV facilitates locating the vein, permitting safe entry with fewer attempts, in less time, and decreases the incidence of arterial puncture. Additionally, some patients who cannot be cannulated using anatomic landmarks alone may be successfully cannulated with ultrasound guidance. In spite of this, the ultrasound may not readily be available during a CVC procedure and not all complications are eliminated by the use of the ultrasound such as the discomfort to patients, infections and nerve injuries.

2.4.2. Louis method (Neck visualization technique)

Almost seven decades have passed since Sir Thomas Louis described a technique for estimating the CVP by measuring the height of the column of blood in the jugular veins. Since then, evaluation of the neck veins for distention has been an integral part of the physical examination process (Lipton 2000). His concept can be pictured as a manometer consisting of a fluid reservoir bulb connected to a partially filled tube. The

bulb symbolizes the right atrium and the tube symbolizes the jugular vein. Now imagine the tube as a very flexible material which bulges outwards when filled and collapses when empty. With such a picture in mind, it is reasonable for a partially filled tube to bulge out from the bottom and collapse at the point (meniscus) where no more filling occurs in the tube. Relating this to the jugular vein, the whole concept about this method is to find the point where the vein collapses and measure its height to a reference point. In a healthy person, the visible jugular veins are fully collapsed when the person is standing and are often distended to a variable degree when the person is supine. Selecting an appropriate intermediate position permits the top of the column (the meniscus) to become visible in the neck between the clavicle and the mandible (Chua Chiaco *et al* 2013). Similar to the CVC method, the IJV is again much preferred for the neck visualization approach. Even though some clinicians are able to use the EJV for the same purpose, the anatomic advantage of the IJV direct route into the right atrium makes its results a true reflection of the pressures in the right atrium.

2.4.2.1. Procedure of the Louis method

Several researchers (Davison and Cannon 1974, Applefield 1990, Lipton 2000, Mangione 2008, and Chua Chiaco 2013) similarly describe the procedure by first placing the patient in a supine position at an angle where the IJV tip of pulsations (meniscus) can be visualized easily. This angle could be between 30 to 40 degrees. To visualize the meniscus, the head of the patient is turned towards the left and the jaw is slightly elevated. A flash light is shown tangentially at an angle of 45 degrees to the right side of

the neck toward the midline. Some have advised the dimming of surrounding lights, helps to identify the pulsation which usually occurs during exhalation.

Two points on the patient are used to determine the height of the column of blood in the IJV. One point is the tip of the pulsations located on the patient's neck and the other is the midpoint of the right atrium usually referred as the zero reference point. Because the midpoint of the right atrium is not directly accessible, it is substituted by the Louis angle. The landmark of Louis' angle is found at the junction of the manubrium and the sternum. This landmark is believed to lie five centimeters above the center of the right atrium regardless of the patient's anatomic position.

When the tip of pulsations (meniscus) of the IJV is located on the neck, the examiner places two rulers at an angle of 90 degrees with the horizontal ruler extrapolated from the meniscus. The vertical ruler is placed on the Louis angle (sternum) and the distance from the intersection of the rulers is read to the sternum. Five centimeters is added to the length of the reading and the total gives the CVP in centimeters of water. This can however be converted to the millimeter mercury using a conversion factor of 1.36 cmH_2O being equal to 1 mmHg. The Louis method is demonstrated in Figure 2.6 (Applefield 1990 and Mangione 2008).

a

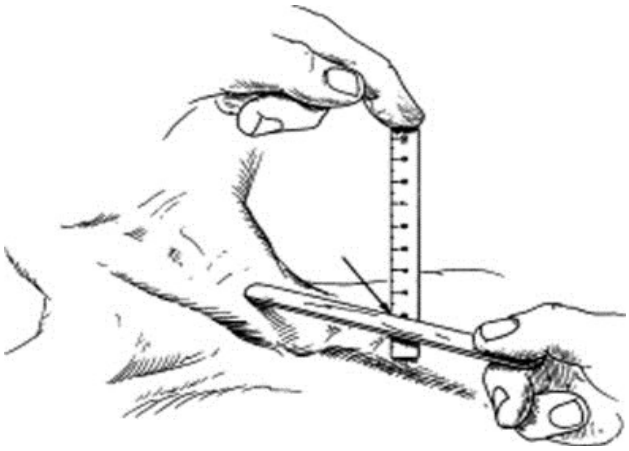

b

Figure 2.6. Estimating CVP using Louis' technique: (a) identifying the tip of pulsations, and (b) measuring the length of blood column in the IJV. Reproduced from (Applefield 1990 and Mangione 2008).

2.4.2.2. Disadvantages of the Louis method

The neck visualization method is still used by some clinicians as a fast way of estimating the CVP. Unlike the CVC approach, it can be performed easily by the bedside without the need of sophisticated equipment or the use of an apparatus. An amount of experience is however required to read off the neck pulsations, making it very difficult for some physicians to implement. The problem gets worse for patients with shorter necks and patients who are overweight, because it becomes difficult for the pulse to travel through the thicker skin to the surface. This approach is also regarded as subjective because of the manual visualization of the neck veins. In order to prevent wrong CVP estimation, there is also a caution to the examiner not to mistake the carotid pulse as the tip of venous pulses. Another drawback to this approach is its inability to continuously monitor the CVP over time because measurements can be taken one at a time in a discrete fashion.

One critical concern which has often been raised with this method is about the Louis angle being five centimeters from the midpoint of the right atrium. Ramana *et al* (2006) did a study to assess the degree of accuracy and consistency of the Louis angle used in the evaluation of CVP. They performed the study on patients with varying weight, body mass index and body surface area. Their analysis indicated a positive relationship between patients' weight and the distance between the Louis angle and the right anatomic landmarks. Hence they concluded that in using the traditional five centimeter "cardiologist's constant," a larger patient's body surface area would result in a greater underestimation of the right arterial pressure. Ratika *et al* (2002) similarly concluded an experiment and stated that the distance from the sternal angle to the level of the mid-right atrium varied considerably between individuals and with patient position. Hence, they advised physicians to consider specific patient factors and positions before calculating the CVP.

2.4.3. Estimating CVP using ultrasound

The use of ultrasound in measuring CVP, even though not widely recognized, is gradually becoming a subject of interest to most researchers and clinicians. This approach may have evolved from the use of ultrasound technology in helping examiners detect the tip of pulsations in the Louis method or from its use as a guide to help physicians carry out successful catheterization. Some researchers have estimated the CVP by observing ultrasound images of the blood dynamics and volume flow in the IJV during various activities. This parameter has been capitalized from the intrinsic mechanical property of veins known as compliance. This property lies in the non-constant relationship between

venous pressure and venous volume. In other words, venous compliance is high at low pressures and low at high pressures. This is characterized by a curvilinear shape (Figure 2.7) between venous pressure and venous volume, with an increase in volume at high pressures and vice versa (Simon *et al* 2010). Chung *et al* (2006) also carried out experiments relying on the theory of the relationship between venous volume and venous pressure. They reasoned that since the volume of venous blood flow represents the venous volume at a particular time in a normal person's IJV, a greater volume of blood flow measured at rest estimates a greater venous volume. This signifies a higher IJV pressure and an elevated CVP. This theory would also hold true in the opposite scenario. Thus, for a lower venous flow there is a lower IJV pressure and a lower CVP.

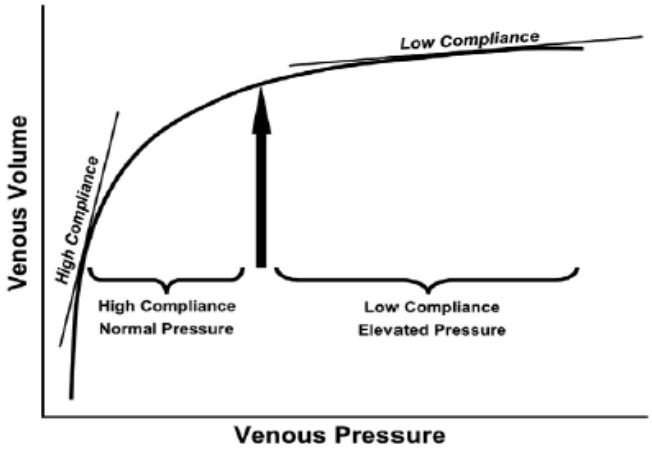

Figure 2.7. Compliance curve of a typical vein. On the steeper portion of the curve, venous compliance, which is equal to the slope of the curve, is large, reflecting low venous pressure. On the flatter portion of the curve, however, venous compliance is much reduced, reflecting elevated venous pressure. Reproduced from (Simon *et al* 2010).

Other researchers have adopted a technique of using the ultrasound to measure CVP by observing the changes in the diameter or cross sectional area of the IJV at different postures. Donahue *et al* (2009) sought to examine noninvasively whether real-

time ultrasonography measurements of the IJV correlated with a patient's known CVP. The experiment was based on a prediction where a positive correlation could be made between the CVP and IJV area or anteroposterior diameter. After the experiments they concluded with certainty that if the IJV's anteroposterior diameter (with the patient lying supine and at end expiration) is between 5.7 and 8.3 mm, then the CVP is less than 10 cmH_2O. If the measurement is between 11.2 and 13.8 mm, the CVP can be predicted with certainty to be greater than 10 cmH_2O (7.36mmHg). Siva *et al* (2012) equally demonstrated by using the cross section of the IJV to conclude that, ultrasonographic estimation of fluid volume status had high specificity and positive predictive values for detecting hypervolemic states.

2.4.3.1. Procedure for estimating CVP using ultrasound

Ultrasound is one of the technologies used predominantly in the field of medical imaging. It is deemed as one of the safest to implement, especially when compared with counterparts like CT (Computed Tomography) scans, MRI (Magnetic Resonance Imaging) and X-ray radiography. Ultrasound is less expensive, much portable, fast and easy to use. It operates on a very simple property of sound waves, such as reflection and diffraction. Its probe/sensor is designed to emit waves through a medium and receive reflected waves, from which images are reproduced.

In similar fashion to the Louis method, the patient is placed in the supine or trendelenburg position to open up the veins. A couplant is applied onto the IJV location of the patient’s neck. With the use of the ultrasound probe, the area is scanned to display images of the IJV. Placing the probe in a transverse plane to the neck gives cross

sectional images of the IJV, whiles a probe in a lateral direction to the neck gives longitudinal images of the IJV. Finally the diagnosis is inferred from the level of blood flow or the changes of the IJV cross sectional area and its diameter or the waveforms. A demonstration of this is shown in Figure 2.8 (Unluer and Kara 2013, and Yan and Seow 2009).

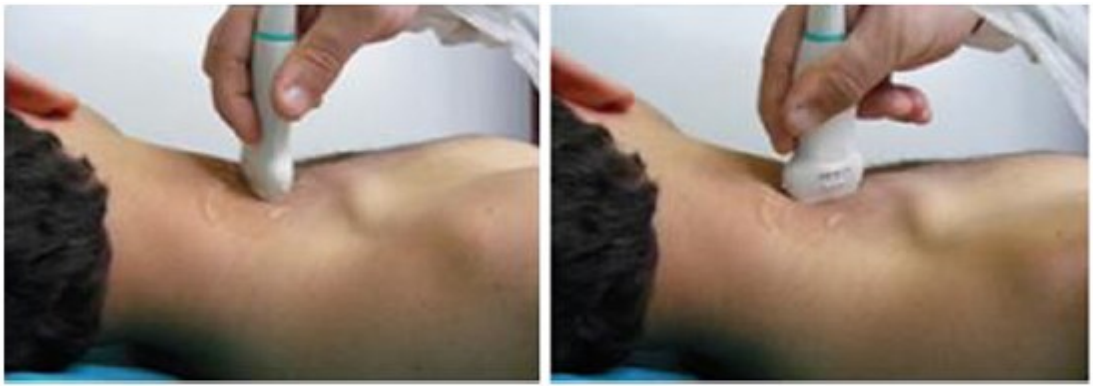

a **b**

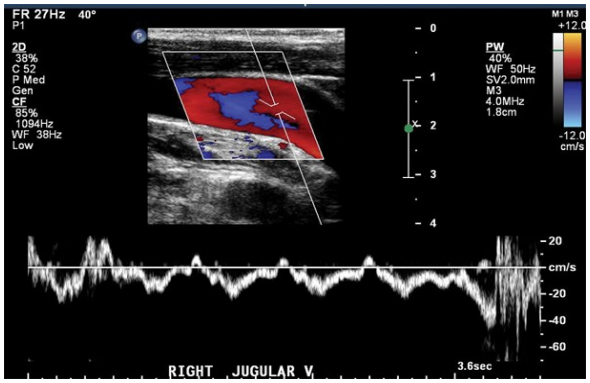

c

Figure 2.8. Detection of CVP using IJV ultrasound: (a) transverse scan, (b) lateral scan, (c) Normal phasic and normal directional venous flow in the right IJV. Reproduced from (Unluer and Kara 2013, and Yan and Seow 2009).

2.4.3.2. Limitations of estimating CVP by ultrasound

The ultrasound technique of estimating CVP has received some level of recommendation from several researchers. The method is lauded primarily because of its noninvasiveness and rapid response. It even gets better now with the development of

portable handheld ultrasound devices which can now be carried conveniently from place to place. As was shown earlier, experiments have shown a good correlation by comparing the ultrasound results with the results from the CVC method. However, it has failed to gain wide spread consideration in estimating CVP due to various discrepancies in its result. Raksamani *et al* (2014) made an assumption that, if the cross-sectional area of the IJV and CVP are gravity dependent, they expect a reproducible correlation of these variables, allowing cross-sectional area to predict CVP. Their results however showed a poor correlation between internal size of both jugular veins (left and right IJV) and CVP in all three positions. Likewise, Doel *et al* (2011) stated emphatically that ultrasound typically underestimated the CVP with discrepancies becoming quite larger, especially at high CVP. Researchers such as Donahue *et al* (2009) and Bellazzini *et al* (2009) after endorsing the ultrasound for CVP measurements still called for further tests to be done. This is because it lacked concrete evidence due to the small sample size during test experiments and the inability to compare the results with a gold standard like the CVC.

2.4.4. Miscellaneous methods of estimation CVP

Three prominent ways of CVP measurements have just been outlined in the previous sections. Apart from these methods, some uncommon techniques have been utilized by other researchers to evaluate the CVP. Some methods drew inspiration from the three major methods, whiles others proposed an entirely new design. A brief account is presented on two of these methods. This are, Impedance based technique for CVP measurement and CVP estimation by neck inductive plethysmography.

2.4.4.1. Impedance-based technique of measuring CVP

Ward *et al* (2010) used a noninvasive method of CVP measurement based on the rate of volume change in the upper extremity in response to low pressure cuff inflation and deflation. The method and principle is similar to the approach used by Davis *et al* (2004) in measuring systemic pressures and volumes. A cuff is applied onto the arm, inflated to a pressure value higher than the CVP but lower than the diastolic arterial pressure (40 mmHg), and kept at that pressure for 45-60 seconds. At this pressure, arterial blood continues to flow into the arm but venous return is interrupted. Because blood is a good conductor of electricity, the displacement in blood volume from under the cuff due to cuff inflation increases impedance which generally approaches a plateau before cuff deflation. During this period, the patient's upper arm underneath the blood pressure cuff is monitored for volume changes via the electrodes. At the end of the inflation hold period, the cuff pressure valve is opened to atmosphere to allow rapid self-deflation. This is shown in Figure 2.9 (Ward *et al* 2010). According to the examiners, the results were promising enough to provide clinically accepted values for CVP estimations. However, limitations like the need for a larger sample size and the need for extended length of patient monitoring was revealed. More studies were therefore advocated to properly ascertain the worthiness of the method.

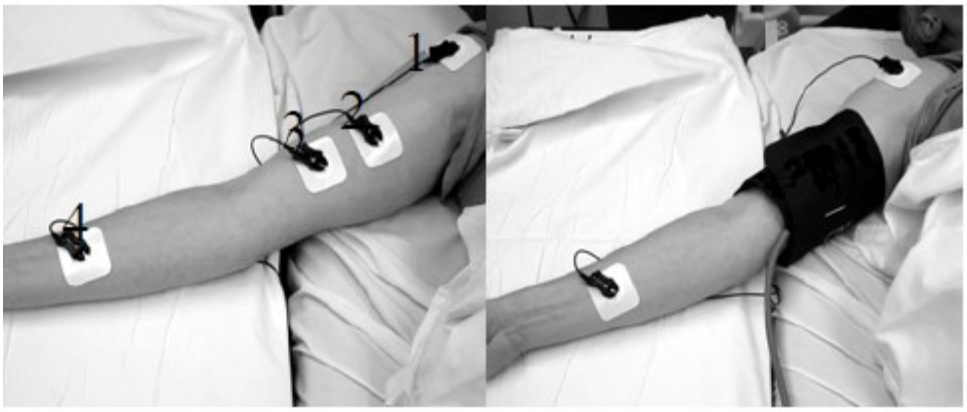

a **b**

Figure 2.9. Impedance based technique in measuring CVP: (a) orientation of electrodes used for impedance plethysmography, and (b) application of inflation cuff. One pair of electrodes injects current towards the other pair allowing for detection of volume changes in the segment of tissue underlying the blood pressure cuff. Reproduced from (Ward *et al* 2010).

2.4.4.2. CVP estimation by neck inductive plethysmography

Bloch *et al* (1991) developed a noninvasive method for estimating CVP. The method was in line with the Louis method but had an aim of abrogating the manual identification of the right IJV. A neck inductive plethysmography transducer was used, which would measure changes in the cross sectional area of the neck and provide analog waveforms of the vascular pulsations. As shown in Figure 2.10 (Bloch *et al* 1991), the idea of the investigation was to use the inductive transducer to pick up the pulsations after the patient had been laid adequately in the supine position. The pressure transducer was referenced to the phlebostatic axis and its accuracy was tested with a water manometer. The results from the inductive transducer were compared to the measurement from a conventional catheter system performed on the patient at the same posture. The results indicated the neck inductive plethysmography provided a recording of the jugular venous waveform even in those with massive obesity. It was therefore concluded that this

noninvasive approach was clinically practical. However, it was admitted that the method was owing to several factors. Including transducer sensitivity, patient transducer interface and the ability to learn and recognize patterns of venous and arterial waveforms.

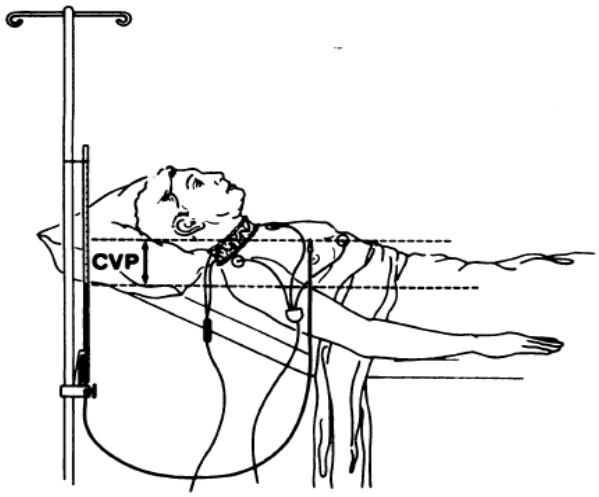

Figure 2.10. Detecting the CVP by neck inductive plethysmography. Reproduced from (Bloch *et al* 1991).

2.5. The central venous pulse/waveform

Having cognizance of the Louis method, it must be noted that the challenge for neck visualization is not only to determine the tip of pulsations. It is also to skillfully identify 'which pulse' emanates from the skin surface. 'Which pulse' in the sense that, at the neck two different pulses are given off simultaneously. There is one from the carotid artery and another from the jugular vein. The onus therefore lies with the physician to clarify and select the JVP from the two pulses. However, clinicians can take respite from the fact that both pulses have separate characteristics which makes them differentiable. Also, the standard CVP pulse or waveform of a normal patient follows a particular pattern or rhythm. This makes it possible for physicians to diagnose health conditions by

observing an abnormal venous waveform. It is therefore very important for scientists and clinicians in this field to familiarize themselves with the central venous pulse.

The blood flowing back to the heart through the jugular veins do not actually have a pulse. As described by Naveen and Nitish (2000), it is the changes in flow and pressure caused by right atrial and ventricular filling which produces the pulsations in the central veins. These pulsations are then transmitted towards the peripheral veins, opposite to their direction of blood flow. In other words, the outline of the venous waveform is just interpretations of the activities going on within the chambers of the heart. To this effect, CVP can interchangeably be referred as the JVP. This owes to the fact that pressure in the venous compartment is transferred to the peripheral vessels including the jugular veins.

A typical normal venous waveform comprises of three positive peaks and two negative troughs. Figure 2.11 (Ronan 2002) shows how a normal CVP waveform corresponds with normal cardiac activities by comparing its outline to the electrocardiogram (ECG). According to Short (1957), Naveen and Nitish (2000), Pittman *et al* (2004), Easby and Dalrymple (2008), and Reems and Aumann (2012), the central venous waveform is described as follows. The *a* wave comes about as a result of the contraction of the right atrium to fill up the right ventricle. The *c* wave, often just a notch on the descending portion of the *a* wave, is caused by the bulging of the closed tricuspid valve during the contraction of the right ventricle. It is often not shown due to its inconsistency but occurs simultaneously with the carotid arterial pulse. The *x* descent is due to the relaxation of the right atrium during ventricular ejection. The *v* wave, which appears towards the end of a systole, represents an increase in the pressure of the right atrium due to the rapid filling of the chamber with a closed tricuspid valve. The *y* descent

is also caused by the reduction in pressure of the right atrium after the tricuspid valve opens for blood to fill the ventricles.

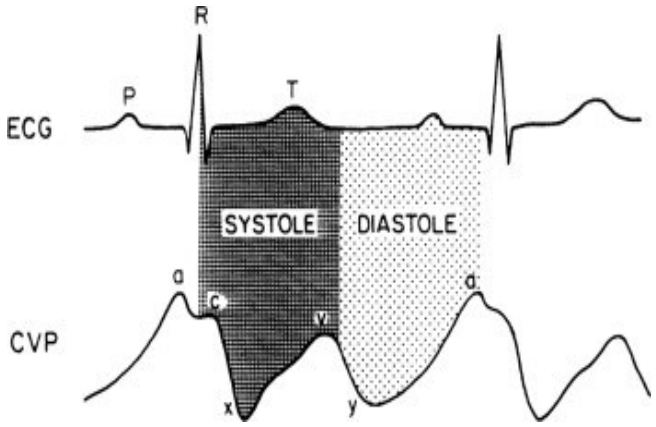

Figure 2.11. Normal CVP waveform with normal electrocardiography tracing. CVP tracings show three positive waves (*a*, *c*, and *v*) and two descents (*x* and *y*). Reproduced from (Ronan 2002).

2.5.1. Diagnosis from abnormal CVP waveforms

Analysis of the central venous waveform tracing can provide additional information about the cardiovascular status of a patient (Watson and Wilkinson 2011). This implies anytime there is an abnormality in the jugular venous waveform, it is often a manifestation of a disease state in the dynamics of the right heart. Some health conditions could be exhibited in an abnormal waveform as tall (canon) peaks, absent waves, or enlarged waves. Easby and Dalrymple (2008) indicated tricuspid regurgitation shows prominent *v* waves, with loss of the *c* waves and *x* descent. On the other hand, tachycardia often causes a fusion of the *a* and *c* waves. Short (1957) also believes the commonest and most important abnormality in the venous pulse is an exaggeration of the normal *a* wave and relates it to pulmonary hypertension and tricuspid stenosis. There are other several medical conditions which can be deduced from an abnormal central venous

waveform. Table 2.6 summarizes the description of some abnormal waveforms and Figure 2.12 illustrates a few of the abnormal waveforms (Shroeder 2010).

Table 2.6. CVP waveform abnormalities (Shroeder 2010).

Condition	Characteristics
Atrial fibrillation	• Loss of *a* wave • Prominent *c* wave
Atrioventricular dissociation	• Cannon *a* wave
Tricuspid regurgitation	• Tall systolic *c*-*v* wave • Loss of *x* descent
Tricuspid stenosis	• Tall *a* wave • Attenuation of *y* descent
Right ventricular ischemia	• Tall *a* and *v* waves • Steep *x* and *y* descents • M or W configuration
Pericardial constriction	• Tall *a* and *v* waves • Steep *x* and *y* descents • M or W configuration
Cardiac tamponade	• Dominant *x* descent • Attenuated *y* descent
Respiratory variation during spontaneous or positive pressure ventilation	• Measure pressures at end of expiration

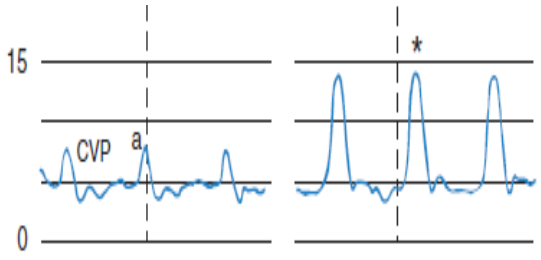

a

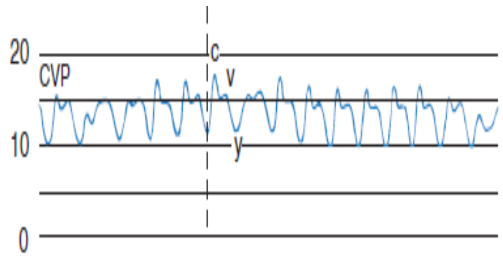

b

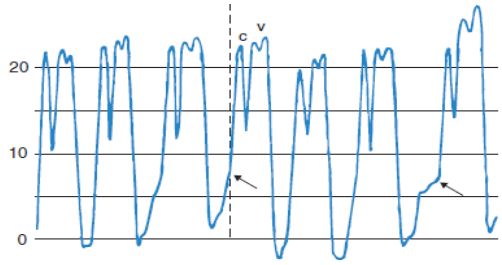

c

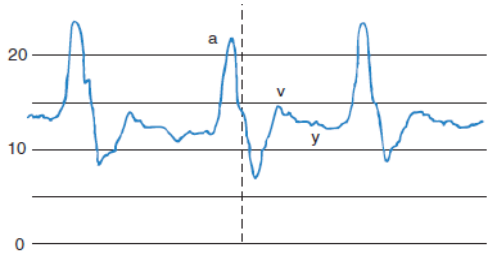

d

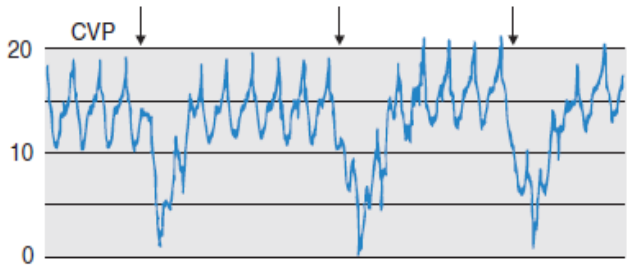

e

Figure 2.12. Waveforms of abnormal CVP: (a)Comparing a normal CVP (left panel) to atrioventricular dissociation (right panel), (b)Atrial fibrillation, (c)Tricuspid regurgitation, (d)Tricuspid stenosis, and (e)Spontaneous breathing during spontaneous ventilation, the onset of inspiration (arrows) causes a reduction in intrathoracic pressure. Reproduced from (Shroeder 2010).

2.5.2. Differences in arterial and venous pulse

During a procedure like the neck visualization, it is very important to observe venous pulsation and not the arterial pulse. The task becomes simple if the patient has visible jugular veins which can easily be examined at different positions. However, this is not always the case and sometimes leads to the carotid pulse been mistaken for the venous pulse. Differentiating the two pulses at the neck region can be done in several ways. It may be done by physically palpating the vessel or by observing the waveforms produced by the vessel. Unlike the central venous waveform, the arterial pressure waveform has two peaks which are in sync with the systolic and diastolic phase of the heart cycle (Watson and Wilkinson 2011). The higher peak emanates from the strong systolic contraction whiles the lower peak is in response to diastole. The arterial pulse is illustrated in Figure 2.13.

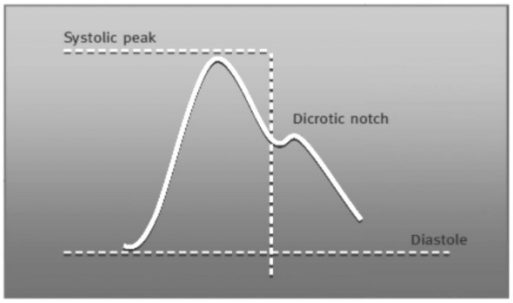

Figure 2.13. The arterial pressure waveform. Reproduced from (Watson and Wilkinson 2011).

Based on the standard outline for both arterial and venous waveforms, one can easily differentiate between the carotid artery pulse and a jugular venous pulse. The hint given by some clinicians to identify venous pulse is to look out for major descents in the wave pattern. Additionally, palpating the base of the neck can also give a clue to the pulse being felt. Arterial pulses are much stronger and are easily palpable with a finger. On the other hand, venous pulses are rarely felt because of the soft and weak pulse. Chua Chiaco *et al* (2013) added to the above differences by pointing out, a venous pulse will easily be obliterated if a light pressure is applied to the vessel. Inversely, the carotid artery will continue to pulsate even if pressure is applied to block the vessel. Also, the waveform is probably a venous type if its peak increases or decreases considerably with abdominal pressure and inspiration. This comes about due to the increased filling of the right sided chamber associated with the decline in intrathoracic pressure (Naveen and Nitish 2000).

2.6. Basics of the research approach

The first part of this chapter was structured to identify the research problem (estimating the CVP/JVP). It covered the existing methods being used to address the

problem currently, the drawbacks of these methods and other pertinent issues required to fully grasp the concept of the research. As indicated earlier, a sensor was designed based on the theory of photoplethysmography to estimate the CVP. The next sections of this chapter focuses on the fundamentals with which the research utilizes to solve the problem. It explains the principles behind the method and considers various aspects useful for the development of the sensor.

2.7. Photoplethysmography

Photoplethysmography (PPG) is a renowned technique implemented by using the properties of light to translate changes within a particular medium into useful information. It is usually an assembly of two basic electronic components which is, a light source and a photo detector. The basis of PPG is to direct light rays through a medium at one point and detect the light intensity emitted out of the medium at another point. The light rays could be reflected, scattered or absorbed depending on the medium. Therefore if any changes occur within the medium, the light intensity reaching the photo detector will also undergo fluctuations. For this reason, the changes in the intensity of light reaching the photo detector will indirectly represent the changes occurring in the medium.

Fluctuations in intensity during the passage of light through a medium could be attributed to the path length of light, the absorbance of material or the level of concentration within the medium. According to Shamir *et al* (2012), the Lambert-Beer law states that when monochromatic light passes through any substance, some of the light is absorbed, thus reducing the intensity of the light. The amount of light intensity

absorbed by the substance is called “absorbance” and is directly proportional to (a) the molar absorption coefficient, which is a unique physical property of the substance for a specific wavelength, (b) the optical path length, which is the distance the light must travel through the substance, and (c) the molar concentration, which is the concentration of the absorbing material in the substance. When the path length of an incident light is increased, the intensity drops and vice versa. Similarly, light intensity will decrease upon an increase in the concentration of the medium and the reverse is also true. Additionally, intensity arriving at a photo detector will largely be dependent on the medium’s absorption coefficient of light. The latter occurs due to the fact that every material has a unique wavelength at which it absorbs light.

In PPG, the information acquired from the photo detectors are usually displayed as a series of sinusoidal waves comprising of parts from an AC (alternating current) and DC (direct current). Allen (2007) points out; the pulsatile AC physiological waveform is attributed to cardiac synchronous changes in the blood volume with each heartbeat. This is usually superimposed on a slowly varying DC baseline with various lower frequency components attributed to respiration, sympathetic nervous system activity and thermoregulation. Sahni (2012) contributed to this and further described the nonpulsatile DC component as a constant voltage offset whose magnitude was determined by the nature of the material through which the light travelled (skin, subcutaneous fat, muscles, cartilage, bones, and venous blood). Shown in Figure 2.14 is a typical PPG waveform describing the various components (Haahr 2006).

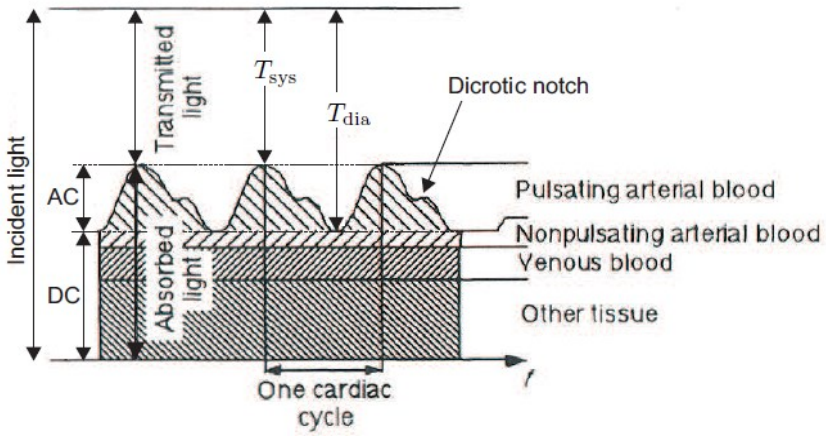

Figure 2.14. Schematic illustration of a PPG i.e. optical measurement of variation in volume of a part of the body (here arterial vessels) due to the cardiac cycle. Reproduced from (Haahr 2006).

The medical field has immensely benefitted from the PPG technology. The technology has been employed in a variety of clinical devices, especially for the noninvasive study and monitoring of patients. Additionally, the components used for the PPG applications are fairly cheap and easy to implement. One typical and mostly used PPG based device is the pulse oximeter.

2.8. Pulse oximetry – how it works

The pulse oximeter is used mainly for the detection of oxygen concentration and arterial pulse within the body. Accordingly, the percent oxygen saturation (SpO_2) in arterial blood measured by a pulse oximeter is used to assess how well oxygen is delivered in the body (Traviglia and Mendelson 2004). The pulse also gives the rate of cardiac systolic and diastolic events. The device has light emitting diodes (LED) which emits light of specific wavelengths and a photodiode (photo detector) which senses the intensity. In the most common setup, the measurement is achieved by shining light from LEDs with two different wavelengths onto a highly perfused tissue, typically on a finger,

toe or earlobe, and detecting the transmitted or backscattered light by means of the photodiode (Glaros and Drakakis 2013).

The pulse oximeter measurements for oxygen concentration are primarily based on spectrophotometry. This means, measuring the absorption coefficients of a medium at specific wavelengths of light. As explained by Reichelt *et al* (2008), standard pulse oximeters estimate partial arterial oxygen saturation by measuring the time-variable, wavelength-dependent transmittance of arterial blood, typically by the use of red (660nm) and infrared (940nm) LEDs. By rapidly blinking (at a frequency much higher than the heart beat rate) the red and infrared (IR) light sources, two photoplethysmograms are recorded from the body with one for each wavelength (Haahr *et al* 2007). It is further revealed that the SpO_2 is a function of the measured magnitude at the systolic and diastolic states of the two photoplethysmograms. Thus,

$$SpO_2 \sim \ln\left(\frac{\mathrm{Red}_{systole}}{\mathrm{Red}_{diastole}}\right) \Big/ \ln\left(\frac{\mathrm{IR}_{systole}}{\mathrm{IR}_{diastole}}\right) \tag{2.1}$$

where $\mathrm{Red}_{systole}$ and $\mathrm{Red}_{diastole}$ are the magnitudes of the red light measured at the systolic state and diastolic state respectively, and $\mathrm{IR}_{systole}$ and $\mathrm{IR}_{diastole}$ are the magnitudes of the infrared light measured at the systolic state and diastolic state respectively (Haahr *et al* 2007). The scope for the research does not involve the estimation of oxygen saturation. For that matter, the basis for its computation will not be discussed any further beyond this point.

Besides the use of absorption coefficients, the pulse oximeter measures the pulse of the body by relying on the fluctuating intensity of the light due to path length and

concentration of the medium. Upon one heartbeat, blood is pumped out from the heart into the peripheral vessels such as the arteries. This increases the pressure in the artery and causes them to widen in order to accommodate more blood. As postulated by the Lambert's law, the absorption of light travelling through the artery will change as the path length (artery diameter) and blood concentration is increased. This will in effect alter the light intensity reaching the photodiode to produce the PPG waveform.

2.8.1. Wavelengths for pulse oximeters

As indicated earlier, the wavelengths used in classical pulse oximeters are 660nm found in the red range and 940nm found in the IR range. These wavelengths are chosen based on the considerations of the absorption spectrum of oxygenated (HbO_2) and deoxygenated (Hb) blood. The mode of operation of the pulse oximeter largely depends on the difference in absorption spectra of these two states of blood present in the body. Numerous experiments has shown HbO_2 blood is found to have a high absorption coefficient at a wavelength in the IR range whiles Hb blood has a high absorption coefficient in the red range. With reference to Figure 2.15, Nitzan and Taitelbaum (2008) showed the different wavelength of absorption for both HbO_2 and Hb blood. From the figure, it can be noticed that wavelengths under 600nm do not clearly distinguish the absorptions coefficient between the two states of blood. However, distinction becomes clearer beyond the 600nm mark with Hb blood having a higher coefficient than HbO_2. This property prevails until 800nm where both blood types are isosbestic (having the same absorbance coefficient). From 800nm upwards, the trend changes with HbO_2 blood having a higher coefficient than Hb blood.

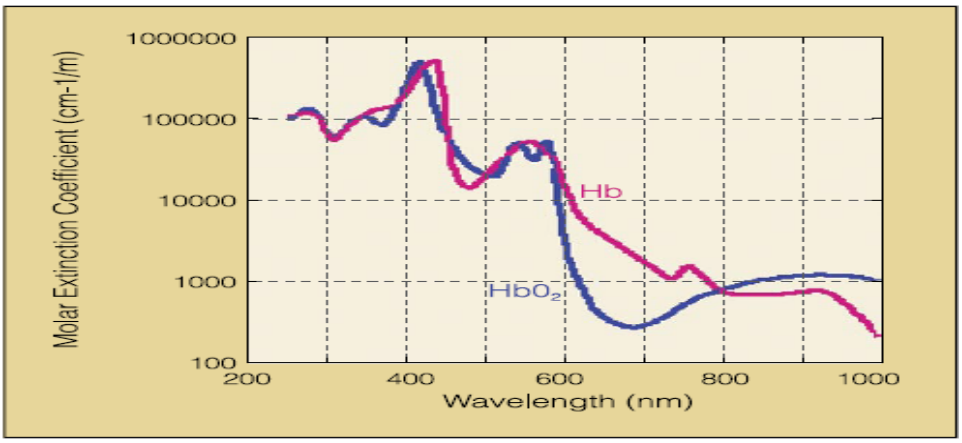

Figure 2.15. The absorption spectra of the oxygenated and deoxygenated hemoglobin molecules. Reproduced from (Nitzan and Taitelbaum 2008). © [2008] IEEE.

This property of absorption differences in the blood states has given other researchers the opportunity to experiment on other wavelengths in the red and IR range. As Mannheimer *et al* (1991) pointed out, the selection of wavelengths should traditionally emphasize on sensitivity to changes in arterial oxygen saturation, with at least one of the wavelengths chosen from a spectral region where the absorption coefficient of oxygenated blood is markedly different from deoxygenated blood. In other words, 660 nm (red) and 940 nm (IR) is mostly used since the absorption ratio between the blood types is large and small at those wavelengths respectively, minimizing the uncertainty of the SpO_2 measurement (Haahr *et al* 2007).

Furthermore, the wavelengths are chosen with respect to how light interact with the skin tissue. The inhomogeneous nature of the skin makes it a medium composing of both light absorbers and scatters. Obviously, the need to get enough light into the body demands going past the skin without losing much light to the absorption and scattering by the skin. Arridge *et al* (1992) bolstered an existing theory stating that, near-infrared (NIR) light in the wavelength range 650nm to 1200nm can penetrate tissues to

considerable depths, making it possible to measure the optical absorption properties of intact organs. Others refer to this range (650-1200nm) as the tissue window because wavelengths falling within the range can permeate skin tissue without being severely attenuated.

2.8.2. Configuration of pulse oximeters

Modelling a pulse oximeter sensor primarily depends on the site of the body where it is to be applied and the responsiveness towards the layout of the sensor. In effect, the mode of the pulse oximeter is classified based on the relative positions of the LEDs and photodiode. The two main configurations used in pulse oximetry probes is the transmittance and reflectance mode. According to Mannheimer (2007), reflectance and transmittance are best thought of as convenient manufacturing terms for sensors which have emitters and detectors located on either adjacent or opposite sides of a tissue bed. These configurations are demonstrated in Figure 2.16 (Kugelman *et al* 2004). The transmittance configuration was the first model to be used in pulse oximeters. With transmittance having LEDs and photodiodes on opposite sides, the configuration makes body attachment very easy. They are usually designed in a form of a peg which makes it very possible to clip body parts like the finger, toe or ear lobe. However there was a need to investigate SpO_2 on other parts of the body, such as the forehead or abdomen, where clipping could not be done. This led to the design of the reflectance configuration where both LED and photodiode are placed beside each other, making it possible for attachment to other body parts. This is illustrated in Figure 2.17.

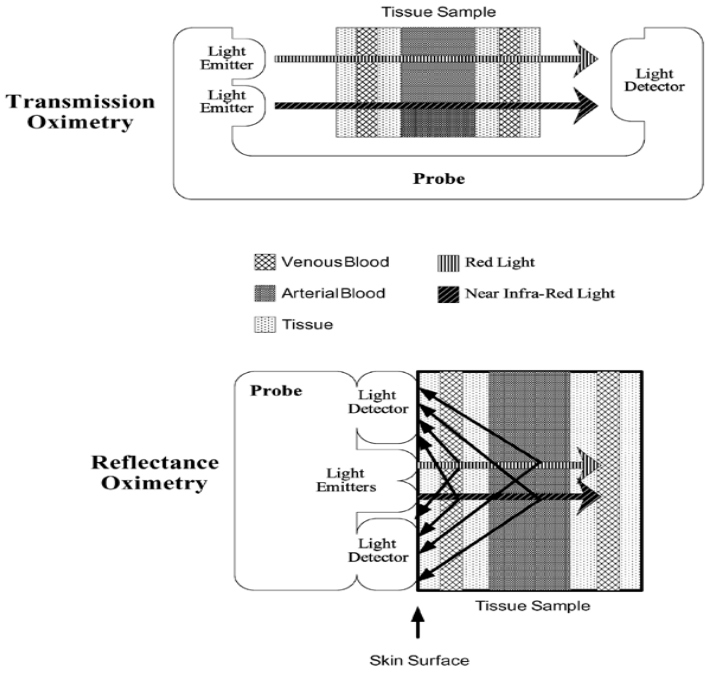

Figure 2.16. The difference between transmission and reflectance pulse oximetry. Reproduced from (Kugelman *et al* 2004).

a **b**

Figure 2.17. The types of oximeter sensors: (a) transmittance configured in a peg model to clip finger. Reproduced from (Wikipedia® 2013), and (b) reflectance configured oximeter attached to the forehead. Reproduced from (ALLMED®.Net 2009).

2.8.2.1. Transmittance versus reflectance configuration

Despite the fact that both configurations give a reliable estimation of SpO_2, the transmittance types are mostly used commercially due to its high signal response and accuracy. Schmitt *et al* (1990) made a very useful remark about the importance of the

sensor geometry or configuration in designing instruments. From results based on simulated measurements of light scattered and absorbed by the skin, it was found that placement of the detector(s) relative to the source affects the average path length and sampling depth of photons and, therefore, influences sensitivity to absorption in the different skin layers. Also, research has shown that signal output from the transmittance sensor is of good quality than the reflectance sensor. Accuracy as well as difficulties in absolute calibration is a major problem with reflectance oximeters (Mendelson and Ochs 1988). By nature, light propagation and scattering is directed forwards and the transmittance configured probe places the LED and photodiode in positions which promotes this property of light. On the contrary, reflectance configured sensors have the photodiodes adjacent to the light source and have to rely on the intensity of backscattered light which are usually not strong enough to enhance PPG signal quality (Shimada *et al* 1991 and Santha *et al* 2006). Furthermore, reflectance configured probes are deemed to produce noisy PPG signals due to motion artifacts. This is influenced by how firmly contact is made between the sensor and the underlying tissue. Unlike transmittance sensors which are firmly clipped, reflectance probes have to be attached to the body with the help of adhesives or bands in order to secure a firm tissue contact. This is not always achieved properly and leads to sensor movements causing motion artifacts. Reflectance probes are also highly affected by interference from ambient light sources, especially if the area of attachment is not secure enough to eliminate unwanted light.

The use of transmittance oximeters provides better PPG results but has limitations with respect to where it can be applied on the human body. On the other hand, reflectance oximeters can virtually be tested on every part of the body provided the place of

attachment is adequately perfused with blood. Its versatility has therefore motivated most researchers to find better ways of improving its PPG signals to make it comparatively better.

2.8.2.2. Signal improvement for reflectance configured sensors

Shimada *et al* (1991) agreed that the reflectance pulse oximeters works with a weaker pulse signal. However, they advocated that the selection of light wavelengths, light intensity, sensor configuration and signal processing were important for the accurate measurement of arterial oxygen saturation. Reuss and Siker (2004) and Huang *et al* (2011) also reiterated that the design of sensors for reflectance pulse oximetry involved making choices of wavelengths, emitter–detector spacing, optical properties of tissue and addition of multiple emitters and detectors.

In view to this, some attention is allocated to the distance between the emitter and detector during the design of a reflectance configured sensor. In an experiment geared towards the improvement of reflectance sensitivity, Liu *et al* (2002) concluded that the optimal source-detector space for red and IR was 2.8mm and 5mm respectively. Hickey and Kyriacou (2007) also contributed to this research by showing how quality PPG signals with large amplitudes and high signal-to-noise ratio were detectable in a separation range of 3mm to 6mm. It was proved that separation distances between 1mm and 2mm produced PPG signals which were erratic with no resemblance to a conventional PPG signal. Also, separation distances greater than 6mm resulted in very small PPG amplitude signal which were not appropriate for processing.

The choice of wavelength is also a contributor which affects the sensitivity and signal quality of the reflectance configured sensor. Wavelengths in the red and near-infrared are particularly useful due to their ability to penetrate tissue based on their strong differential absorbance (Reus and Siker 2004). Huang *et al* (2011) erased some doubts when they reemphasized by claiming red light travels a longer distance in tissue than other wavelengths. This is due to the fact that red light has much smaller absorption and scattering properties than other wavelengths.

Improving signal strength in the reflectance mode has also been linked to the light intensity reaching the photo detectors. Assuredly, an increase in light intensity will improve signal strength. Many researchers have approached this technique in several ways. As hinted by Thomson *et al* (2006), previous sensors used a single photodiode to acquire the reflectance signals from individual red and infrared LED's. More functional designs can utilize an array of photodiodes wired in parallel to encircle the LED. In an effort to increase the intensity of light, Shimada *et al* (1991) also placed an array of LEDs in a circle with a single photodiode in the middle. To alternatively obtain a good signal at minimal light intensity, the surface area of the photodiodes has to be large enough to receive maximum light (König *et al* 1998). Nevertheless, it is alerted that the design has to eliminate "direct light," i.e. light passing directly from the LEDs to the photodiodes without going through the tissue or medium. To this effect, most designers place a non-reflective optical shield as a barrier between the LEDs and the photodiodes to avoid such a phenomenon. Figure 2.18 gives a schematic diagram of designs used to improve light intensity in reflectance configured sensors (Haahr 2006 and Shimada *et al* 1991).

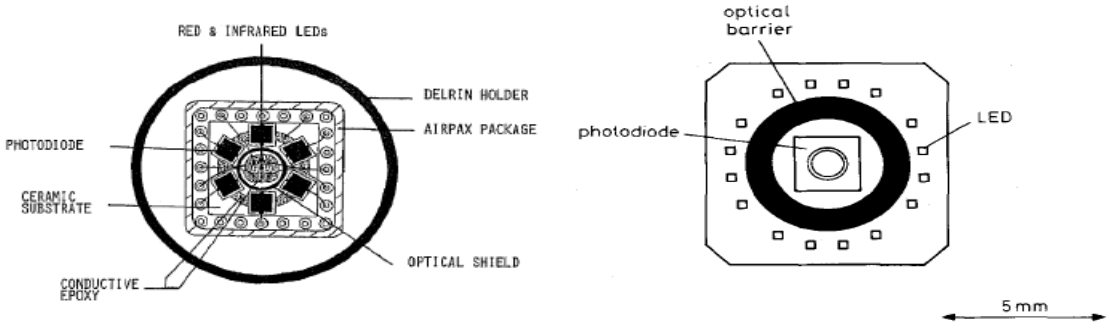

a **b**

Figure 2.18. Top view of different designs in reflectance oximeters: (a) an array of photodiodes encircling one LED, and (b) an array of LEDs encircling one photodiode. Reproduced from (Haahr 2006 and Shimada *et al* 1991).

2.9. Motivation towards the research approach

The task was to conveniently measure the pressure or waveform within the jugular veins in order to estimate the CVP. Prior to the selection of the PPG technique, the dynamics of the veins and the principle behind PPG were considered. The choice to use this strategy was based on one initial premise. Thus, the continuous inflow and outflow of blood in the jugular veins will effectively vary the diameter or shape of the veins resulting to fluctuations of the light intensity propagated through it. Even though the premise sounded plausible, there were still doubts in terms of the sensor's ability to capture volume changes emanating from veins which has very low pressure.

As shown from literature, arterial perfusion is a contributor to signal generation of the pulse oximeter. Thus, its involvement makes it possible for the separation of the AC and DC components of the PPG waveform. Moreover, Walton *et al* (2010) indicated the movement of venous blood could be detected using the PPG because the venous signals had been seen as a source of artifact which interfered with the calculation of arterial

saturation. From the results described in their work, they suggested the possibility to harness physiologic sources of periodic volume changes in the venous compartment.

Thiele *et al* (2011) and Colquhoun *et al* (2012) did an experiment to find the venous oxygen concentration by placing reflectance oximeters on the jugular veins. The former decomposed the acquired signals into individual frequency components and postulated that, oscillations of venous blood at the heart rate may be attributable to either subtle changes in venous pressure transmitted from the right heart. The latter also said near IR spectroscopy devices placed directly over the IJV were most likely to reflect global changes in cerebral oxygen supply. From these observations and remarks, there was an indication of a probability of capturing changes within the jugular veins irrespective of its low blood pressure.

Chapter 3

3.0. Materials and methodology

The objective of the research was to develop a new approach of measuring the JVP or waveform. Bearing in mind the problems and complications posed by the existing methods, an assignment was presented to develop an approach which is noninvasive, fast, less expensive, simple to use, accurate and reproducible. Using the PPG based technique with emphasis on the reflectance pulse oximeter, a sensor was modelled to tackle the problem. The sensor was then tested in vitro using a mock circulatory loop and was further tested on a single subject (author). Presented in this chapter, is the procedure for designing the sensor as well as the development of the in vitro setup.

3.1. Sensor design

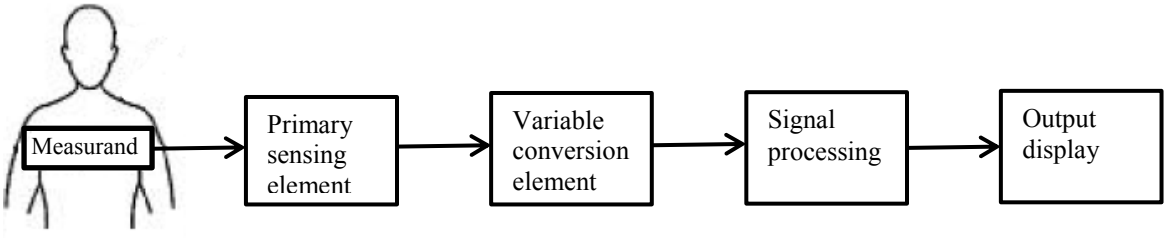

Figure 3.1. Block diagram of a generalized instrumentation system.

According to Olson (2010), any generalized medical instrumentation device has the functional components shown in Figure 3.1. It starts with the measurand, which is the physical quantity or control to be measured and serves as the signal source. The primary sensing element is the part which interfaces with the environment to capture the physical measurand. The mechanism through which the measurand is converted into electrical

information is the variable conversion element. They are often referred as transducers. A typical example is a photodiode converting incident light into an electrical signal. The signal processing block is where the signal is enhanced to make it viewable on an output display. Here, the signal could be amplified, filtered or converted into another convenient form in order to make it perceivable by the observer. Therefore to achieve a good and standard instrumentation device, it was necessary to factor all the following functional blocks into the sensor design process.

3.1.1. Primary sensing elements

The sensing elements were designed and configured with similar properties to the reflectance pulse oximeter. However, it was modified in several ways to suite the research objective. In particular, only one wavelength of light source was used instead of the traditional two wavelengths used in pulse oximeters. It was not convenient or feasible to use two wavelengths since the research was not estimating oxygen saturation. Additionally, the research was interested in the pulses emanating from deoxygenated blood carrying vessels such as the jugular veins. Hence eliminating the 940nm for oxygenated blood also simplified the design and application. The wavelength used for the sensor was therefore 660nm. This wavelength was used in reverence to the high absorption coefficient of deoxygenated blood which is primarily transported in the jugular veins. In order to also enhance the light intensity reaching the photodiodes, a 5mW laser was substituted for the conventionally used light emitting diodes LEDs.

The photodiodes used for the research were selected based on some directives from Schowalter (1997). Some considerations for selecting the appropriate photodiode

included a larger surface area, a high spectral response at the 660nm wavelength, a very low level of dark current and a diode packaging that would enhance the sensor design. Two Everlight® PD438C/S46 photodiodes were used. A copy of its data sheet can be found in Appendix C of this thesis. The two photodiodes were connected in parallel by soldering and were placed on each side of the laser. The laser diode was covered by a miniature lens to focus the light intensity and was optically shielded from the photodiodes with a black ring. The distance of separation between the laser source and a photodiode (measured from their centers) was seven millimeters. The three components (laser and two photodiodes) were mounted in a reflectance mode and housed into a flat cardboard as shown in Figure 3.2.

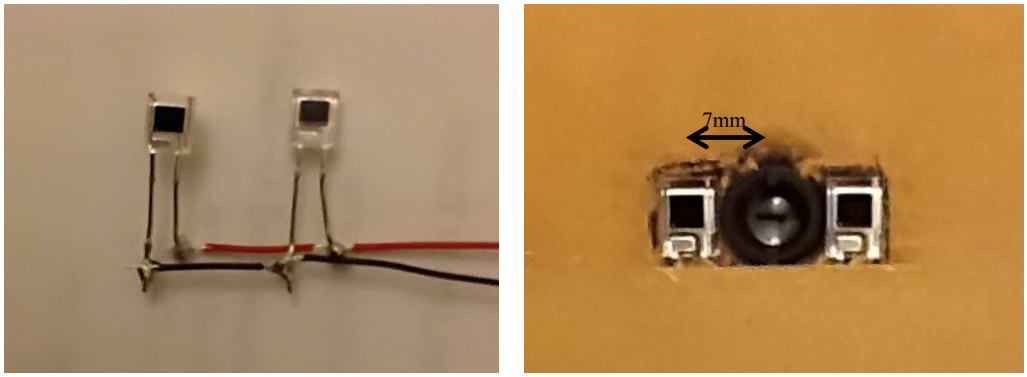

a **b**

Figure 3.2. Developed reflectance configured sensor: (a) photodiodes connected in parallel, and (b) laser and photodiodes mounted together in a reflectance mode and housed in a cardboard.

3.1.2. Signal processing

A signal processing circuit was also designed to process the information from the photodiodes. The design of the circuit was adopted from a circuit of a heartbeat monitor built by Darrah (2013). However, certain components of the circuit had to be altered to suite the desired response of the photodiodes. The components for the circuit were

assembled on a solder-less breadboard according to the circuit diagram shown in Figure 3.3. For the sake of simplicity, the circuit diagram displays only one photodiode instead of two. It should also be noted that the diagram does not include the driver circuit for the laser diode. Upon the purchase of the laser module, the driver circuit was incorporated into its design. The driver circuit ensures a stable current is delivered to the laser diode to prevent unnecessary fluctuations of the light intensity.

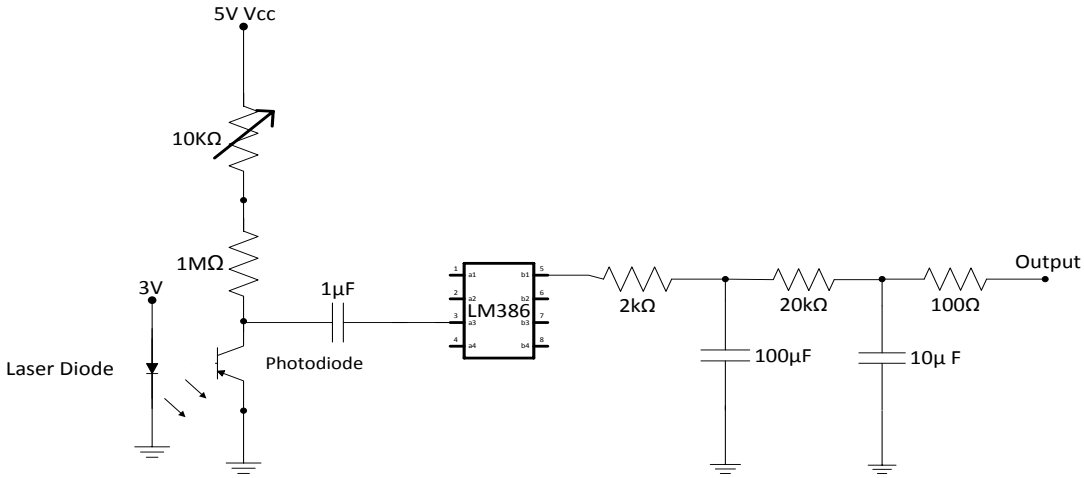

Figure 3.3. Signal processing circuit diagram.

From the circuit diagram, the laser and photodiodes have a voltage supply of three and five volts respectively. These voltages were supplied using an Arduino Uno® board. The photodiodes was powered through a 10kΩ potentiometer which was used to set the drive current to regulate the sensitivity of the photodiodes. The photodiodes are PIN silicon diodes which supports a connection in a reverse bias mode. Thus, the positive terminals of the photodiodes were connected to the negative terminal of the voltage source and vice versa. In such a mode, no current runs through the circuit until the surface of the photodiode is illuminated by light, inferring the level of current in the circuit is proportional to the intensity of light. The current was then channeled to a

capacitor to smooth out any alternating current before entering the amplifier (LM386). The detailed pin connections of the LM386 amplifier is also not shown in the circuit diagram. However, the connection of the pins was done according to the datasheet presented in Appendix C.

The amplified voltage signal was then fed through a second order low pass filter to remove noise and high frequency components. The high frequency referred here is related to pulses from cardiac or arterial activity. Since the venous pulses are characterized by lower frequencies, the filter was designed to pass low frequency components and reject high frequency components. Walton *et al* (2010) in an effort to find oxygen saturation at the cardiac frequency, split the PPG signal according to a cardiac algorithm which found frequency in the range of 0.75 – 2 Hertz (Hz). Similarly, Colquhoun *et al* (2012) did a fast Fourier transform (FFT) on the absorbance waveform of the red and IR wavelengths of a pulse oximeter and identified the cardiac frequency at 1Hz. Based on these references, the design of the circuit worked towards achieving a low pass filter with a threshold of 0.75Hz. From theory, the cut off frequency of a low pass filter is given as;

$$f_c = \frac{1}{2\pi RC} \tag{3.1}$$

where f_c is the cut off frequency, R is the resistance of the resistor and C is the series capacitance of the capacitor (Cox 2001). Using the values of the first low pass filter in Figure 21, the following was obtained;

$$f_c = \frac{1}{2 \times \pi \times 2000 \times 100 \times 10^{-6}}$$

$$f_c = 0.796\text{Hz}$$

This gives an approximate value of 0.8Hz which is closer to the anticipated value of 0.75Hz. The same cut off frequency of 0.8Hz is achieved using the values of the components of the second low pass filter. These two low pass filters cascaded together form the second order low pass filter. This was done to ensure complete removal of any high frequencies above the 0.8Hz threshold. One assumption made about this filter was to conveniently pass venous frequency components without damping their waveforms considerably.

For quicker preliminary tests, the output signal from the circuit was mostly viewed on a GwINSTEK GDS-1152A oscilloscope. However for the purpose of large data storage and detail analysis of results, the circuit was linked to a NI USB-6212 DAQ device connected to a laptop computer. The results were displayed in real time using the LabVIEW™ 2012 software developed by National Instruments. The complete device setup including the sensing elements, signal processing circuit, power source and output display equipment are shown below in Figure 3.4.

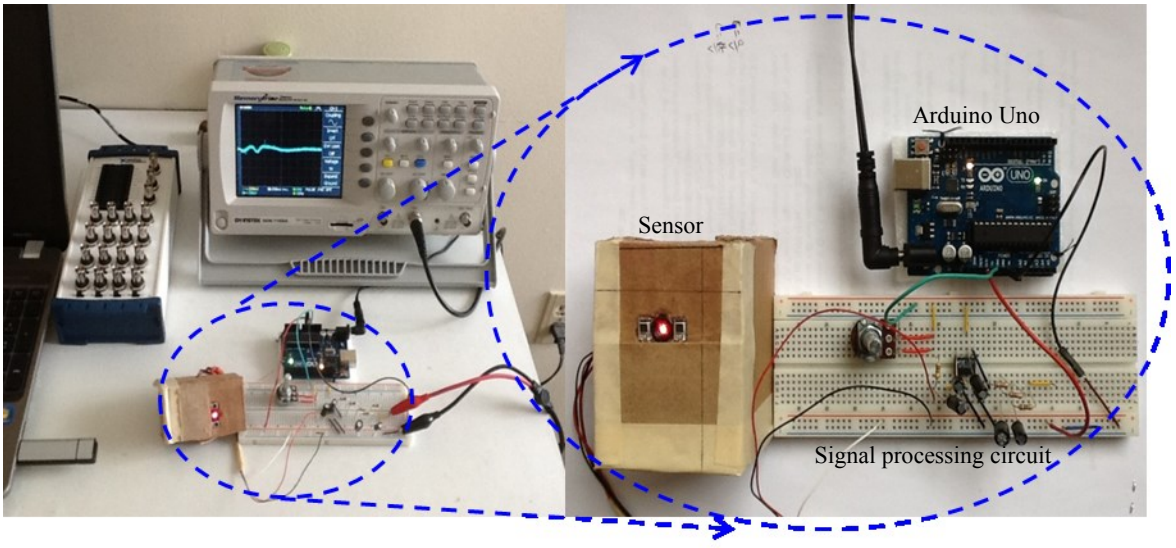

Figure 3.4. The measuring device setup: (a) complete sensor instrumentation setup, and (b) close up view of sensor, Arduino and processing circuit.

3.2. The in-vitro setup

The in-vitro setup was done to provide a platform to test the sensor's capabilities at pressures found within the jugular veins. From literature, it was recognized that the appropriate layout would be a MCL. A MCL provides a suitable test platform by mechanically representing a human system of interest and it is a necessary step prior to in vivo testing. This approach allows for the effective selection of physical loop characteristics, such as pneumatic drive parameters to create pressure and flow, pipe dimensions to replicate the resistance, compliance, and fluid inertia of the venous system (Timms *et al* 2011). The flow of the mock circulatory loop progresses serially through separate devices, with each simulating a parameter of the venous system (Taylor and Miller 2012).

3.2.1. Requirements for the MCL

There are several MCL systems available in research depending on the parameters one seeks to measure. However, this project relied on a MCL system utilized by Fischer *et al* (2002) and Molas *et al* (2003). The MCL system used by both researchers were made up of a pump, a perfusion line, a Windkessel chamber (dampener), a fluid reservoir, a pressure monitoring device and a test object. Figure 3.5 shows a schematic diagram of the MCL used for the in-vitro experiment. In its operation, the pump draws and propels the fluid from the reservoir and channels it through the Windkessel chamber to the test sample. Between the Windkessel chamber and the testing platform is a pressure monitoring device which indicates the pressure within the loop at any point in time. The fluid is returned back to the reservoir and the process is repeated. By adjusting the

parameters in the pump and Windkessel chamber, pressure levels in the jugular veins are simulated to test the sensor.

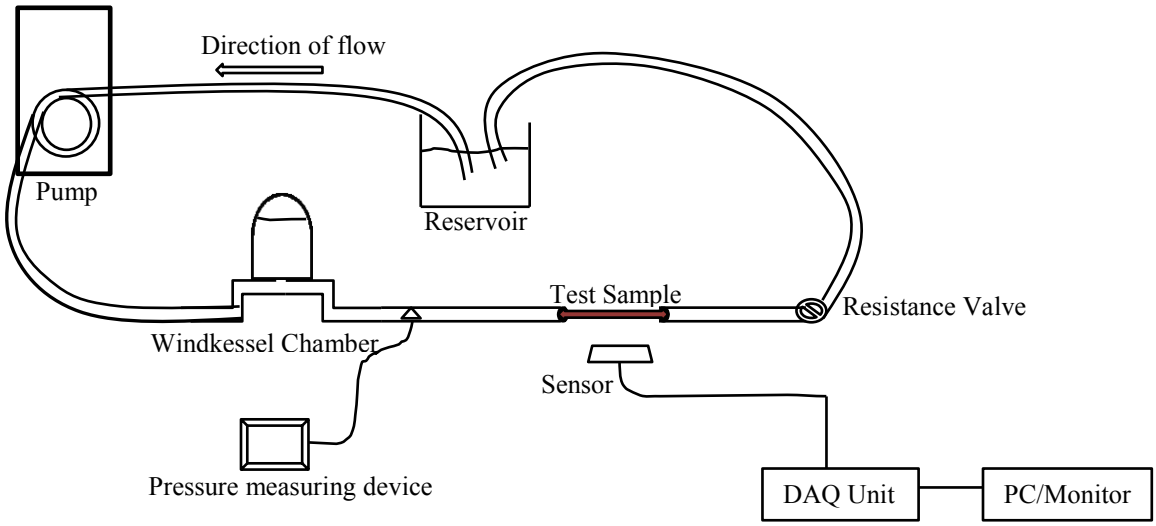

Figure 3.5. Schematic of the MCL system.

3.2.1.1. The pump and perfusion line

In view of the pulsatile flow within the jugular veins, it was appropriate to use a pump which could deliver flow in a pulsatile fashion. This could be achieved with a peristaltic pump or a diaphragm pump. Also, a pump with regulatory functions was also considered in order to regulate the level of the pressure. Therefore, a custom made micro diaphragm pump was purchased from TOPSFLO Ltd., with model number GLP-W4/ W6-C00110. This liquid pump was equipped with a five volts pulse width modulator (PWM) which regulated the pressure as shown in Figure 3.6.

Ideally, the perfusion line should have had similar dimensions to the jugular veins in order to present a realistic simulation. However, constraints were introduced by the devices in the setup which made this impossible. The perfusion line for the system was selected based on the dimensions of the inflow and outflow connectors of the micro

pump. Therefore, clear vinyl tubing with dimensions 6.35mm x 4.31mm (outer diameter x inner diameter) was employed for the perfusion line.

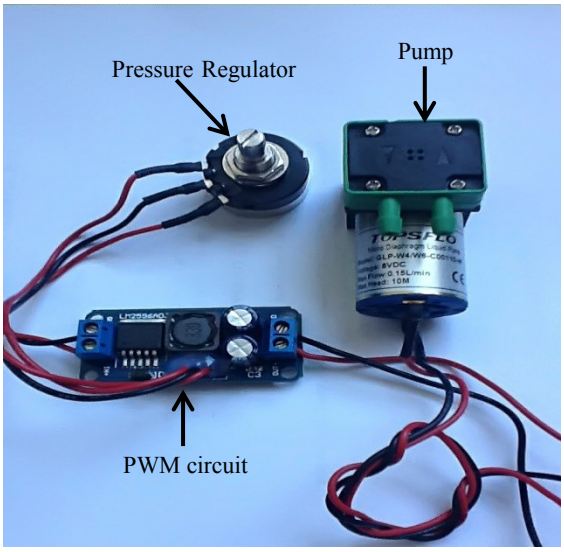

Figure 3.6. Micro diaphragm pump with PWM.

3.2.1.2. The Windkessel chamber (Dampener)

Even though pulsatile pressure was required in the loop, the pulse level had to be within limits in order to experience a certain degree of pressure. This phenomenon could not be achieved by regulating the pump. It could however be done by using the Windkessel chamber or pulse dampener. The chamber was placed between the pump and the test material in order to dampen the pulses emanating from the pump. In its function, the fluid enters the inlet, fills the chamber trapping a volume of air above the liquid, and then exits the outlet. By regulating the proportions of the fluid and air space within the chamber, the pulses can be damped to a certain level or cancelled out entirely to achieve a continuous fluid flow. For this setup, the Cole-Parmer MASTERFLEX® pulse dampener (07596-20) was utilized (Figure 3.7).

Figure 3.7. MCL Windkessel apparatus.

3.2.1.3. The MCL pressure monitoring device

The primary purpose of the in-vitro setup was to establish jugular venous pressure levels. It was therefore necessary to equip the setup with a pressure monitoring device which would indicate the pressure in the loop during the testing process. For this purpose, the Statham® P23Db pressure transducer was exploited. This pressure transducer works as a strain gauge based on the Wheatstone bridge circuit theory. Although it was acquired as a standalone device, a calibrated gauge response was programmed on LabVIEW for the pressure transducer by connecting it to the NI USB-6212 DAQ device. Prior to the calibration process, it was standardized with the Dwyer® Series 490 Wet/Wet Digital Manometer. The LabVIEW calibration program and the standardization process of the pressure transducer can be found in Appendix B. Figure 3.8 shows the P23Db pressure transducer and the digital manometer.

a **b**

Figure 3.8. MCL pressure monitoring device: (a) P23Db pressure transducer, and (b) Handheld digital manometer.

3.2.1.4. Blood mimicking fluid

The fluid in any vascular research has to mimic human blood with respect to dynamic viscosity so as to obtain realistic blood-flow modeling measurements (Yousif *et al* 2009). It was also hinted earlier in Chapter 2 that, the absorption coefficient of the medium of light propagation influenced the level of light intensity reaching the photo detectors. Furthermore, an emphasis was made about the 660nm absorption coefficient of deoxygenated blood. In view of this, there was a need to simulate similar blood properties of absorbance and viscosity in the MCL fluid.

To mimic the viscosity of blood, a mixture of water and glycerol was employed. Although, Ramnarine *et al* (1998) and Yousif *et al* (2009) used similar proportions of water and glycerol to mimic the viscosity of blood, the latter achieved a fluid which exhibited a dynamic viscosity of 4.31 ±0.03 centipoise (cP) which lied within the range of blood viscosity (4.4 ±0.6 cP). The fluid was composed of water (47.38% by weight), glycerol (36.94% by weight) and sodium iodide salt (15.68% by weight). The sodium iodide was added to improve the refractive index of the fluid. However since the

refractive index was not being considered for this case, it was ignored and the percentage was split equally and added to the percentages of glycerol and water. The resulting percentages by weight for glycerol and water became 44.5% and 55.5% respectively.

The term 'percentage by weight' means a ratio of an amount of substance in grams contained in 100ml of solution (weight/volume).

$$\%(w/v) = \frac{\text{grams of substance}}{\text{milliliters of solution}} \times 100 \tag{3.2}$$

where weight/volume percent is abbreviated $\%(w/v)$ (Seager and Slabaugh 2010).

In preparing the fluid, it was assumed a final fluid volume of 800ml was required for the MCL reservoir. To calculate the volume of glycerol (44.5%) in the overall fluid, the following calculations were done. First, the actual weight of the glycerol in the proposed volume was calculated by rearranging Equation (3.2):

$$800\text{ml} \times \frac{44.5\text{g}}{100\text{ml}} = 356\text{g}$$

Therefore 356g of glycerol had to be converted to its equivalent volume using its density. The density of glycerol is 1259.37kg/m^3 (Springer 2013), meaning there is 1259.37g of glycerol in every 1000ml of solution (Density theory) (Seager and Slabaugh 2010). By using ratio and proportion:

$$\text{glycerine volume} = \frac{1000\text{ml} \times 356\text{g}}{1259.37\text{g}} = 282.68\text{ml}$$

Similarly for water (55.5%),

$$800\text{ml} \times \frac{55.5\text{g}}{100} = 444\text{g}$$

The volume equivalent of 444g of water was calculated from the density of water (1000kg/m^3) (Springer 2013). From the density theory, this implies 1000g of water is contained in 1000ml of solution (Seager and Slabaugh 2010). Therefore from ratio and proportions, 444g is equivalent to 444ml of water.

Therefore, the fluid prepared for the MCL was a mixture of approximately 283ml of glycerol and 444ml of water. The glycerol was a product of Rougier Pharma and was purchased locally from the pharmacy. Although the viscosity of the final fluid was not tested, it was assumed the viscosity was nearly equal to blood. This assumption was made with confidence based on the results of other researchers, who had recorded good results by using similar proportions of water and glycerol.

Mimicking blood with a fluid having an absorption coefficient of 660nm was also very important. Several colors were tried on the fluid but the closest absorbance wavelength that was achieved with a blue marker was approximately 620nm. The tip of a blue Sharpie® permanent marker was dipped into the fluid to spread out the color uniformly. The dipping processes made it quite difficult to control and quantify the concentration of the color in the fluid. After several trials, an absorbance of 620nm was recorded using a Varian Cary® 50 UV-Vis Spectrophotometer. Even though the 620nm is off the 660nm mark expected, it was used based on the fact that both wavelengths lie close to each other in the absorption spectrum.

3.2.1.5. The test sample

Among the interconnected segments of the MCL was the test segment. This region of the loop served as the point of contact for the sensor. In other words, this

segment is responsible for delivering the measurand needed to demonstrate the sensitivity of the sensor. It therefore required a vein or an object which could substitute the vein. To this effect, a vein-like object was created at the test segment to transfer the physical quantity from the loop onto the sensor. One major characteristic of the jugular veins which was taken into consideration is its flexible wall, which allows the transmission of pulses onto the skin surface. The material had to be flexible and compliant enough to relay the pulsatile flow in the MCL onto the sensing elements of the sensor. Additionally, the color of the material had to be taken into account to prevent it from interfering with the absorbance of the mimicked blood fluid.

The vein-like vessel was therefore created from a grey latex glove. A section of the perfusion line of the MCL was removed and the latex material was stretched and wound around the gap created between the two ends of the line. It was fitted and firmly secured by tying both ends with strips of latex. The outcome of the design is illustrated in Figure 3.9. The wall thickness of the test object could not be reliably measured. However, it had three layers of the latex material wound on each other. Furthermore, the extent at which the material was stretched before winding could not easily be quantified. Stretching at a higher degree caused the material to contract upon completion, which blocked the lumen of the object. On the other hand, stretching at a lower degree also caused the object to bulge out during fluid transmission. Nevertheless, several trials were done in order to realize a suitable simulated vessel which could allow the smooth movement of the fluid with a reliable degree of compliance.

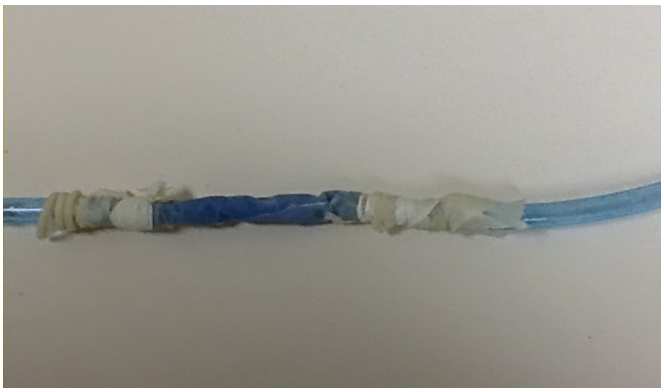

Figure 3.9. Vein-like object for MCL setup.

Chapter 4

4.0. Experiments and results

The response of the sensor was ascertained in two different ways. As a prior requirement for in vivo analysis, the sensor was first tested in vitro on the MCL. Based on the good results from the in vitro analysis, the in vivo experiment was also conducted. Unlike the in vivo test, the response expected of the sensor for the in vitro experiments was not peculiar. However, there was a need to establish a specific trend in its response to varying pressures in the MCL. For the in vivo analysis, the sensor was expected to demonstrate a unique response similar to the central venous waveform. Outlined in the following sections are the experimental procedures, the results and some analysis of the results.

4.1. In vitro experiment

In the previous chapter, the schematic structure of the MCL was identified. Based on this, an in vitro experiment was set up as illustrated in Figure 4.1. The system was primed and initialized to rid the setup of any bubbles which could interfere with the tests. By using the pump regulator and adjusting the fluid level in the dampener, the needed pressure was reached and maintained in the loop. The pressure within the loop was monitored on the computer through the P23Db transducer gauge which was setup on LabVIEW. To minimize the interference of ambient light on the sensor, the experiment was conducted in a dark room. Once the required pressure level was realized, the sensor was applied to the test object and its response was observed and stored. A screenshot of the pressure monitoring gauge as well as the sensor response is shown in Figure 4.2.

During the experiments, the pressure within the loop was mostly regulated with a step change of 2mmHg. A 2mmHg factor change was used due to the difficulty in adjusting loop components to attain a 1mmHg change. Two separate scenarios were used in the in vitro experiment, in relation to the relative positions of the sensor and the test object. Either the sensor was placed on the test object whiles lying on a flat surface (first scenario), or the test object was placed directly on the surface of the sensor (second scenario).

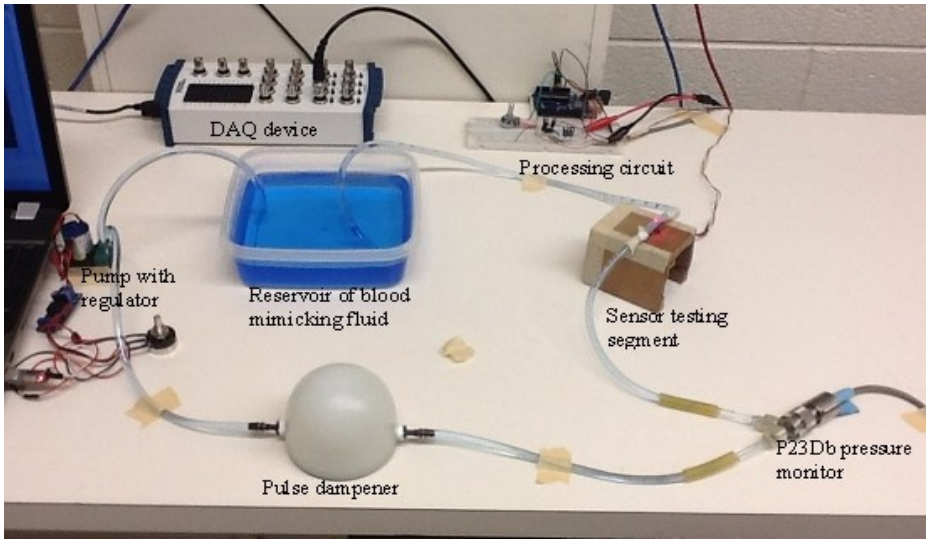

Figure 4.1. In vitro experimental setup.

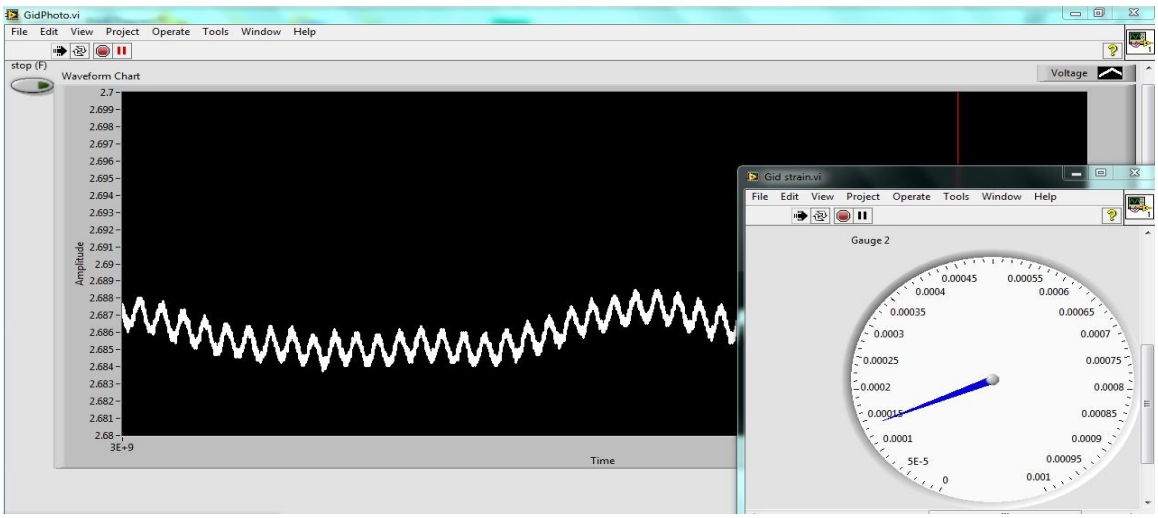

Figure 4.2. The graphical interface on LabVIEW during the in-vitro analysis for the PPG sensor response. Bottom right corner is the pressure monitoring gauge for the MCL.

4.1.1. In vitro results

Illustrated in Figure 4.3 is the sensor response for a varying loop pressure from 6mmHg to 16mmHg for the two different situations. Using MATLAB, different sections of Figure 4.3 (a) and (b) are focused to illustrate the trend in the response of the sensor. Figure 4.4 shows the sensor response observed at some selected pressure levels for the first scenario. It should be noted that the waveforms displayed in Figure 4.4 were exhibited in real time during the experiments.

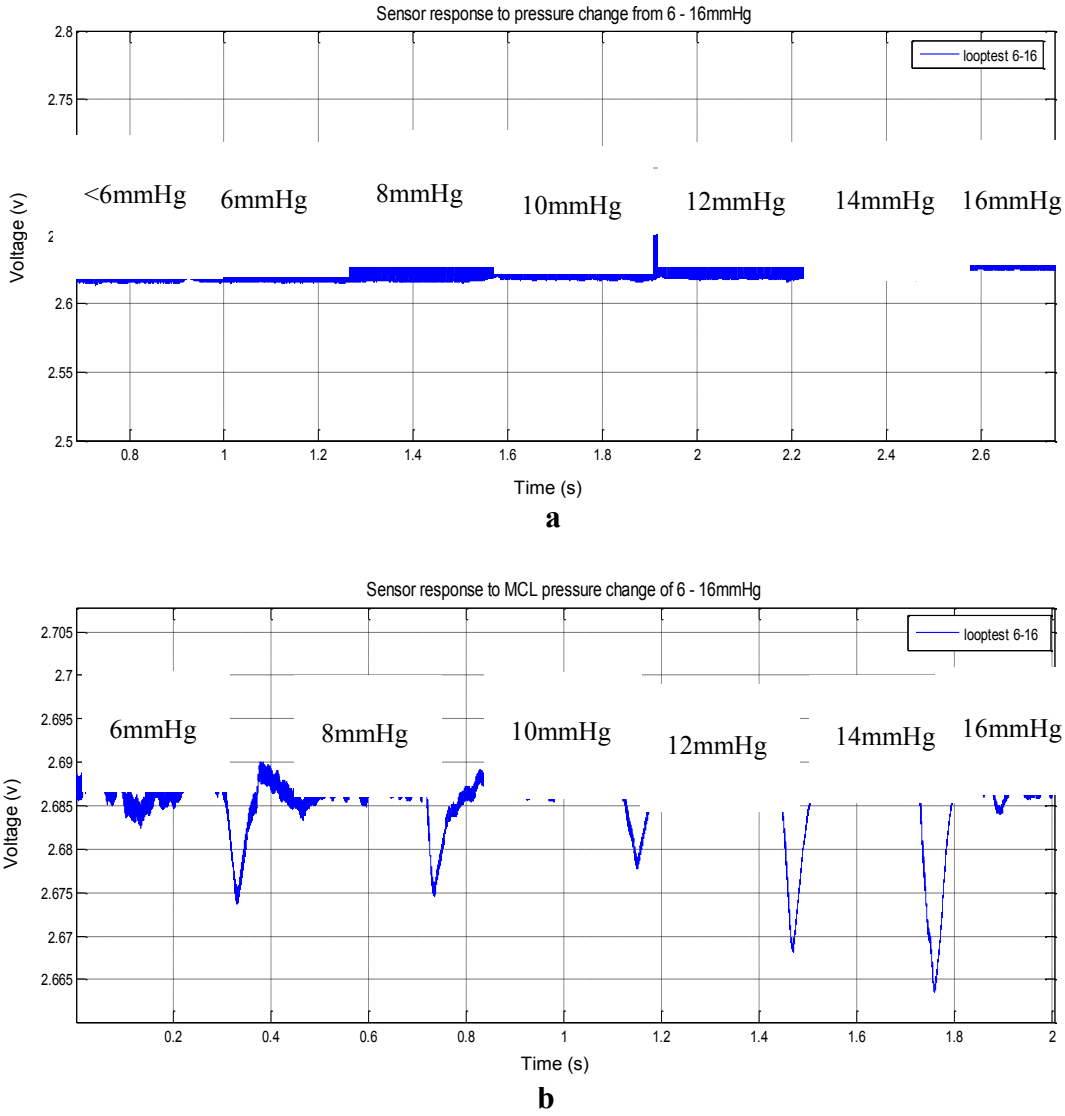

Figure 4.3. Sensor response to MCL pressure variation: (a) First scenario - sensor placed on test object, and (b) Second scenario - test object placed on sensor.

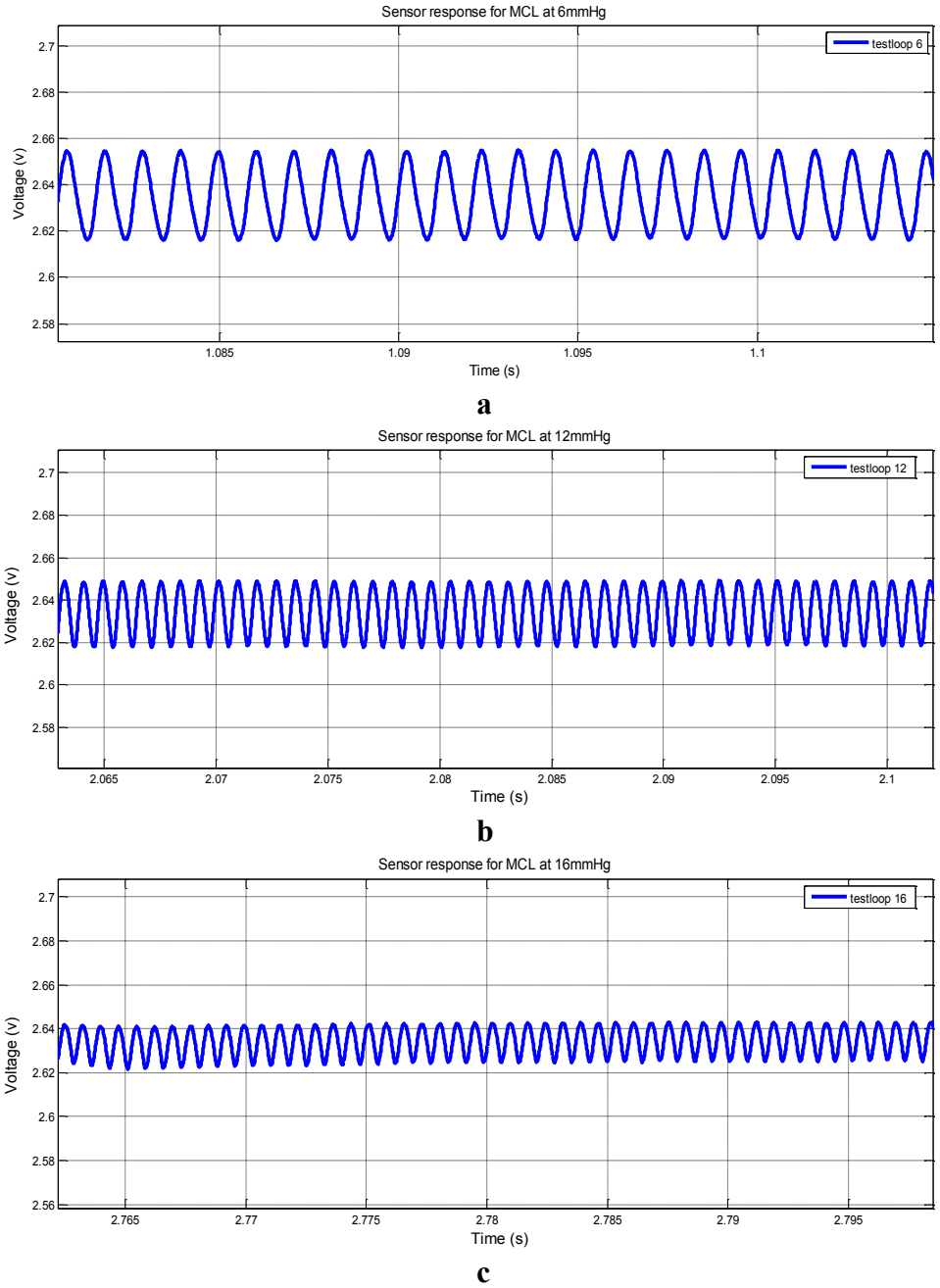

Figure 4.4. Waveform trend of sensor response at different pressures in first scenario: (a) 6mmHg, (b) 12mmHg, and (c) 16mmHg.

Similarly, Figure 4.5 illustrates the real time display of the sensor response at different pressures for the second scenario.

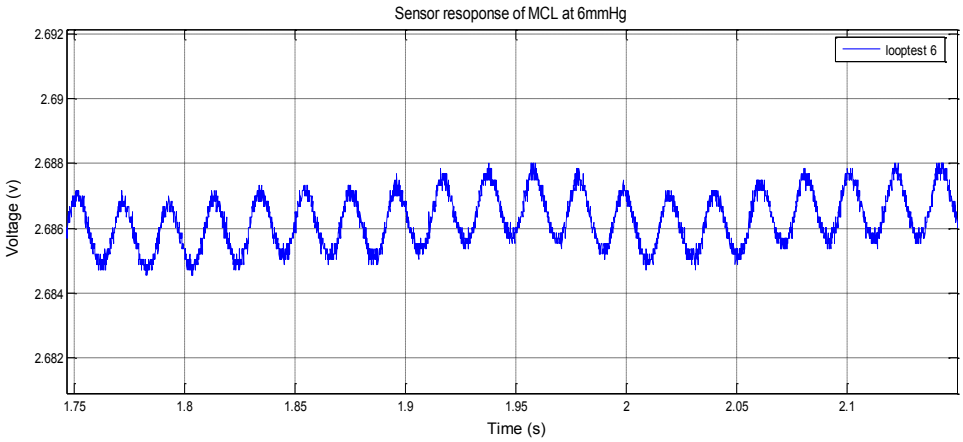

a

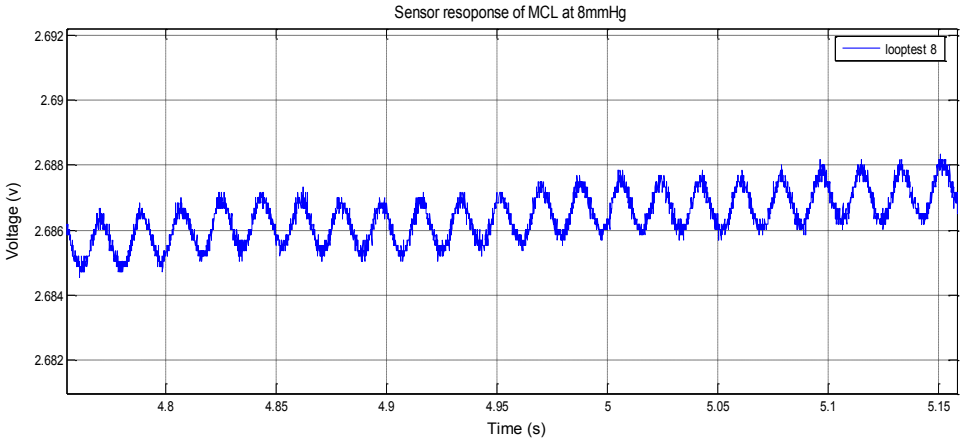

b

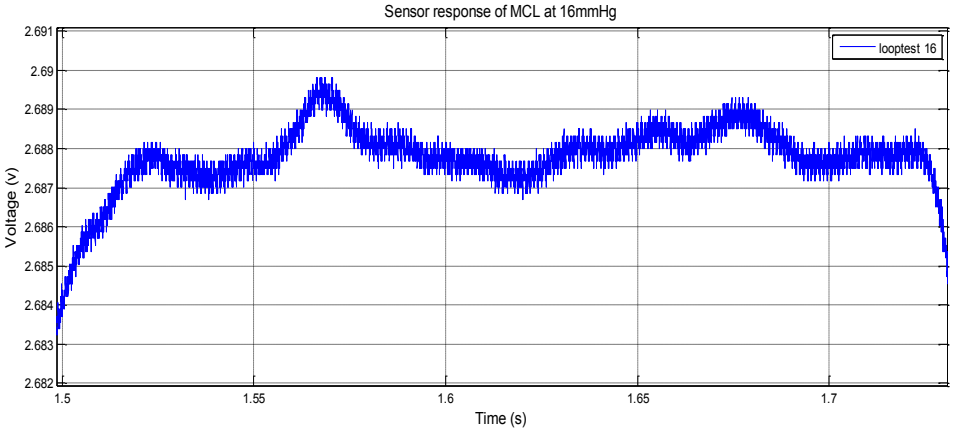

c

Figure 4.5. Waveform of sensor response at different pressures in second scenario: (a) 6mmHg, (b) 8mmHg, and (c) 16mmHg.

4.1.2. In vitro result analysis

A look at the results from both scenarios reveals a similar trend in the sensor response. As the pressure increases, the waveform changes with a decrease in both amplitude and wavelength, but an increase in frequency. It can therefore be concluded from this trend that if the pressure continues to increase beyond a certain level, the amplitude will continue to decrease with a probability of the waveforms deteriorating into a straight line. This occurrence verifies the research of Molas *et al* (2003) who showed that an enhanced sensibility of the compliance response can be experienced in lower pressures. However, as the pressure increases the compliance level of veins diminishes. In view of this, the trend observed in the in vitro test also confirms how closely the vein-like test object is able to mimic the compliance of a true vein.

In a reverse case, the waveform observed at lower pressures is very distinct and clearly defined. The pressure variation in the MCL started at 6mmHg. Based on this direction, one can state confidently that those pressures below 6mmHg will give a finer waveform with clearly defined peaks and troughs. It should be remembered that the pressure levels in the jugular veins are very low. Ultimately, it can be concluded with a good level of confidence that the designed reflectance configured sensor will give a better response at lower pressures than higher ones. This infers the sensor is effective enough to estimate the CVP waveforms in the jugular veins.

4.2. In vivo test

With some results accomplished at the in vitro level, it became desirable to test the sensor on myself. The size of the housing cardboard of the sensing elements was

reduced to fit the neck and was also extended about one meter away from the processing circuit. Using the valsalva maneuver, the right and left EJV was marked on the neck as shown in Figure 4.6. The sensor was then tied to the marked portions of the neck using a flexible rubber band and the supine position was assumed. Some quick preliminary tests were conducted on both left and right EJVs. However, from the preliminary results it became necessary to neglect the left EJV in the final tests since its results did not carry the full information for a central venous waveform.

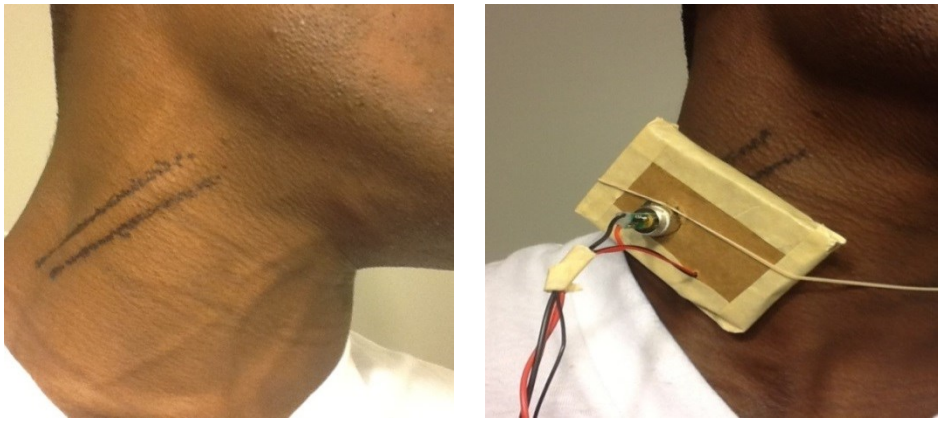

a **b**

Figure 4.6. In vivo experiment: (a) marked outline of right EJV, and (b) sensor placed on marked EJV.

4.2.1. In vivo preliminary test results

This test was done to primarily ascertain the response of the sensor to the jugular veins. It was also done with the hope of identifying if the right or left EJV would yield better results. The test was conducted in a dark room, whiles the body of the subject laid in a 30^0 supine position. The screenshots of the oscilloscope display is illustrated in Figure 4.7. From the preliminary results, a good level of sensor sensitivity was noticed. Additionally, the waveforms observed from the right EJV carried detailed information about the dynamics of the CVP. Some peaks in the waveform of the left EJV were either

reduced, missing or out of place. More light will be shed on this claim in the result analysis section.

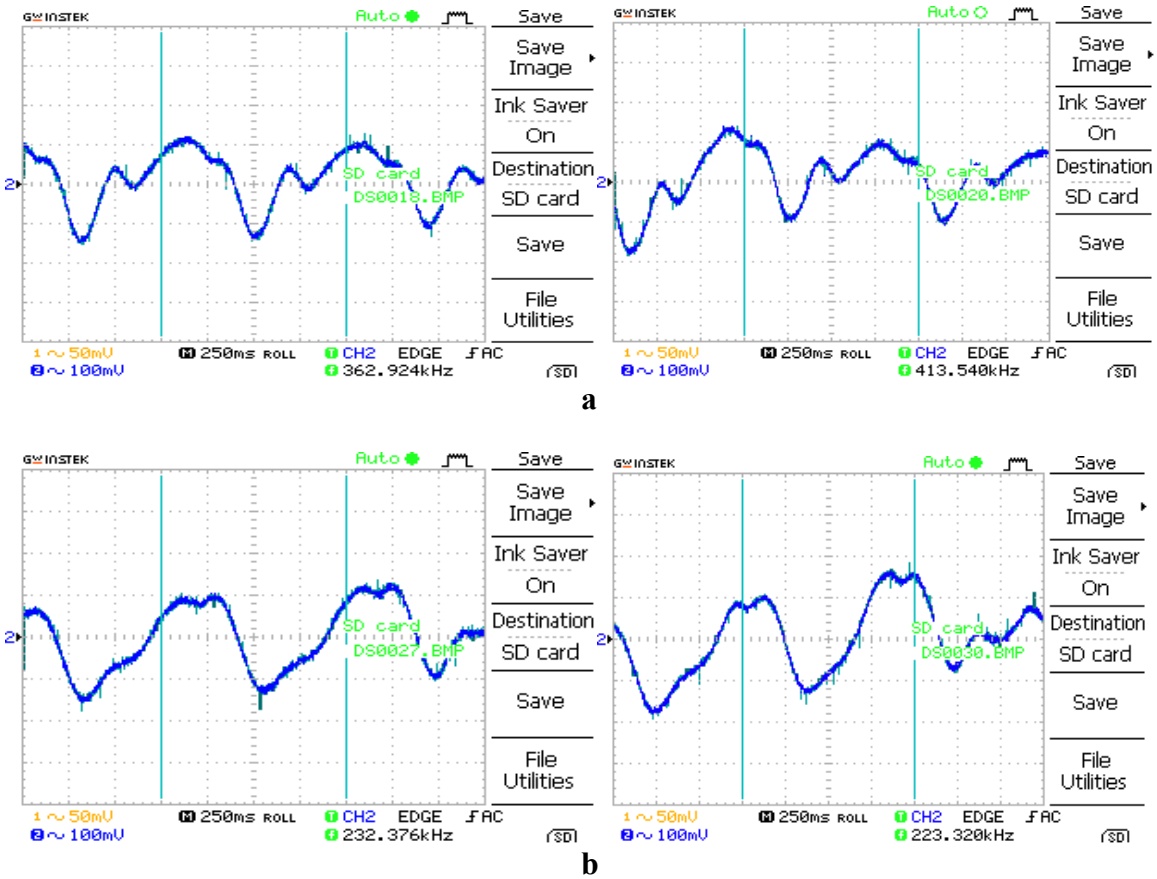

Figure 4.7. In vivo preliminary results showing consecutive screen shots of the oscilloscope: (a) waveform from right EJV, and (b) waveform from left EJV.

4.2.2. In vivo final test results

The final test was conducted to supplement the preliminary one. It was carried out over longer periods in order to identify any trends present in the right EJV. Using the same preparations for the preliminary test, measurements were conducted in two different supine positions. Either the head was elevated to a 30^0 angle or the head was laid flat with no elevation. Some results from the final tests are shown in Figures 4.8 and 4.9.

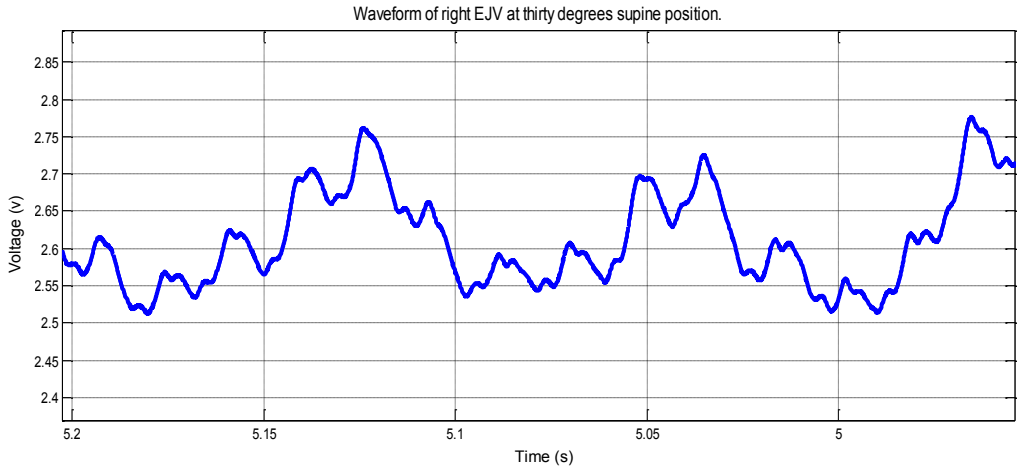

Figure 4.8. Waveform of right EJV at 30^0 supine.

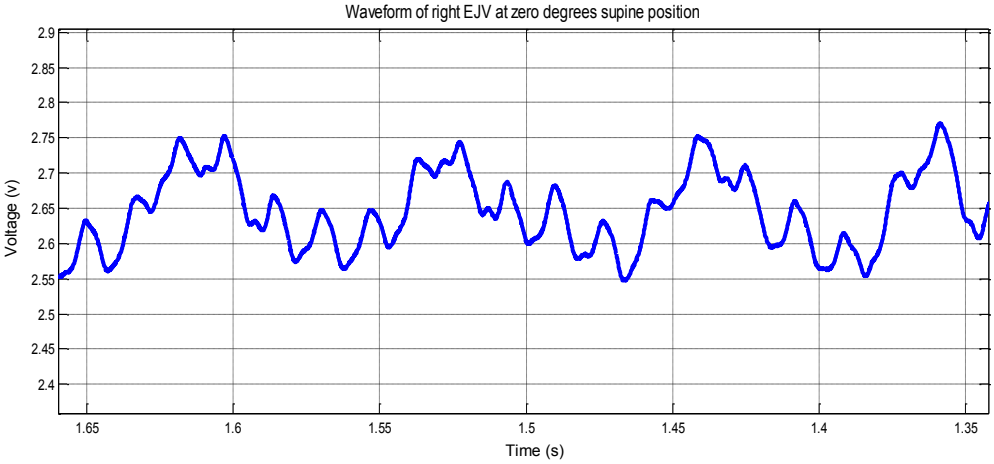

Figure 4.9. Waveform of right EJV at 0^0 supine.

4.2.3. In vivo result analysis

Even though the preliminary tests were conducted for trail reasons, the response from the sensor was very good. Its sensitivity was convincing enough to advocate the final tests towards the right EJV. This is because the waveform produced by the right EJV reveals all the characteristics of the central venous waveform. To bolster this statement, a comparison has been made in Figure 4.10 between a standard central venous waveform and the screenshot of the right EJV from the preliminary test. From the

comparison, (i.e., *a*, *c* and *v*) and two troughs (i.e., *x* and *y*) have been identified and labelled on the screenshot of the oscilloscope. This illustration does not only promote the right EJV for CVP measurements, but more importantly, shows how well the designed PPG sensor can estimate the waveform in the jugular veins.

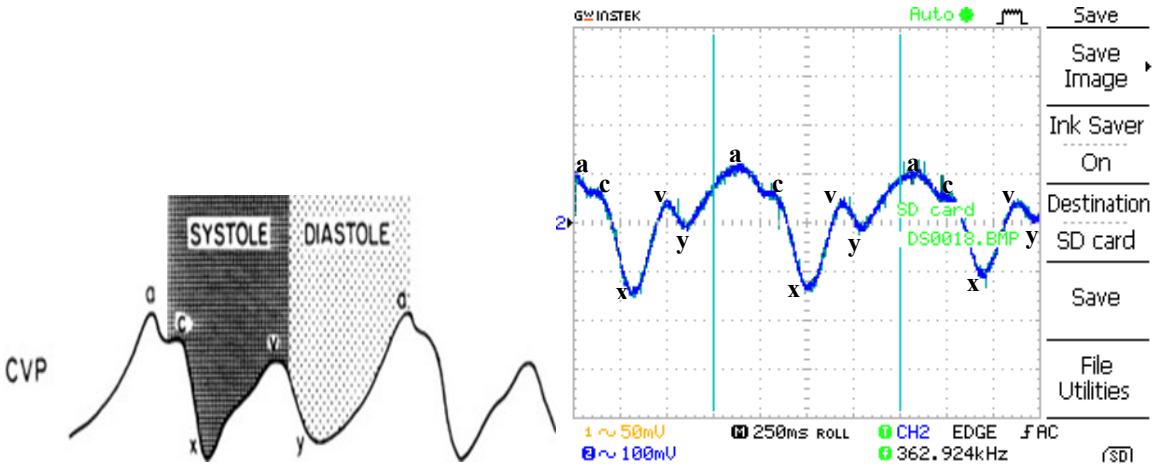

Figure 4.10. Comparing the standard central venous waveform (left part of the figure) to the preliminary response of the sensor on the right EJV (left part of the figure).

With reference to the final test results displayed in Figures 4.8 and 4.9, a critical look shows the waveform produced with the subject's head raised at an angle of 30^0 carries the full information. The waveform generated in the 0^0 supine position fails to clearly distinct the *a, c,* and *v* peaks. Nevertheless, the waveforms generated in the two positions exhibits a characteristic rise and fall pattern. In Chapter 2, it was stated from literature that the CVP was influenced by spontaneous or positive pressure breathing and it was also advised to take CVP readings at the end of expiration. Building on these points, another comparison is made from literature to support that a central venous response was recorded by the PPG sensor. In Figure 4.11, the venous waveform generated from a catheter (Meyers and Weingart 2007) is compared to the waveform generated from the PPG sensor on the right EJV at 30^0 supine. In both waveforms, a rise

in wave occurs during expiration and a fall in wave occurs during inspiration. Furthermore, the waveform generated from the catheter points out the *a*, *c*, and *v* peaks. Likewise, the peaks are also identified in the waveform response obtained from the PPG sensor and this is illustrated in Figure 4.12. Undoubtedly, the difference in length of the rise and fall periods of the waveform will vary depending on the rate of breathing. A shorter segment is portrayed for faster breathing while a longer segment is portrayed for slower breathing.

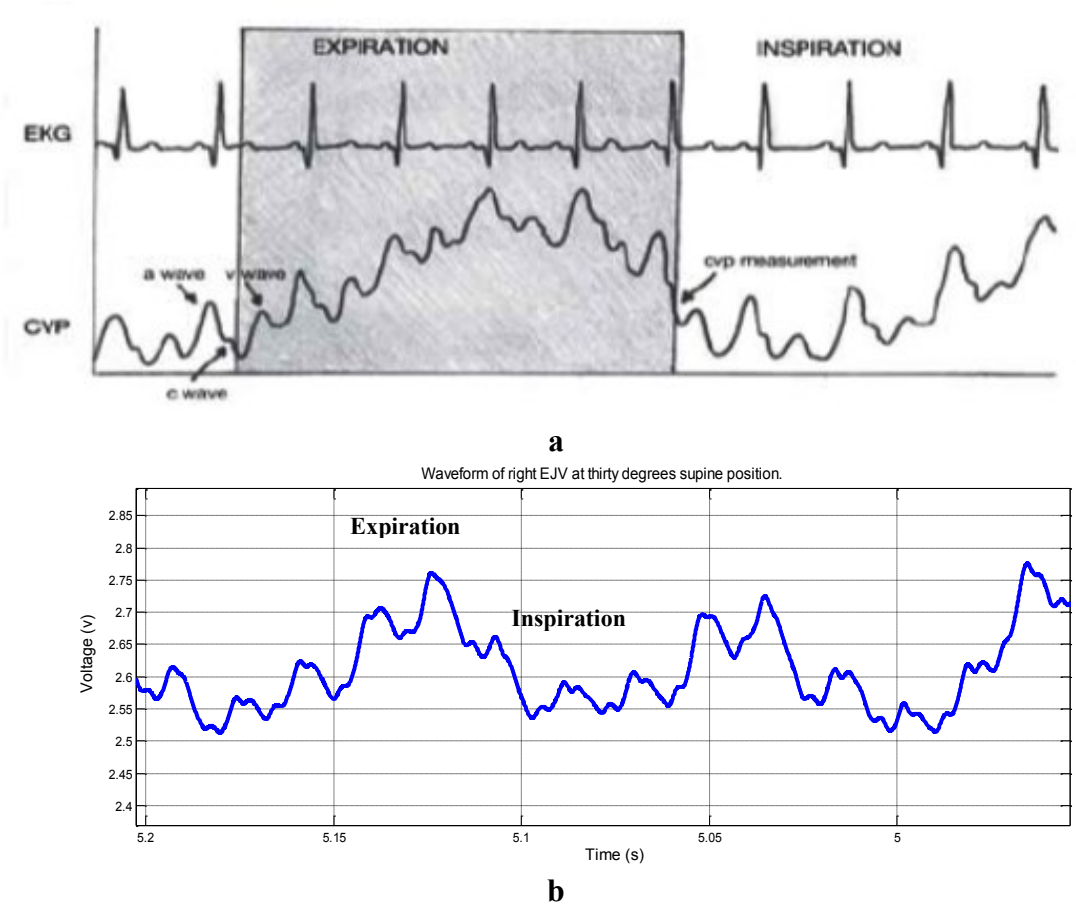

Figure 4.11. Comparing two CVP waveforms: (a) waveform generated from a catheter, (b) waveform generated from the developed PPG sensor.

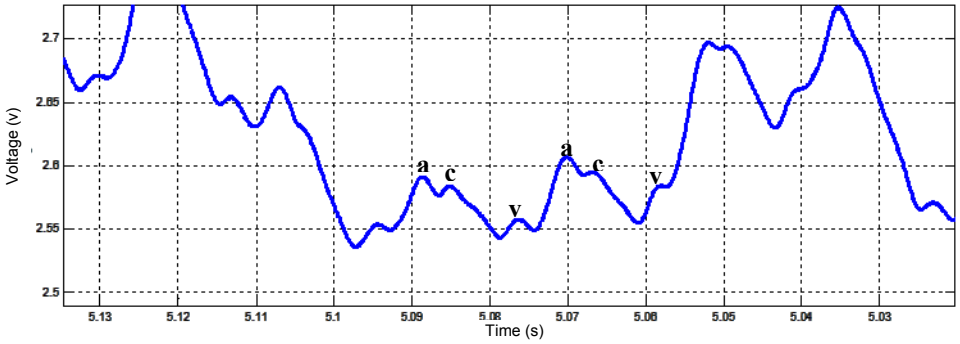

Figure 4.12. Sensor generated central venous waveform with identified peaks.

4.2.4. Confirmatory tests

In the literature, it was explained how the central venous pressure or waveforms were mostly modulated by respiratory and cardiac activities. In the last section, a characteristic rise and fall pattern was observed in the waveform of the right EJV. By comparing it to a catheter based waveform from literature, the inspiration and expiration times were revealed. To confirm that the central venous waveform was dependent on respiration, another experiment was done with the PPG sensor in a 30^0 supine position. In this instance, the subject held the breath a couple of times at the end of expiration during the experiment. The result indicating the events of respiratory hold is shown in Figure 4.13. This event is characterized by a uniform progression of waves as compared to the times of respiration where an upward and downward trend is found.

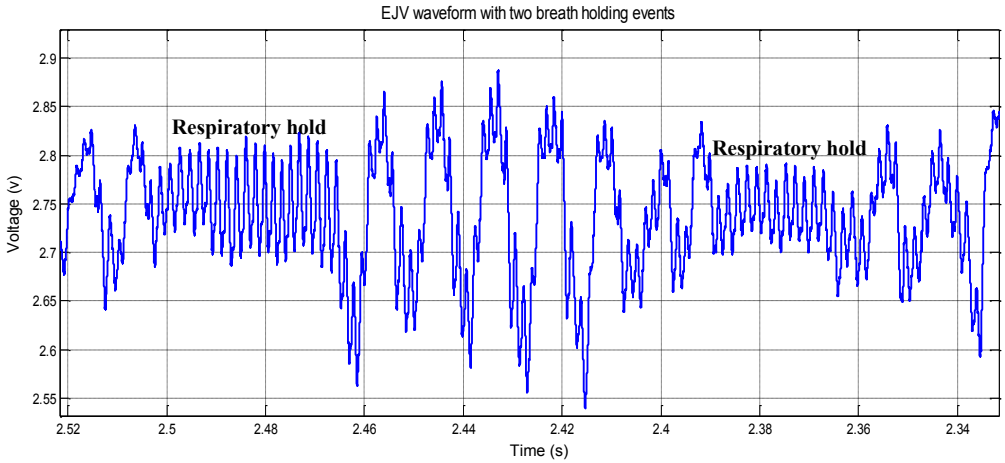

Figure 4.13. EJV waveform showing respiratory activities.

Another experiment was performed to investigate the effect of cardiac activity on the central venous pulse of the subject. A jogging exercise was performed by the subject for approximately 10 minutes. First, the EJV waveform was taken using the PPG sensor in a 30^0 supine position immediately after the exercise. Two other waveforms were subsequently recorded from the subject's EJV after 10 and 20 minutes of the exercise and the results are shown in Figure 4.14. From the results it can be observed that the waveforms generated from the EJV immediately after the exercises possess very large peaks, with some extending beyond the voltage window of 2.5 to 2.9volts. In Figure 4.14(a), it is also difficult to examine the wave pattern as well as its trend. However one recognizable feature is the sharply pointed peaks, which corresponds to the *a* and *v* peaks of the central venous waveform. The waveforms after 10 and 20 minutes of exercise are similar due to the fact that both exhibit the characteristic upward and downward trend in wave propagation. In spite of this, a closer look reveals slightly longer peaks in Fig. 4.14(b) than 4.14(c). Also, the waveform generated after 20 minutes of exercise demonstrates a clearer patterned waveform with a uniform trend than the other two

occasions. Clearly, the varying waveforms denote the changes in cardiac activity from exercise to rest. However, it should be remembered the above waveforms are also affected by respiration, which are more responsible for the graph trend. On the other hand, difference in pressure due to heart pumping rates, can be linked to the different peaks and troughs shown in the waveforms.

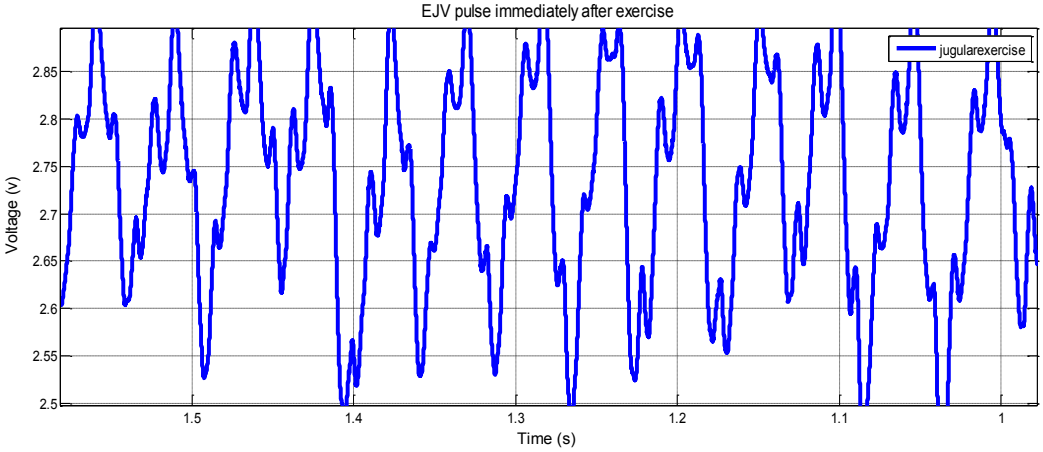

a

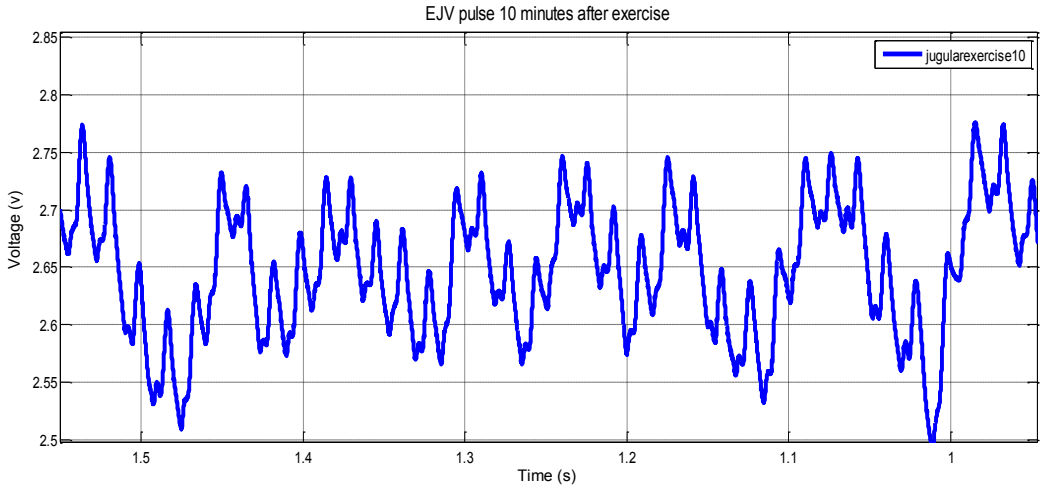

b

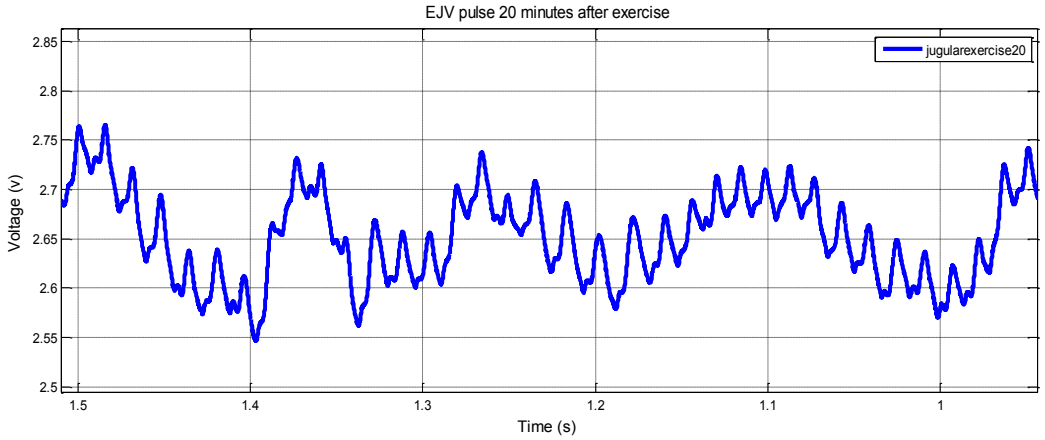

c

Figure 4.14. EJV waveform after exercise: (a) immediately after exercise, (b) 10 minutes after exercise, and (c) 20 minutes after exercise.

Even though this research demonstrates the dependence of the venous waveform on respiration and cardiac activities, Pitman *et al* (2004) makes it clear that these characteristics also apply to arterial pressure. In Chapter 2 it was mentioned that differentiating central and arterial waveforms was very important in the proper identification of central venous pressure. There can be instances where an abnormal venous waveform can take up the shape of an arterial pulse and similarly, an abnormal arterial waveform could also show up as a venous pulse. Since the in vivo study was done on a single subject whose health status is unknown, there are chances that an abnormal arterial pulse could be represented in the research results as the central venous waveform. In light of this, there was a need to identify and distinguish the test subject's arterial pulse to rule out the chances of an abnormal arterial pulse posing as a central venous waveform.

To achieve this, a pulse oximeter was dismantled and the red wavelength source was disconnected leaving only the infrared source. This was done to target the arterial oxygenated blood flow. The laser of the developed PPG sensor was also disconnected

and its photodiodes were used in conjunction with the infrared source of the pulse oximeter. The filter of the processing circuit was reconfigured to increase the frequency threshold to about 16Hz in order to allow the passage of high frequency signals. In a transmittance mode, the arterial pulse of the subject was measured through the right index finger. The results for the arterial test are shown in Figure 4.15.

From both displays, a perfect arterial pulse is exhibited by the test subject. By comparing the graph in Figure 4.15(b) to Figure 2.13 of this thesis, one can clearly identify the systolic and diastolic phase of the pulse, as well as the diacrotic notch. This result therefore confirms the test subject has a normal arterial pulse which is distinguishable from the central venous pulses earlier recorded. Therefore, it can be concluded with confidence that the waveform reported in the in vivo experiment is truly a central venous pulse emanating from the EJV.

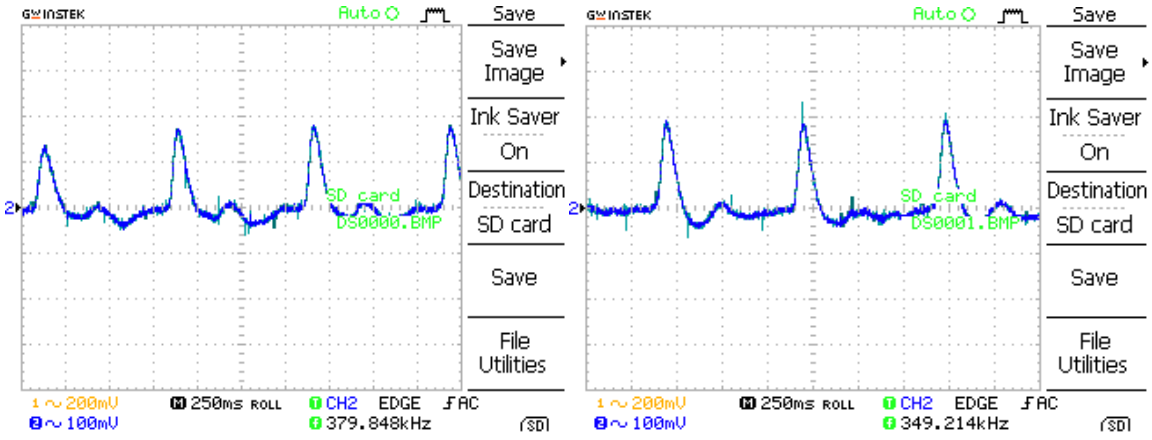

a

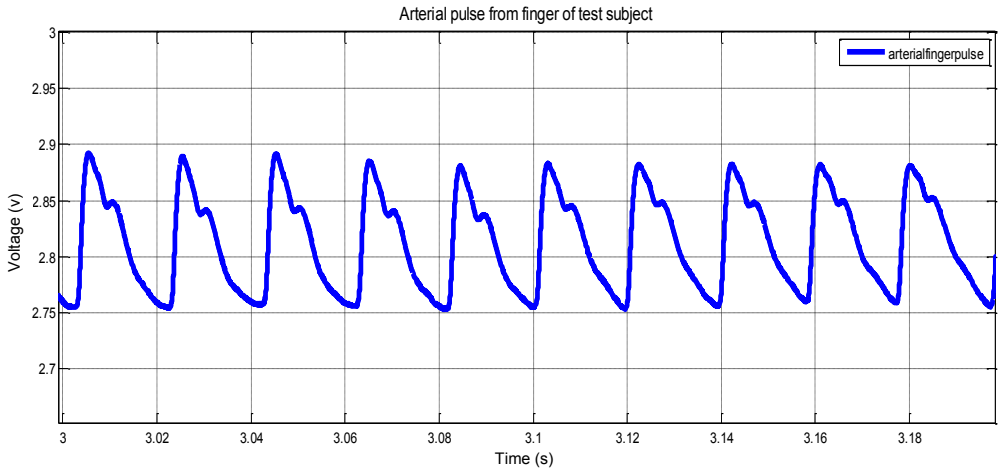

b

Figure 4.15. Arterial pulse/waveform of test subject: (a) consecutive screen shots from the oscilloscope, and (b) LabVIEW generated waveform.

Chapter 5

5.0. Conclusion and recommendation

5.1. Discussion

In this research, a laser diode was adopted in designing the PPG sensor. This was done to boost the light intensity reaching the photodiodes after the propagation through a medium. However, concerns are raised about the potential harm posed by laser sources. Upon careful considerations, a 5mW 660mm laser was chosen. According to Thomas and Isaacs (2011), the revised system implemented in 2002 defines classes of lasers based on the maximum permissible exposure levels and effects on the eyes and skin (1, 1M, 2, 2M, 3R, 3B, 4). This refers to a range of Class one with no potential damage, to Class four with high degree of potential damage. Rainer (2011) classified the 5mW laser under 3R which agrees with laser classification under risk management at the University of Ottawa, stating that it has no serious skin hazard. According to the American National Standard (2007), 3R laser system is potentially hazardous under some direct and specular reflection viewing condition if the eye is appropriately focused and stable on the beam. However, the probability of an actual injury is very low. It is safe to state that this laser type will not pose either a fire hazard or diffuse-reflection hazard.

Despite the level of safety declared for this laser type, there was a small level of heat generated at the EJV area over the prolonged use of this sensor. This was felt between twenty to thirty minutes of continuous sensor attachment. As indicated earlier, the light in this sensor was covered by a small lens to concentrate the light and this may have resulted to the heating of the skin. However, the level of heat was not intense to cause any harm or burn to the skin. Interestingly, this phenomenon could have also

played a part in achieving good results from the in vivo study. Mendelson and Ochs (1988) validated skin heating as a feasible method of increasing the size of reflected photoplethysmograms. By heating the skin surface to 45 degrees celsius, they noticed a five-fold increase in the pulsatile component could be achieved. It was indicated that by heating the skin, the vascular bed under study became vasodilated. Therefore, the reflected photoplethysmograms become more stable resulting in smaller beat-to-beat amplitude fluctuations. Nevertheless, there is a need to perform even longer tests with this sensor to formulate a time frame at which heating could cause discomfort or burns to the skin.

In connection to the results of the in vitro experiments, observing the results from both scenarios revealed a steadier wave progression for the first scenario whiles a noisier wave pattern existed in the second scenario. This can be explained as follows. When the sensor was placed on the test sample, a close contact between the photodiodes and the test object was made. Also, the weight from the sensing block kept the test object very steady during the experiment. On the contrary, a slight gap was experienced between the sensing components and the test object for the second scenario. This gap may have caused artifacts from reflected light, which had not propagated through the test object, to influence the response of the photodiodes. The unsteady wave progression observed in the second scenario is likely attributed to relative motions between the object and sensor. Even though the object was held in place on the sensor, there were still movements during fluid flow and pressure adjustments. The latter is evident in Figure 4.3(b) as huge downward peaks.

During the course of the research, there were a few areas of concern which needs to be deliberated. Some of these situations were unavoidable and may have altered the outcome of this research. A greater part of the discrepancies fell within the in vitro setup such as monitoring the pressure levels within the MCL. The inlet and outlet of the P23Db pressure transducer had a smaller dimension than the perfusion line in terms of their inner diameters. Since pressure in fluids is affected by the dimension of the containing vessel, there is a possibility that the pressure recorded by the transducer was slightly higher than what was present in the loop. Also, the gauge set up on LabVIEW for the pressure transducer had an analogue interface with a slightly unstable pointer. This made the monitoring of MCL pressures very difficult and inconsistent.

Another area of uncertainty was the vein-like test object designed for the in vitro setup. Apart from the compliance which was taken into consideration, no other physical characteristic or property of veins were considered in making the test object. It was designed to suite the response of the experiment and this could have introduced some biased results. The test sample also failed to incorporate a skin simulator. What was portrayed in the experiment was the direct application of a sensor to a vein. In a real circumstance, this cannot be the case due to the fact that the jugular veins underlie the skin. Furthermore, the presence of a skin simulator would have definitely influenced the results. In spite of this, the result from the in vivo experiment compensates and complements this omission.

During the literature review, it was brought to light that the pressure levels within the jugular veins ranged from 0 – 8mmHg. In principle, the in vitro experiment should have varied the pressure starting from zero or at least one millimeter mercury. However,

this could not be done due to the fact that the pump's operation became unstable, and sometimes ceased to work below 6mmHg. As the pump manufacturing company tried to make the pump to meet the specifications for the research, this occurrence was communicated prior to its purchase. According to the manufacturer, adjusting the PWM of the micro pump below two volts could stop the pump from working. For this reason, the in vitro setup could only start the pressure variation beyond 6mmHg.

In preparing the blood mimicking fluid, the volume quantities of glycerol and water in the final mixture had to be calculated from their densities. Practically, the calculations for glycerol should have been done based on a datasheet accompanying the product, especially with its density value. However, since the product was bought from a local pharmacy, such information was not readily available. To this effect, an assumption was made and a density value was chosen from a database which corresponded to a purity level of 95%. Since the viscosity of the final blood mimicking fluid was not determined, it is likely the final fluid might have failed to attain the blood viscosity range which was targeted.

In the course of the in vivo study, one other aspect which needed to be taken into account was the proper alignment of sensor to the jugular vein. The response of the sensor was better when all the three sensing components were aligned parallel to the path of the vein as shown in the schematic diagram in Figure 5.1(a). Since the pulsations occurs along the vein, aligning the components perpendicularly to the vein as shown in Figure 5.1(b), causes the photodiodes to fall outside the pulsating area leading to reduced or no response. Also with the parallel alignment, it increases the chances of at least one photodiode falling exactly on the tip of pulsations where a greater effect is felt. In

addition to this, the sensor should not be attached to the vein with too much pressure. This blocks the veins with no sensor response. The pressure on the vein should be as light as possible to keep the vein fully open for optimum sensor response

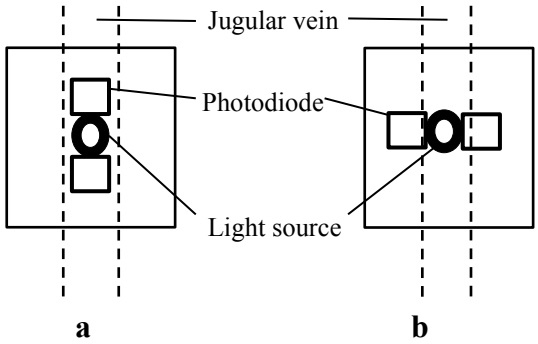

Figure 5.1. Sensor alignment to jugular vein: (a) parallel alignment to vein path, and (b) perpendicular alignment to vein path.

From the confirmatory in vivo tests, the PPG sensor was able to track respiratory and cardiac changes in the EJV. The respiratory trend is characterized by very low frequency which modulates the activity of the EJV. This is in response to the differential changes in cardiac pressure during inspiration and expiration. During inspiration, air flows into the lungs increasing the volume of the thoracic cavity. This in effect decreases the intrathoracic pressure which reduces the CVP and leads to fall in the waveform trend. On the other hand, expiration forces air out of the lungs reducing thoracic volume and increasing intrathoracic pressure. This results to an increase in CVP leading to the rise of the waveform pattern. Due to the varying pressures, it is advised to take the CVP measurements at the end of expiration. At that moment, air would have been expelled from the lungs giving rise to a normal volume which will reflect a real intrathoracic pressure.

Similarly, varying cardiac activity from exercises was translated to the jugular venous pressure. In the literature review, the *a* peak of the central venous waveform symbolized the contraction of the right atrium to fill up the right ventricle. From the results shown for the different times after the exercise, a decrease in peak *a* was established as time increased. During rigorous body activities, the pressure in the heart increases with a faster cycle due to the demand of supplying oxygenated blood. Immediately after the exercise, the filling pressure in the heart was high and this was demonstrated by the extremely long *a* peaks in the graph. As time passed, the body was able to recoup from the exercise leading to a more relaxed cardiac function which was illustrated in the reduced *a* peaks of the subsequent waveforms. Under the same circumstance, a decrease in peak *v* was also realized for subsequent times. This peak denotes an increase in the pressure of the right atrium due to the rapid filling of the chamber with a closed tricuspid valve. This is a good response demonstrated by the PPG sensor. This infers if a patient has an increased CVP, the sensor will be capable of showing waveforms to establish this fact. Even though this sensor does not give actual pressure values inherent in the central venous system, the waveforms recorded by it carry useful information which can be depended on for medical monitoring and diagnosis.

5.2. Conclusion

Using a newly developed laser PPG reflectance configured sensor, this research has demonstrated a way of estimating the waveforms in the jugular veins. In other words, this new sensor is capable of detecting the central venous waveform.

1. A MCL, which mimicked the pressure of the central venous system, was used to test the sensor in vitro.
2. The sensor was further tested in vivo on a single subject.
3. By comparing the waveforms recorded from the sensor to the standard central venous waveform, it was established that the PPG sensor was able to reproduce the standard waveform from the right EJV of the researcher.
4. The sensor is made from inexpensive components and is very simple to implement. It is noninvasive, fast, capable of continuous monitoring, and easy to use.

5.3. Recommendation and future research

This research has a number of improvements that can be made. It also presents a couple of interesting aspects which can be exploited for further research work. A good place to begin is to incorporate the sensing elements and its processing circuit onto a single prototype chip. As a remainder, the sensing component was about one meter away from the processing circuit during the in vivo study. This is not advisable since signals could have been lost or compromised before the amplification stage. By integrating all the components on one chip, there is a greater chance of improving the results.

Moreover, there is a need to carry out more tests using a larger sample size in order to validate the response of the sensor to CVP. The sensor can be tested on patients having a standard approach like CVC. The results can then be compared to evaluate the correlation between the results from the two methods.

Due to the constraints posed by the dimensions of the devices used, the possible separating distance between the photodiode and the laser was seven millimeters. A similar sensor with a smaller separation distance can be investigated for this purpose. Also, research can be dedicated to the alternative use of other brands and models for the electronic components used in designing the PPG sensor. For instance, a highly powerful amplifier and better filtering architecture can be substituted in the sensor design for enhanced CVP response.

Finally, the sensing elements were housed in a cardboard and the hard flat surface made skin contact quite difficult. One way to promote a good contact is probably the use of a flexible sensor housing material which can adequately wrap around the curved section of the neck. Motion artifacts between the sensor and skin will always be a challenge. However, more work is required in implementing better ways of attaching the sensor securely to the neck without necessarily occluding the veins.

References

Aggarwal, V., Chatterjee, A., Cho, Y., and Cheung, D., 2006, Ultrasound-guided noninvasive measurement of a patient's central venous pressure. *Proceedings of the 28th Annual International Conference of the IEEE Engineering in Medicine and Biology Society,* New York, USA, 3843-3849.

Allen, J., 2007, Photoplethysmography and its application in clinical physiological measurement. *Physiological Measurement*, **28**(3), R1-R39.

Alliance Medical Inc., http://www.allmed.net/catalog/item/1,417,489,503,505. (Accessed December 2013).

American National Standard for Safe Use of Lasers, ANSI 2136.1-2007, Laser Institute of America, Orlando, FL.

Applefeld M.M., 1990, The jugular venous pressure and pulse contour. in Walker H.K., Hall, W.D., and Hurst, J.W., (eds), *Clinical Methods: The History, Physical, and Laboratory Examinations*, 3rd ed., (Boston: Butterworths), 107-111.

Arridge, S.R., Cope, M., and Delpy, D.T., 1992, The theoretical basis for the determination of optical path lengths in tissue: temporal and frequency analysis. *Physics in Medicine and Biology*, **37**(7), 1531-1560.

Bellazzini, M.A., Rankin, P.M., Gangnon, R.E., and Bjoernsen, L.P., 2009, Ultrasound validation of maneuvers to increase internal jugular vein cross-sectional area and decrease compressibility. *American Journal of Emergency Medicine*, **27**(4), 454-459.

Bloch, K.E., Krieger, B.P., and Sackner, M.A., 1991, Noninvasive measurement of central venous pressure by neck inductive plethysmography. *Chest*, **100**(2), 371-375.

Brennan, J.M., Blair, J.E., Goonewardena, S., Ronan, A., Shah, D., Vasaiwala, S., Brooks, E., Levy, A., Kirkpatrick, J.N., and Spencer, K.T., 2007, A comparison by medicine residents of physical examination versus hand-carried ultrasound for estimation of right atrial pressure. *The American Journal of Cardiology*, **9**(11), 1614-1616.

Chua Chiaco, J.M., Parikh, N.I., and Fergusson, D.J., 2013, The jugular venous pressure revisited. *Cleveland Clinic Journal of Medicine*, **80**(10), 638-644.

Chung, C.P., Hsu, H.Y., Chao, A.C., Wong, W.J., Sheng, W.Y., and Hu, H.H., 2007, Flow volume in the jugular vein and related hemodynamics in the branches of the jugular vein. *Ultrasound in Medicine and Biology*, **33**(4), 500-505.

Cirovic, S., Walsh, C., Fraser, W.D., and Gulino, A., 2003, The effect of posture and positive pressure breathing on the hemodynamics of the internal jugular vein. *Aviation, Space, and Environmental Medicine*, **74**(2), 125-131.

Cole, E., 2007, Measuring central venous pressure. *Nursing Standard*, **22**(7), 40

Colquhoun, D.A., Tucker-Schwartz, J.M., Durieux, M.E., and Thiele, R.H., 2012, Non-invasive estimation of jugular venous oxygen saturation: a comparison between near infrared spectroscopy and transcutaneous venous oximetry. *Journal of Clinical Monitoring and Computing*, **26**(2), 91-98.

Colquhoun, D.M., and Jenkins Glenn., 2010, Measurement of jugular venous pressure. *The Medical Journal of Australia*, **193**(1), 64.

Cox, F.J., 2001, Filter circuits, *Fundamentals of Linear Electronics: Integrated and Discrete*, 2nd ed., (Kentucky: Delmar Cengage), 439-460.

Darrah, K., 2013, How to: heartbeat monitoring-arduino/processing, http://www.kevindarrah.com (accessed 18 September 2013)

Davis, C.L., Thong, T., Belzberg, H., Phillips, C., Holden, W.E., and Thornburg, K.L., 2004, Direct coextensive plethysmography for non-invasive measurement of systemic pressures and volumes. *Proceedings of the 26th International Conference of the IEEE in Medicine and Biology Society*, California, USA, 2318-232.

Davison, R., and Cannon, R., 1974, Estimation of central venous pressure by examination of jugular veins. *American Heart Journal*, **87**(3), 279-282.

Defalque, R.J., 1974, Percutaneous catheterization of the internal jugular vein. *Anesthesia & Analgesia*, **53**(1), 116-121.

Deol, G.R., Collett, N., Ashby, A., and Schmidt, G.A., 2011, Ultrasound accurately reflects the jugular venous examination but underestimates central venous pressure. *Chest*, **139**(1), 95-100.

Donahue, S.P., Wood, J.P., Patel, B.M., and Quinn, J.V., 2009, Correlation of sonographic measurements of the internal jugular vein with central venous pressure. *American Journal of Emergency Medicine,* **27**(7), 851-855.

Easby, D., and Dalrymple, P., 2009, Monitoring arterial, central venous and pulmonary capillary wedge pressure. *Anaesthesia & Intensive Care Medicine*, **10**(1), 38-44.

Enderle, J.D., 2006, *Bioinstrumentation*, 1st ed., (San Rafael: Morgan & Claypool).

Enderle, J.D., Blanchard, S. M., and Bronzino, J.D., 2005, Anotomy and Physiology, in Blanchard, S. (eds), *Introduction to biomedical engineering*, 2nd Ed., (Burlington: Elsevier), 94-96.

English, I.C.W., Frew, R.M., Pigott, J.F., and Zak, M., 1969, Percutaneous catheterisation of the internal jugular vein. *Anaesthesia*, **24**(4), 521–531.

Feldman, R., 2003: Central venous access. in Reichman, E.F., and Simon, R.R., (eds), *Emergency Medicine Procedures* (New York: McGraw-Hill), 314-337.

Fischer, E.I., Armentano, R.L., Pessana, F.M., Graf, S., Romero, L., Christen, A.I., Simon, A., and Levenson, J., 2002, Endothelium-dependent arterial wall tone elasticity modulated by blood viscosity. *American Journal of Physiology. Heart and Circulatory Physiology*, **282**(2), H389-H394.

Glaros, K., and Drakakis, E.M., 2013, A Sub-mW fully-integrated pulse oximeter front-end. *IEEE Transactions on Biomedical Circuits and Systems*, **7**(3), 363-375.

Graves, C.L., and Klein, R. L., 1968, Central venous pressure monitoring during routine spinal anesthesia. *Archives of Surgery*, **97**(5), 843-847.

Grubb, N., Spratt, J., and Bradbury, A., 2013, The cardiovascular system, in Douglas, G., Nicol, F., Robertson, C. (eds), *Macleod's Clinical Examination*, 13th ed., (Churchill Livingstone: Elsevier), 97-136.

Haahr R.G., 2006, *Reflectance Pulse Oximetry Sensor for the Electronic Patch*, M.Sc. thesis, Department of Micro and Nanotechnology, Technical University of Denmark, Denmark.

Haahr, R.G., Duun, S., Birkelund, K., Raahauge, P., Petersen, P., Dam, H., Nørgaard, L., and Thomsen, E.V., 2007, A novel photodiode for reflectance pulse oximetry in low-power applications. *Proceedings of the 29th Annual International Conference of the IEEE EMBS*, Lyon, France, 2350-2353.

Hickey, M., and Kyriacou. P.A., 2007, Optimal spacing between transmitting and receiving optical fibres in reflectance pulse oximetry. *Journal of Physics: Conference series*, **85**(1), 1-8.

Huang, F.H., Yuan, P.J., Lin, K.P., Chang, H.H., and Tsai, C.L., 2011, Analysis of reflectance photoplethysmograph sensors, *World Academy of Science, Engineering and Technology*, **59**(241), 1266-1269.

James, D., 2011, Central venous catheter insertion, in Pfinninger, J.L., and Fowler, G.C., (eds), *Procedures for Primary Care*, 3rd ed., (Philadelphia: Mosby Elsevier), 1443-1450.

König, V., Huch, R., and Huch, A., 1998, Reflectance pulse oximetry – principles and obstetric application in the zurich system. *Journal of Clinical Monitoring and Computing*, **14**(6), 403-412.

Kugelman, A., Wasserman, Y., Mor, F., Goldinov, L., Geller, Y., and Bader, D., 2004, Reflectance pulse oximetry from core body in neonates and infants: comparison to arterial blood oxygen saturation and to transmission pulse oximetry. *Journal of Perinatology*, **24**(6), 366-371.

Lee, P.J., Prince, W., and Ramsay, J.G., 2007, Central venous pressure monitoring, in Atlee, J.L. (eds), *Complications in Anesthesia*, 2nd ed., (Philadelphia: Saunders), 582-587.

Lin, S.K., Chang, Y.J., and Yang, F.Y., 2009, Hemodynamics of the internal jugular vein: an ultrasonographic study. *Tzu Chi Medical Journal*, **21**(4), 317-322.

Lipton, B., 2000, Estimation of central venous pressure by ultrasound of the internal jugular vein. *American Journal of Emergency Medicine*, **18**(4), 432-434.

Liu, Y., Zhu, J., and Luo, Y., 2002, Design of new type of reflectance pulse oximetry sensor. *Proceedings of SPIE of Optics in Health Care and Biomedical Optics: Diagnostics and Treatment*, Shangai, China, 98-102.

Lobato, E.B., Florete, O.G., Paige, G.B., and Morey, T.E., 1998, Cross-sectional area and intravascular pressure of the right internal jugular vein during anesthesia: Effects of trendelenburg position, positive intrathoracic pressure and hepatic compression. *Journal of Clinical Anesthesia*, **10**(1), 1-5.

Magder, S., 2005, How to use central venous pressure measurements. *Current Opinion in Critical Care*, **11**(3), 264-270.

Mangione, S., 2008, The cardiovascular exam, in *Physical Diagnosis Secret*, 2nd ed., (Philadelphia: Elsevier), 251-268.

Mannheimer, P.D., 2007, The light–tissue interaction of pulse oximetry. *Anesthesia and Analgesia*, **105**(6), S10-S17.

Mannheimer, P.D., Cascini, J.R., Fein, M.E., and Nierlich, S.L., 1997, Wavelength selection for low-saturation pulse oximetry. *IEEE Transactions on Biomedical Engineering*, **44**(3), 148-158.

Marc A. Simon, M.A., Kliner, D.E., Girod, J.P., Moguillansky, D., Villanueva, F.S., and Pacella, J.J., 2010, Detection of elevated right atrial pressure using a simple bedside ultrasound measure. *American Heart Journal*, **159**(3), 421-427.

Mendelson, Y., and Ochs, B.D., 1988, Noninvasive pulse oximetry utilizing skin reflectance photoplethysmography. *IEEE Transactions on Biomedical Engineering*, **35**(10), 798-805.

Meyers, C.M., and Weingart, S.D., 2007, Critical care monitoring in the emergency department. *Emergency Medicine Practice*, **9**(7), 1-29.

Molas, M. C., Armentano, R., Bia, D., Zocalo, Y., Craiem, D., and Risk, M. R., 2003, Enhanced venous compliance sensibility at physiological ranges of pressure: experimental validation of a biphasic model. *Proceedings of the 25th Annual*

International Conference of the IEEE Engineering in Medicine and Biology Society, Cancun, Mexico, 297-300.

Muralidhar, K., 2002, Central venous pressure and pulmonary capillary wedge pressure monitoring. *Indian Journal of Anesthesia*, **46**(4), 298-303.

Naveen, G., and Nitish, G., 2000, Jugular venous pulse: an appraisal. *Journal, Indian Academy of Clinical Medicine*, **1**(3), 260-269.

Nishihara, J., Takeuchi, Y., Miyake, M., and Nagahata, S., 1996, Distribution and morphology of valves in the human external jugular vein: indications for utilization in microvascular anastomosis. *Journal of Oral and Maxillofacial Surgery*, **54**(7), 879-882.

Nitzan, M., and Taitelbaum, H., 2008, The measurement of oxygen saturation in arterial and venous blood. *IEEE Transactions in Instrumentation and Measurement Magazine*, **11**(3), 9-15.

Olson, W.H., 2010, Basic concepts of medical instrumentation. in Webster, J.G., (eds), *Medical Instrumentation: Application and Design*, 4th ed., (New Jersey: John Wiley & Sons), 1-39.

Parker, J.L., Flucker, C.J., Harvey, N., Maguire, A.M., Russell, W.C., and Thompson, J.P., 2002, Comparison of external jugular and central venous pressures in mechanically ventilated patient. *Anesthesia*, **57**(6), 596-600.

Pittman, J.A.L., Ping, J.S., and Marc, J.B., 2004, Arterial and central venous pressure monitoring. *International Anesthesiology Clinics*, **42**(1), 13-30.

Rainer, D., 2011, Laser safety review. *Journal of Chemical Health and safety*, **18**(6), 29-30.

Raksamani, K., Udompornmongkol, V., Suraseranivongse, S., Raksakietisak, M., and von Bormann, B., 2014, Correlation between cross-sectional area of the internal jugular vein and central venous pressure. *European Journal of Anesthesiology*, **31**(1), 50-51.

Ramana, R.K., Sanagala, T., and Lichtenberg, R., 2006, A new angle on the angle of Louis. *Congestive Heart Failure*, **12**(4), 196-199.

Ramnarine, K.V., Nassiri, D.K., Hoskins, P.R., Lubbers, J., 1998, Validation of a new blood-mimicking fluid for use in Doppler flow test objects. *Ultrasound in Medicine and Biology*, **24**(3), 451-459.

Ratika, S., Peter, M., Matzinger, F., and Van Walraven, C., 2002, How far is the sternal angle from the mid-right atrium. *Journal of General Internal Medicine*, **17**(11), 861-865.

Reems, M.M., and Aumann, M., 2012, Central venous pressure: principles, measurement, and interpretation. *Compendium*, **34**(1), E1-E10.

Reichelt, S., Fiala, J., Werber, A., Forster, K., Heilmann, C., Klemm, R., and Zappe, H., 2008, Development of an implantable pulse oximeter. *IEEE Transactions on Biomedical Engineering*, **55**(2), 581-588.

Reuss, J.L., and Siker, D., 2004, The pulse in reflectance pulse oximetry: modeling and experimental studies. *Journal of Clinical Monitoring and Computing*, **18**(4), 288-299.

Rhodes, A.,Grounds, R.M., and Bennett, E.D., 2011, *Textbook of Critical Care*, 6th ed., (Philadelphia: Elsevier Saunders), 533-537.

Ronan, K.P., 2002, Effect of cardiac function on central venous pressure. in Faust, R.J., (eds), *Anesthesiology Review*, 3rd ed., (Pennsylvania: Churchill Livingston), 240-241.

Russell W.J., 1974, The cardiovascular system, *Central Venous Pressure: Its Clinical Use and Role in Cardiovascular Dynamics*, (London:Butterworth), 1-3.

Sahni, R., 2012, Noninvasive monitoring by photoplethysmography. *Clinics in Perinatology*, **39**(3), 573-583.

Santha, H., Stuban, N., and Harsanyi, G., 2006, Design considerations of small size reflective type pulse oximeter heads in special applications. *Electronics Systemintegration Technology Conference*, **1**(1), 404-408.

Schmitt, J.M., Zhou, G.X., Walker, E.C., and Wall, R.T., 1990, Multilayer model of photon diffusion in skin. *Journal of the Optical Society of America*, **7**(11), 2141-2153.

Schowalter, J.S., 1997, Photodetectors and amplifiers. In Webster, J.G., (eds), *Design of Pulse Oximeters* (New York: Taylor & Francis Group), 71-84.

Seager, S., and Slabaugh, M., 2010, Solutions and colloids, *Introductory Chemistry for Today*, 7th ed., (Scarborough: Cengage Learning), 214.

Shah, P.N., Kane, D., and Appukutty, J., 2013, Depth of central venous catheterization by intracardiac electrocardiogram in adults. *Anesthesiology and Pain Medicine*, **2**(3), 111-114.

Shamir, M.Y., Avramovich, A., and Smaka, T., 2012, The current status of continuous noninvasive measurement of total, carboxy, and methemoglobin concentration. *Anesthesia and Analgesia*, **114**(5), 972-978.

Shimada, Y., Nakashima, K., Fujiwara, Y., Komatsu, T., Kawanishi, M., Takezawa, J., and Takatani, S., 1991, Evaluation of a new reflectance pulse oximeter for clinical applications. *Medical and Biological Engineering and Computing*, **29**(5), 557-561.

Short, D.S., 1957, The jugular venous pulse. *Postgraduate Medical Journal*, **33**(382), 389-394.

Shroeder, R.A., Barbeito, A., Bar-Yosef, S., and Mark, J.B., 2010, Cardiovascular monitoring. in Miller, R.D., (eds), *Miller's Anesthesia*, 7th ed., (Pennsylvania: Churchill Livingstone), 1267-1328.

Siva, B., Hunt, A., and Boudville, N., 2012, The sensitivity and specificity of ultrasound estimation of central venous pressure using the internal jugular vein. *Journal of Critical Care*, **27**(3), 315.e7-315.e11.

Springer Materials, 2013, The Landolt-Bornstein Database. Material science data for 250,000 substances, www.springermaterials.com. (accessed December, 2013)

Taylor, C.E., and Miller, G.E., 2012, Mock circulatory loop compliance chamber employing a novel real-time control process. *Journal of Medical Devices*, **6**(4), 450031-450038

Thiele, R.H., Tucker-Schwartz, J.M., Lu, Y., Gillies, G.T., and Durieux, M.E., 2011, Transcutaneous regional venous oximetry: a feasibility study. *Anesthesia and Analgesia*, **112**(6), 1353-1357.

Thomas, G., and Isaacs, R., 2011, Basic principles of lasers. *Anesthesia & Intensive Care Medicine*, **12**(12), 574-577.

Thompson, D., Wareing, A., Day, D., and Warren, S., 2006, Pulse oximeter improvement with an ADC-DAC feedback loop and a radial reflectance sensor. *Proceedings of the 28th International Conference on the IEEE Engineering Medicine and Biology Society*, Kansas, USA, 815-818.

Timms, D.L., Gregory, S.D., Greatrex, N.A., Pearcy, M.J., Fraser, J.F., and Steinseifer, U., 2011, A compact mock circulation loop for the in vitro testing of cardiovascular devices." *Artificial Organs*, **35**(4), 384–391.

Traviglia, D., and Mendelson, Y., 2004, A portable setup for comparing transmittance and reflectance pulse oximeters for field testing applications. *Proceedings of the IEEE 30th Annual Northeast Bioengineering Conference*, Springfield, USA, 212-213.

Troianos, C.A., Jobe, D.R., and Ellison, N., 1991, Ultrasound-guided cannulation of the internal jugular vein. A prospective randomized study. *Anesthesia & Analgesia*, **72**(6), 823-826.

Uflacker, R., 2006, *Atlas of Vascular Anatomy: An Angiographic Approach*, 2nd ed., (Philadelphia: Lippincott Williams & Wilkins).

University of Ottawa risk management. http://www.uottawa.ca/services/ehss/ClassificationofLasers.html (accessed 13 December 2013).

Unluer, E.E., and Kara, P.H., 2013, Ultrasonography of jugular vein as a marker of hypovolemia in healthy volunteers. *American Journal of Emergency Medicine*, **31**(1), 173-177.

Vinayak, A.G., Levitt, J., Gehlbach, B., Pohlman, A.S., Hall, J.B., and Kress, J.P., 2006, Usefulness of the external jugular vein examination in detecting abnormal central venous pressure in critically ill patients. *Archives of Internal Medicine*, **166**(19), 2132-2137.

Walton, Z.D., Kyriacou, P.A., Silverman, D.G., and Shelley, K.H., 2010, Measuring venous oxygenation using the photoplethysmograph waveform. *Journal of Clinical Monitoring and Computing*, **24**(4), 295-303.

Ward, K.R., Tiba, M.H., Barbee, R.W., Ivatury, R.R., Arrowood, A.J., Spiess, B.D., and Hummel, R., 2006, A new noninvasive method to determine central venous pressure. *Resuscitation*, **70**(2), 238-246.

Ward, K.R., Tiba, M.H., Draucker, G.T., Proffitt, E.K., Barbee, R.W., Gunnerson, K.J., Reynolds, P.S., and Spiess, B.D., 2010, A novel noninvasive impedance-based technique for central venous pressure measurement. *Shock*, **33**(3), 269-273.

Watson, A.C., and Wilkinson, M.B., 2012, Monitoring central venous pressure, arterial pressure and pulmonary wedge pressure. *Anaesthesia & Intensive Care Medicine*, **13**(3), 116-120.

Yan, W., and Seow, S., 2009, Reversed internal jugular vein flow as a sign of brachiocephalic vein obstruction. *Australian Journal of Ultrasound in Medicine*, **12**(2), 39-41.

Yousif, M.Y., Holdsworth, D.W., and Poepping, T.L., 2009, Deriving a blood-mimicking fluid for particle image velocimetry in sylgard-184 vascular models. *Proceedings of* the *31st Annual International Conference IEEE Engineering Medicine and Biology Society*, Minnesota, USA, 1412-1415.

Zamani, H., Babazadeh, K., Ghaffari, R., Karami, H., Fattahi, S., and Mokhtari Esbuie F., 2012, The successful withdrawal of a migrated central venous catheter. *Caspian Journal of Internal Medicine*, **3**(4), 550-553.

Appendix A: LabVIEW code

Labview program for sensor instrumentation interface.

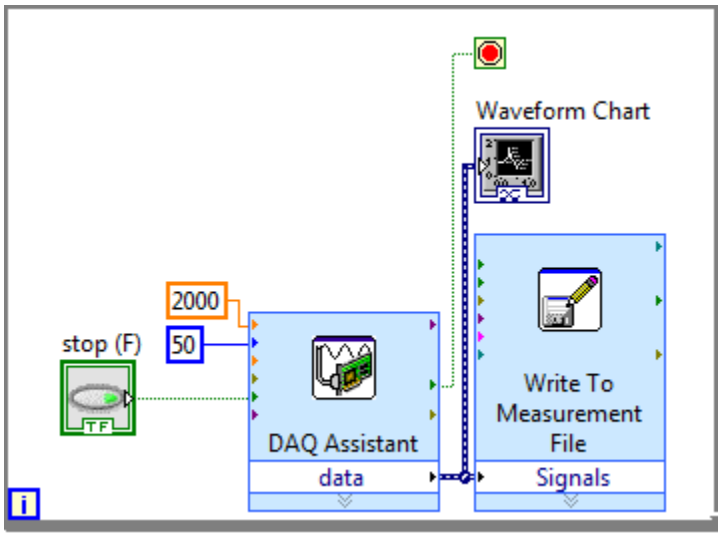

Parameters used for the DAQ assistant in the above program are also shown below.

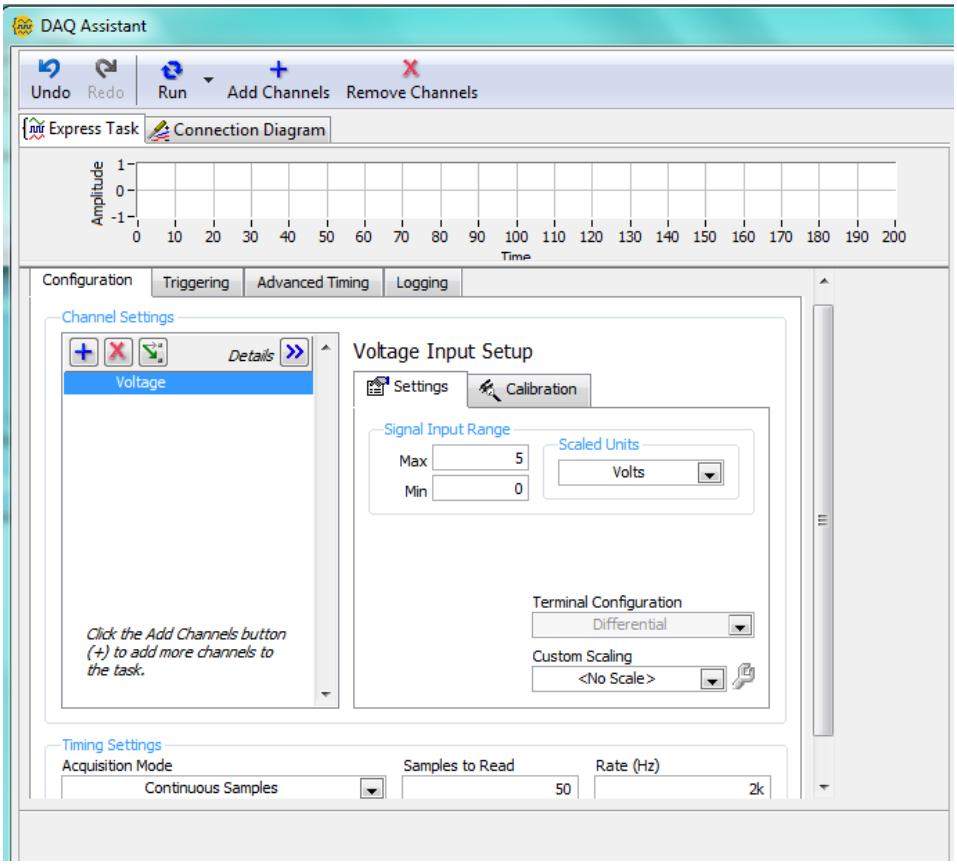

Appendix B: P23Db standardization and calibration

The standardization of the P23Db was done with the Dwyer® 490 digital manometer, a vinyl tubing with an internal diameter of 4.138mm, a 10ml syringe barrel and water. The water was left at room temperature for about an hour to attain a uniform temperature. The tubing was mounted vertically on a wall and attached to the manometer as shown below.

With the help of the 10ml syringe, several volumes of water were dispensed into the tubing and their respective pressures were noted in mmHg. Three measurements were done for the volumes of 2ml, 3ml, 4ml, 5ml and 7ml and a respective mean pressure value of 7.2, 12.8, 17.7, 22.6, and 33.7mmHg was recorded.

The P23Db device was interfaced to a gauge on LabVIEW through a DAQ device. Since the pressure transducer was configured as a Wheatstone bridge, two of its wires were connected to the terminals of a five volts power supply and the other two wires were connected to the DAQ device which served as outputs. The program used to calibrate the transducer is shown below.

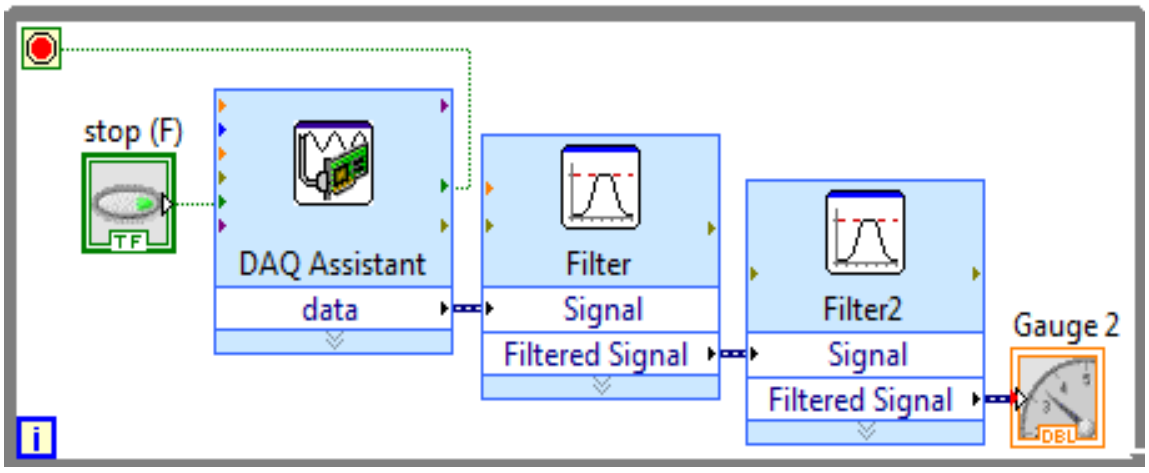

The parameters for the DAQ Assistant, first and second filters, and the voltage gauge are shown below.

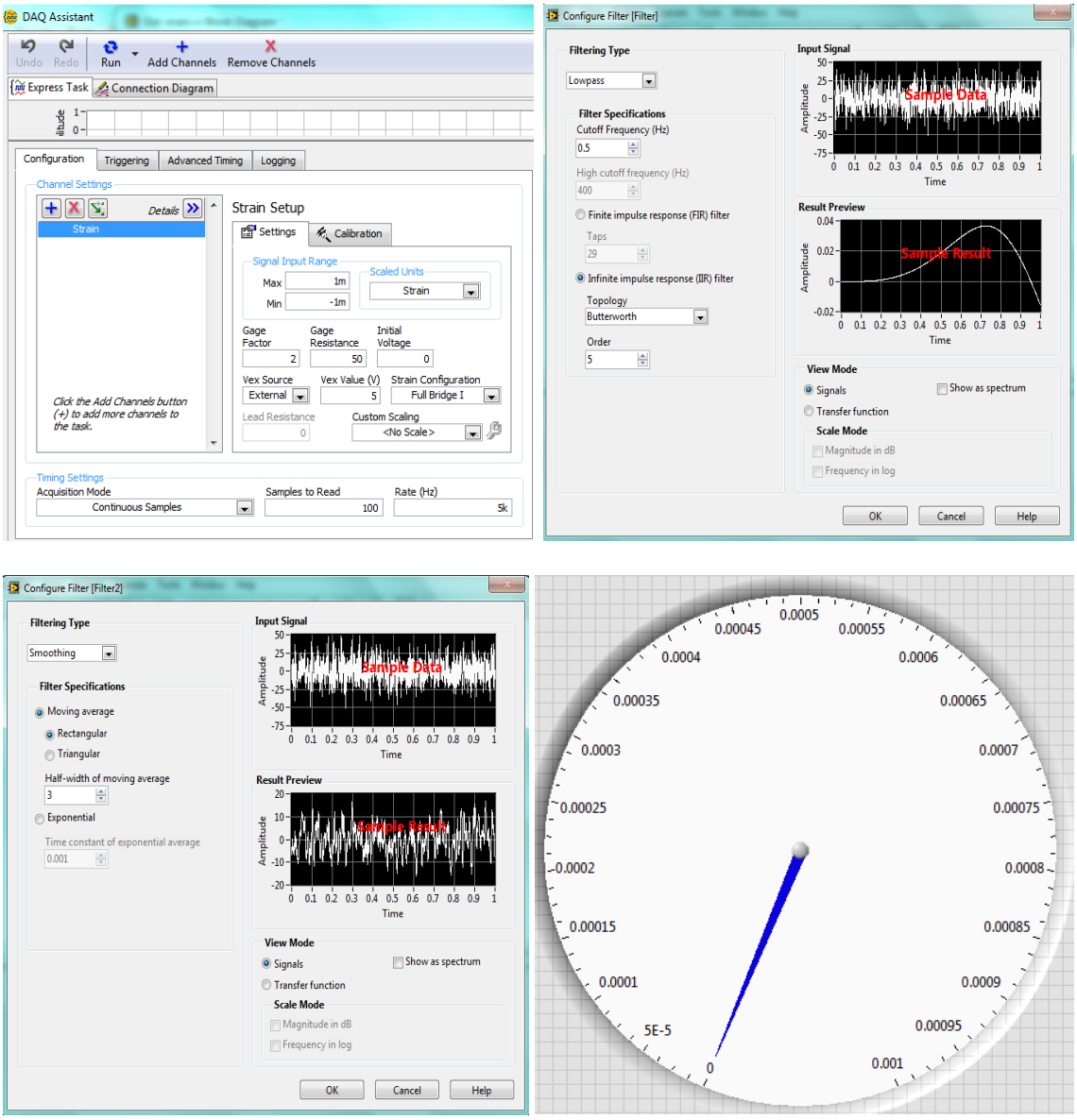

Once calibration of the P23Db was done successfully on LabVIEW, its inlet was connected to the wall mounted tubing as shown below.

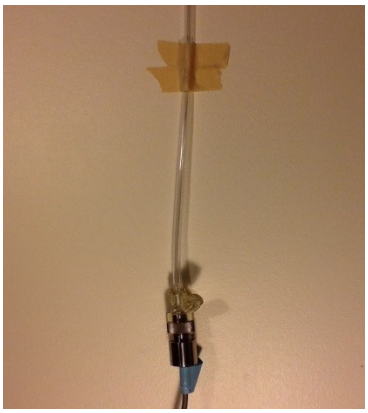

The same water volumes of 2ml, 3ml, 4ml, 5ml and 7ml were dispensed into the tubing with the help of the syringe barrel. Corresponding values on the gauge for these volumes were recorded. So indirectly, the pressure values that were recorded for the manometers corresponded to the values recorded on the gauge by the P23db. There was a zero error of $+5.0*10^{-5}$v on the gauge. Hence every result on the gauge had this value deducted to get the actual value.

The values recorded on the gauge after zero error deductions were;

2ml (7.2mmHg) = $3.75*10^{-5}$v $\pm 1.25*10^{-5}$
3ml (12.8mmHg) = $1.0*10^{-4}$v $\pm 1.25*10^{-5}$
4ml (17.7mmHg) = $1.25*10^{-4}$v $\pm 1.25*10^{-5}$
5ml (22.6mmHg) = $1.375*10^{-4}$v $\pm 1.25*10^{-5}$
7ml (33.7mmHg) = $1.625*10^{-4}$v $\pm 1.25*10^{-5}$

NB: The values presented are mean values calculated from three trials. However, due to the pulsed nature of the pressure signals, the pointer on the gauge was not completely stable for values to be taken. This may have altered the results during the exercise.

Appendix C: Datasheets

PD438C/S46 photodiode

Technical Data Sheet
4.8mm Semi-Lens Silicon PIN Photodiode

PD438C/S46

Features

- Fast response times
- High photo sensitivity
- Small junction capacitance
- Pb free
- The product itself will remain within RoHS compliant version.

Descriptions

PD438C/S46 is a high speed and sensitive PIN photodiode in a flat side view plastic package. Due to its water clear epoxy the device is sensitive to visible and infrared radiation.

Applications

- High speed photo detector
- Camera
- Optoelectronic switch
- VCRs , Video camera

Device Selection Guide

LED Part No.	Chip Material	Lens Color
PD	Silicon	Water clear

Package Dimensions

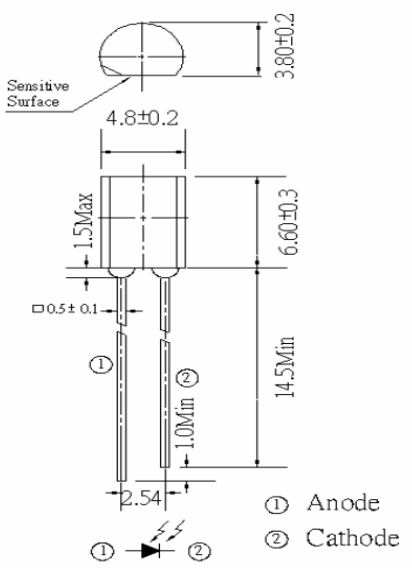

Notes: 1.All dimensions are in millimeters
2.Tolerances unless dimensions ±0.25mm

Absolute Maximum Ratings (Ta=25℃)

Parameter	Symbol	Rating	Units
Reverse Voltage	V_R	32	V
Power Dissipation	Pd	150	mW
Lead Soldering Temperature	Tsol	260	℃
Operating Temperature	Topr	-40 ~ +85	℃
Storage Temperature	Tstg	-40 ~ +85	℃

Notes: *1:Soldering time≦5 seconds.

Electro-Optical Characteristics (Ta=25℃)

Parameter	Symbol	Condition	Min.	Typ.	Max.	Units
Rang of Spectral Bandwidth	$\lambda_{0.5}$	-----	400	---	1100	nm
Wavelength of Peak Sensitivity	λ_p	-----	---	940	---	nm
Open-Circuit Voltage	Voc	Ee=5m W/cm^2 λ p=940nm	---	0.35	---	V
Short- Circuit Current	I_{SC}	Ee=1m W/cm^2 λ p=940nm	---	18	---	μA
Reverse Light Current	I_L	Ee=1m W/cm^2 λ p=940nm V_R=5V	10.2	18	---	
Dark Current	Id	Ee=0m W/cm^2 V_R=10V	---	5	30	nA
Reverse Breakdown	BV_R	Ee=0m W/cm^2 I_R=100 μA	32	170	---	V
Total Capacitance	Ct	Ee=0m W/cm^2 V_R=3V f=1MHZ	---	25	---	pF
Rise/Fall Time	t_r/t_f	V_R=10V R_L=1KΩ	---	50/50	---	nS

Typical Electro-Optical Characteristics Curves

Fig.1 Power Dissipation vs. Ambient Temperature

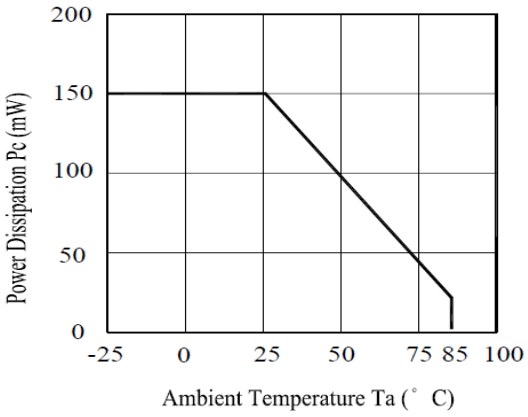

Fig.2 Spectral Sensitivity

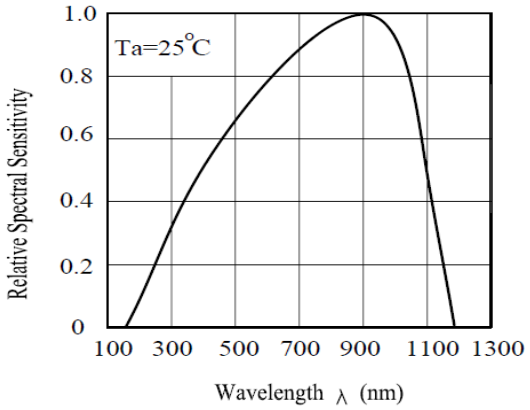

Fig.3 Dark Current vs. Ambient Temperature

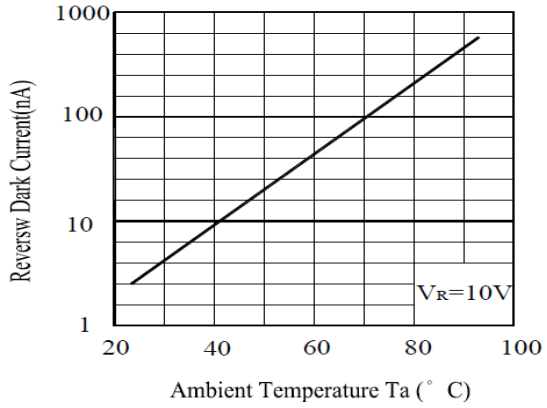

Fig. 4 Reverse Light Current vs. Ee

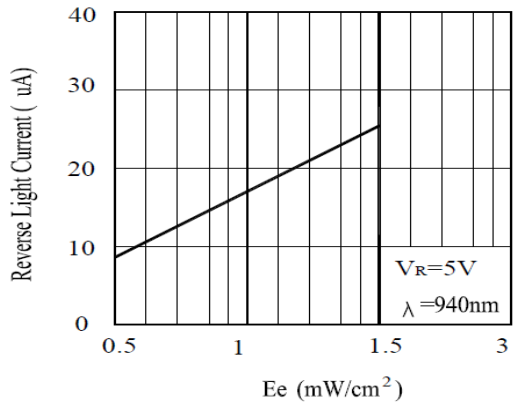

Fig.5 Terminal Capacitance vs. Reverse Voltage

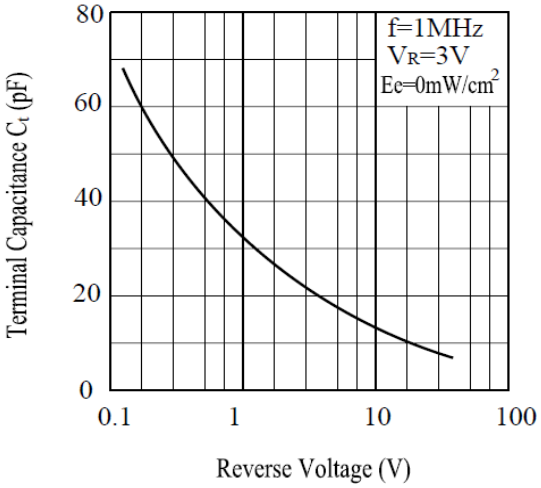

Fig.6 Response Time vs. Load Resistance

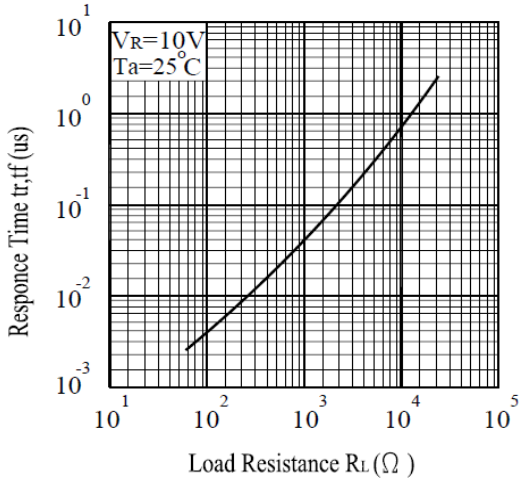

National Semiconductor

August 2000

LM386
Low Voltage Audio Power Amplifier

General Description

The LM386 is a power amplifier designed for use in low voltage consumer applications. The gain is internally set to 20 to keep external part count low, but the addition of an external resistor and capacitor between pins 1 and 8 will increase the gain to any value from 20 to 200.

The inputs are ground referenced while the output automatically biases to one-half the supply voltage. The quiescent power drain is only 24 milliwatts when operating from a 6 volt supply, making the LM386 ideal for battery operation.

Features

- Battery operation
- Minimum external parts
- Wide supply voltage range: 4V–12V or 5V–18V
- Low quiescent current drain: 4mA
- Voltage gains from 20 to 200
- Ground referenced input
- Self-centering output quiescent voltage
- Low distortion: 0.2% (A_V = 20, V_S = 6V, R_L = 8Ω, P_O = 125mW, f = 1kHz)
- Available in 8 pin MSOP package

Applications

- AM-FM radio amplifiers
- Portable tape player amplifiers
- Intercoms
- TV sound systems
- Line drivers
- Ultrasonic drivers
- Small servo drivers
- Power converters

Equivalent Schematic and Connection Diagrams

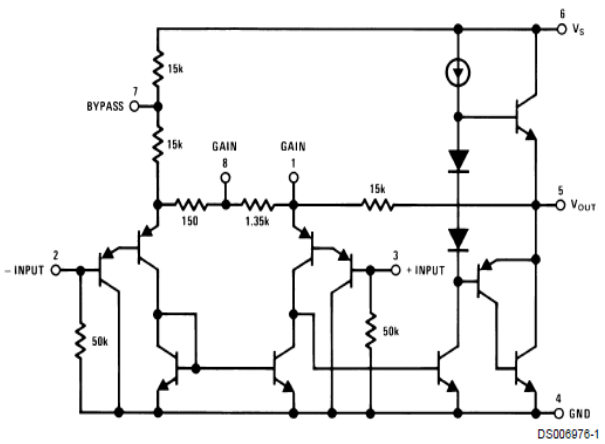

DS006976-1

Small Outline, Molded Mini Small Outline, and Dual-In-Line Packages

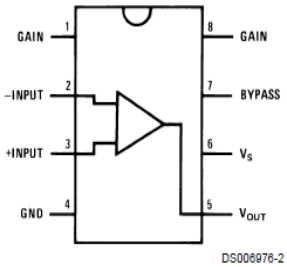

DS006976-2

Top View
Order Number LM386M-1, LM386MM-1, LM386N-1, LM386N-3 or LM386N-4
See NS Package Number M08A, MUA08A or N08E

Absolute Maximum Ratings (Note 2)

If Military/Aerospace specified devices are required, please contact the National Semiconductor Sales Office/ Distributors for availability and specifications.

Supply Voltage	
(LM386N-1, -3, LM386M-1)	15V
Supply Voltage (LM386N-4)	22V
Package Dissipation (Note 3)	
(LM386N)	1.25W
(LM386M)	0.73W
(LM386MM-1)	0.595W
Input Voltage	±0.4V
Storage Temperature	−65°C to +150°C
Operating Temperature	0°C to +70°C
Junction Temperature	+150°C
Soldering Information	
Dual-In-Line Package	
Soldering (10 sec)	+260°C
Small Outline Package	
(SOIC and MSOP)	
Vapor Phase (60 sec)	+215°C
Infrared (15 sec)	+220°C

See AN-450 "Surface Mounting Methods and Their Effect on Product Reliability" for other methods of soldering surface mount devices.

Thermal Resistance	
θ_{JC} (DIP)	37°C/W
θ_{JA} (DIP)	107°C/W
θ_{JC} (SO Package)	35°C/W
θ_{JA} (SO Package)	172°C/W
θ_{JA} (MSOP)	210°C/W
θ_{JC} (MSOP)	56°C/W

Electrical Characteristics (Notes 1, 2)

T_A = 25°C

Parameter	Conditions	Min	Typ	Max	Units
Operating Supply Voltage (V_S)					
LM386N-1, -3, LM386M-1, LM386MM-1		4		12	V
LM386N-4		5		18	V
Quiescent Current (I_Q)	V_S = 6V, V_{IN} = 0		4	8	mA
Output Power (P_{OUT})					
LM386N-1, LM386M-1, LM386MM-1	V_S = 6V, R_L = 8Ω, THD = 10%	250	325		mW
LM386N-3	V_S = 9V, R_L = 8Ω, THD = 10%	500	700		mW
LM386N-4	V_S = 16V, R_L = 32Ω, THD = 10%	700	1000		mW
Voltage Gain (A_V)	V_S = 6V, f = 1 kHz		26		dB
	10 µF from Pin 1 to 8		46		dB
Bandwidth (BW)	V_S = 6V, Pins 1 and 8 Open		300		kHz
Total Harmonic Distortion (THD)	V_S = 6V, R_L = 8Ω, P_{OUT} = 125 mW		0.2		%
	f = 1 kHz, Pins 1 and 8 Open				
Power Supply Rejection Ratio (PSRR)	V_S = 6V, f = 1 kHz, C_{BYPASS} = 10 µF		50		dB
	Pins 1 and 8 Open, Referred to Output				
Input Resistance (R_{IN})			50		kΩ
Input Bias Current (I_{BIAS})	V_S = 6V, Pins 2 and 3 Open		250		nA

Note 1: All voltages are measured with respect to the ground pin, unless otherwise specified.

Note 2: Absolute Maximum Ratings indicate limits beyond which damage to the device may occur. Operating Ratings indicate conditions for which the device is functional, but do not guarantee specific performance limits. Electrical Characteristics state DC and AC electrical specifications under particular test conditions which guarantee specific performance limits. This assumes that the device is within the Operating Ratings. Specifications are not guaranteed for parameters where no limit is given, however, the typical value is a good indication of device performance.

Note 3: For operation in ambient temperatures above 25°C, the device must be derated based on a 150°C maximum junction temperature and 1) a thermal resistance of 107°C/W junction to ambient for the dual-in-line package and 2) a thermal resistance of 170°C/W for the small outline package.

Application Hints

GAIN CONTROL

To make the LM386 a more versatile amplifier, two pins (1 and 8) are provided for gain control. With pins 1 and 8 open the 1.35 kΩ resistor sets the gain at 20 (26 dB). If a capacitor is put from pin 1 to 8, bypassing the 1.35 kΩ resistor, the gain will go up to 200 (46 dB). If a resistor is placed in series with the capacitor, the gain can be set to any value from 20 to 200. Gain control can also be done by capacitively coupling a resistor (or FET) from pin 1 to ground.

Additional external components can be placed in parallel with the internal feedback resistors to tailor the gain and frequency response for individual applications. For example, we can compensate poor speaker bass response by frequency shaping the feedback path. This is done with a series RC from pin 1 to 5 (paralleling the internal 15 kΩ resistor). For 6 dB effective bass boost: R ≃ 15 kΩ, the lowest value for good stable operation is R = 10 kΩ if pin 8 is open. If pins 1 and 8 are bypassed then R as low as 2 kΩ can be used. This restriction is because the amplifier is only compensated for closed-loop gains greater than 9.

INPUT BIASING

The schematic shows that both inputs are biased to ground with a 50 kΩ resistor. The base current of the input transistors is about 250 nA, so the inputs are at about 12.5 mV when left open. If the dc source resistance driving the LM386 is higher than 250 kΩ it will contribute very little additional offset (about 2.5 mV at the input, 50 mV at the output). If the dc source resistance is less than 10 kΩ, then shorting the unused input to ground will keep the offset low (about 2.5 mV at the input, 50 mV at the output). For dc source resistances between these values we can eliminate excess offset by putting a resistor from the unused input to ground, equal in value to the dc source resistance. Of course all offset problems are eliminated if the input is capacitively coupled.

When using the LM386 with higher gains (bypassing the 1.35 kΩ resistor between pins 1 and 8) it is necessary to bypass the unused input, preventing degradation of gain and possible instabilities. This is done with a 0.1 µF capacitor or a short to ground depending on the dc source resistance on the driven input.

Typical Performance Characteristics

Quiescent Supply Current vs Supply Voltage

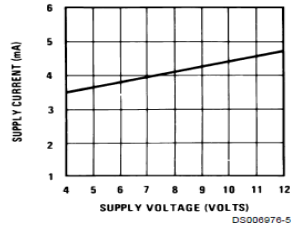

Power Supply Rejection Ratio (Referred to the Output) vs Frequency

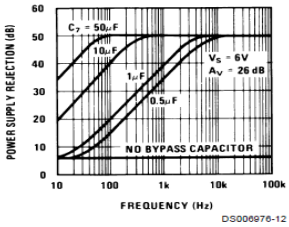

Peak-to-Peak Output Voltage Swing vs Supply Voltage

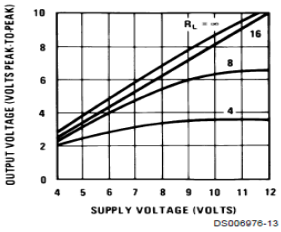

Voltage Gain vs Frequency

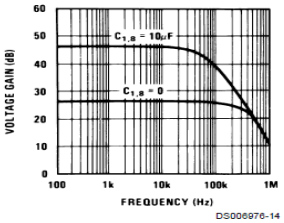

Distortion vs Frequency

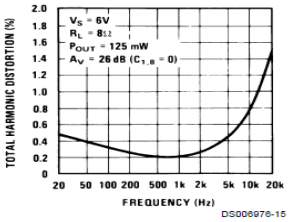

Distortion vs Output Power

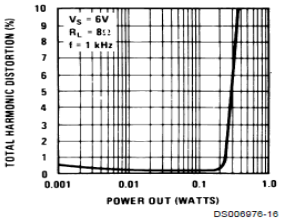

Device Dissipation vs Output Power—4Ω Load

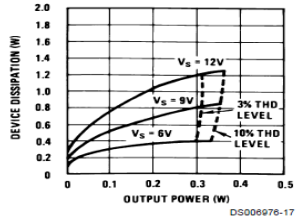

Device Dissipation vs Output Power—8Ω Load

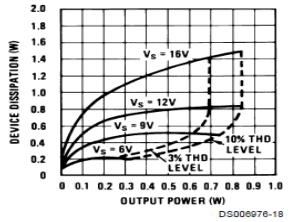

Device Dissipation vs Output Power—16Ω Load

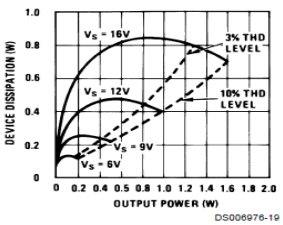

Physical Dimensions inches (millimeters) unless otherwise noted (Continued)

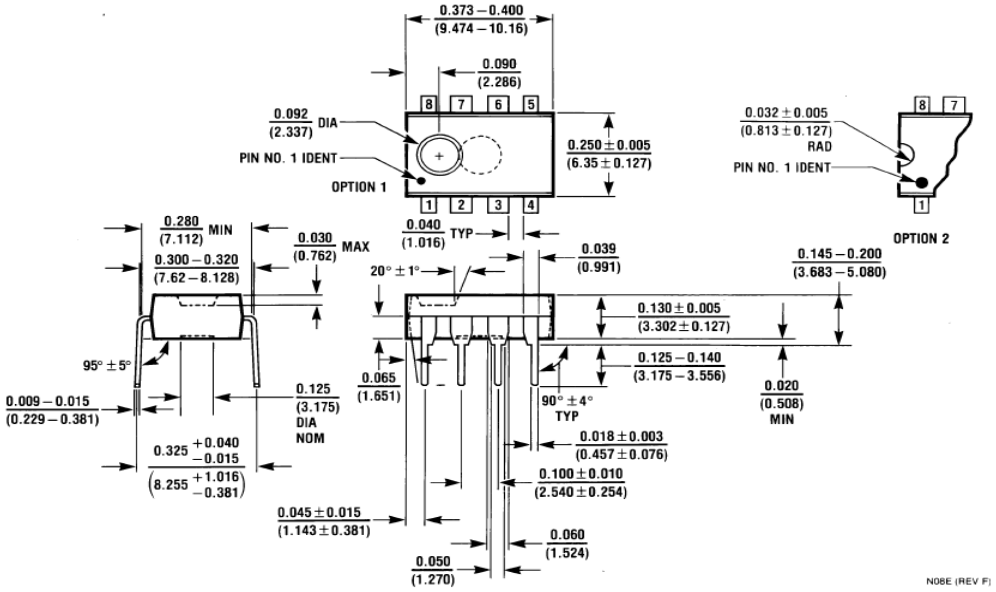

Dual-In-Line Package (N)
Order Number LM386N-1, LM386N-3 or LM386N-4
NS Package Number N08E

GLP-W4/ W6-C00110 Pump

Brushless Motor Membrane Water Pump

GLP-WL1 Brushless Membrane Water&Vacumm Pump Series

Model	Water Pump (Item Number)	Vacuum Pump (only vacuum reference GLP-ML3) (Item Number for mix-usage)	Rated Voltage (Vdc)	No-load Current (A)	MaxHead (M)	Max Vacuum (KPa)	Max Flow (L/min)
GLP-WL1	GLP-WL1/ W6,W12,W24-C00210	GLP-WL1/ V6,V12,V24-C6005	6 /12 / 24	1.5/1/ 0.8	⩾10	-60	water: 0.2 gas : 5
	GLP-WL1/ W6,W12,W24-C00310	GLP-WL1/ V6,V12,V24-C6504	6 /12 / 24	1.5/1/ 0.8	⩾10	-65	water: 0.35 gas: 4.5
	GLP-WL1/ W6,W12,W24-C00410	GLP-WL1/ V6,V12,V24-C7004	6 /12 / 24	1.5/1/ 0.8	⩾10	-70	water: 0.4 gas 4
	GLP-WL1/ W6,W12,W24-C0110	GLP-WL1/ V6,V12,V24-C5505	6 /12 / 24	1.5/1/ 0.8	⩾10	-55	water: 1 gas: 5
	GLP-WL1/ W6,W12,W24-C00310-W (outside controller)	GLP-WL1/ V6,V12,V24-C6504-W (outside controller)	6 /12 / 24	1.5/1/ 0.8	⩾10	-65	water: 0.35 gas: 4.5
	GLP-WL1/ W6,W12,W24-C00410-W (outside controller)	GLP-WL1/ V6,V12,V24-C7004-W (outside controller)	6 /12 / 24	1.5/1/ 0.8	⩾10	-70	water:0.4 gas: 4
	GLP-WL1/ W6,W12,W24-C0110-W (outside controller)	GLP-WL1/ V6,V12,V24-C5505-W (outside controller)	6 /12 / 24	1.5/1/ 0.8	⩾10	-55	water:1 gas: 5

" / W " means water pump, " / V " means vacuum pump, **3, 6, 9, 12, 24 means different voltages.**

C type: weight 250g, size 61.5*30.5*80.5mm Materials: pump head Nylon, membrane EPDM / PTFE, valve EPDM / FPM (PTFE/FPM type should be ⩽0.8L).

Note: 1. ***"W" means pump with outside controller*** can realize functions of PWM 0～5V speed adjustment, brake, instant starting work ; no "W" mark means normal 2 wires connection type, no additional functions. 2. super silent noise motor ＜50dB, motor long lifetime ＞15,000hours. 3.other water flow rates of 0.3L/0.5L/0/6L/0.7L/0.8L/0.9L can be customized as requirements.

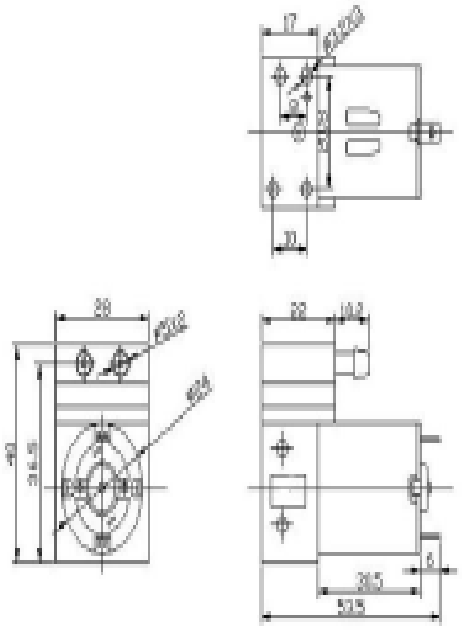

GLP-W4

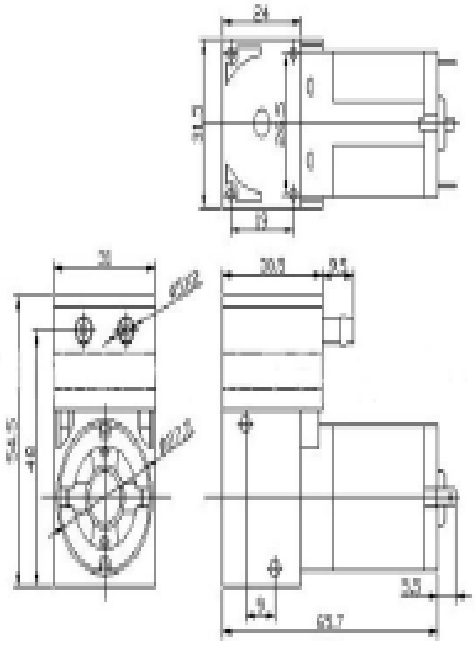

GLP-W5

Bulletin D-24

Series 490 Wet/Wet Handheld Digital Manometer

Specifications - Installation & Operating Instructions

Series 490 Digital Manometers are versatile, hand-held, battery operated manometers available in several basic ranges from 0-15.0 psi up to 0-500 psi. All models measure either positive, negative or differential pressures with ±0.5% of full scale accuracy. You can select from up to seven common English and metric pressure units so conversions are not necessary. A memory function allows storage of up to 40 readings for later recall and a backlight provides auxiliary lighting for hard-to-see locations. Also standard are a hold feature plus both visual and audible overpressure alarms.

SPECIFICATIONS

Service: Compatible, non-combustible gases & liquids.
Wetted Materials: Type 316L SS.
Accuracy: ±0.5% F.S., 60 to 78°F (15.6 to 25.6°C); ±1.5% F.S. from 32 to 60°F and 78 to 104°F (0 to 15.6°C and 25.6 to 40°C).
Pressure Hysteresis: ±0.1% of full scale.
Pressure Limits: See chart.
Temperature Limits: 32 to 104°F (0 to 40°C).
Storage Temperature Limits: -4 to 176°F (-20 to 80°C).
Display: 4-digit LCD (.425 H x .234 W digits).
Resolution: See chart.
Power Requirements: 9 volt alkaline battery. Battery included but not connected.
Weight: 14.1 oz (400 g).
Connections: Two 1/8" (3.18 mm) female NPT.
Agency Approvals: CE.

Model Number	English Range	Metric Range	Maximum Pressure
490-1	0-15.00 psi	0-103.4 kPa	30 psi (2.7 bar)
490-2	0-30.00 psi	0-206.9 kPa	60 psi (4.13 bar)
490-3	0-50.00 psi	0-344.8 kPa	100 psi (6.89 bar)
490-4	0-100.0 psi	0-689.5 kPa	200 psi (13.78 bar)
490-5	0-500.0 psi	0-3448 kPa	1000 psi (68.9 bar)
490-6	0-200.0 psi	0-1379 kPa	400 psi (27.57 bar)